AN INVESTIGATION OF NEW IN-SITU-GENERATED ACID FOR CARBONATE MINERAL DISSOLUTION IN SANDSTONE AND CARBONATE CORES

A Thesis

by

THANAKRICH PUMMARAPANTHU

Submitted to the Office of Graduate and Professional Studies of
Texas A&M University
in partial fulfillment of the requirements for the degree of

MASTER OF SCIENCE

Chair of Committee,	Hisham Nasr-El-Din
Committee Members,	Berna Hascakir
	Mahmoud El-Halwagi
Head of Department,	A. Daniel Hill

August 2016

Major Subject: Petroleum Engineering

ABSTRACT

Matrix acidizing is a well stimulation technique in which an acid solution is injected into the formation to dissolve some of the minerals to recover or increase the permeability in the near-wellbore region. The most common acid used in matrix acidizing is hydrochloric acid (HCl). HCl has been used as a stand-alone stimulating fluid to decrease skin damage, create highly conductive wormholes in carbonate reservoirs, and stimulate sandstone reservoirs as a part of mud acid treatment. However, HCl in high-pressure/high-temperature (HP/HT) wells is problematic because of its rapid reactivity, resulting in face dissolution, corrosion, and associated increased inhibition costs.

Therefore, an acidizing system that is comparable to HCl in terms of availability and cost is required; however, the drawbacks associated with HCl, such as its fast reaction rate and high corrosion rate, should be taken into account in any newly developed systems. To answer these challenges, this study will investigate the effectiveness of a new in-situ-generated HCl acid (Urea Hydrochloride) that will provide slower reaction rates and lower corrosion rates in high-temperature reservoirs.

The objectives of this work are to investigate the performance of an in-situ-generated acid system as an alternative to regular HCl in the dissolution of carbonates in dolomite cores and in the preflush stage for sandstone cores, to identify the effect of additives on the outcome of the in-situ-generated acid system treatment, and to evaluate the effect of temperature on treatment outcome. The new in-situ-generated acid treatment will be applied to stimulate two types of sandstone cores (Grey Berea and Bandera) and

Silurian dolomite. The effects of the treatment fluid at high temperature will be investigated based on results from coreflood experiments, chemical analysis of effluent samples, and X-ray computed tomography (CT).

This study's outcome will assist in developing a more cost-effective and efficient design of acid treatments.

DEDICATION

I dedicate this thesis to my family and friends for their support and encouragement during my time at Texas A&M University.

ACKNOWLEDGEMENTS

I would like to express my gratitude to my supervisor professor Dr. Hisham A. Nasr-El-Din for his assistance and guidance throughout my studies and research. Also, I would like to thank Dr. Berna Hascakir and Dr. Mahmoud El-Halwagi for devoting their time to review my research work. Furthermore, I would like to thank PTTEP for sponsorship during my time at Texas A&M University. Moreover, I would like to thank Khatere Sokhanvarian for her help and guidance throughout the project. Finally, I would like to thank the technical staff at Lubrizol Company for their help in providing chemicals and knowledge in this project.

NOMENCLATURE

CI	Corrosion Inhibitor
FA	Fixing Agent
ICP-OES	Inductively Coupled Plasma-Optical Emission Spectroscopy
Psi	Pound Per Square Inch
PV	Pore Volume
SEM-EDS	Scanning Electron Microscope and Energy Dispersive X-Ray Spectrometer
XRD	X-ray Diffraction
CT	Computed Tomography

TABLE OF CONTENTS

Page

LIST OF FIGURES

Page

LIST OF TABLES

Page

CHAPTER I

INTRODUCTION AND LITERATURE REVIEW

Regarding the history of well stimulation, acidizing is certainly the oldest techniques still in use nowadays. Other techniques such as hydraulic fracturing were developed much more recently. The primary objective of an acidizing job is to bypass the nearby wellbore damage to enhance the well productivity or injectivity.

In sandstone reservoirs, the key objective is to accomplish deep penetration into the formation region caused by completion and drilling operations. The goal is to bypass formation damage and restore the flow capacity in the near wellbore zone without fracturing the producing regions. In carbonate acidizing, the primary purpose is to dissolve significant amounts of alkaline-earth metals to form channels or effective wormholes to increase the productivity and injectivity index of the reservoir rock.

The earliest records indicate that the first acid treatments were probably performed in 1896 (Walker et al. 1991). The Standard Oil Company used concentrated hydrochloric acid (HCl) to stimulate oil wells producing from carbonate formation in Lima, Ohio, at their Solar Refinery (Kalfayan 2008).

Herman Frasch, the chief chemist of the Solar Refinery at that time, is credited with the invention of the acidizing technique (Putnam 1933). His first patent was issued on March 17, 1896 (Frasch 1896). He proposed commercial muriatic acid (30-40% by weight of HCl, a highly water-soluble gaseous acid).

Many wells in the Lima, Ohio, wells were acidized with remarkable results in the short term. However, its use soon declined until the late of 1920s. The decline may have

been related to the lack of an efficient method for limiting acid corrosion. In 1928, the use of acidizing rose again. The Gypsy Oil Company, a subsidiary of Gulf Oil Company, used HCl to remove calcareous scale deposited in the pipe and on equipment, in Oklahoma wells (Chapman 1933). These treatments included the use of Rodine No.2, an acid corrosion inhibitor used in acid pickling in steel mills. The lack of good corrosion inhibitors prevented popularity of acid in stimulating oil wells until arsenic inhibitors were discovered in the early 1930's. (Nitter et al. 2000).

Since the first commercial use in 1932, HCl has remained the primary acid for stimulating carbonate formations. In 1961, Harris introduced the use of acetic acid to the industry (Harris 1961). The benefits of acetic were it was less corrosive than HCl and could replace HCl in certain applications, particularly at high temperatures. Later, formic acid was also found to be useful in solving particular problems relating to acidizing with HCl. In many cases, the different properties of higher HCl concentration provided deeper acid penetration.

In May 1933, Halliburton conducted the first sandstone acidizing treatment using a mixture of HCl and hydrofluoric acid (HF). The treatment was pumped in a test well belonging to the King Royalty Company, near Archer City, Texas. It was 1,532 feet (ft) deep with 11 ft of open-hole production interval. The exact composition and strength of the mixture are not known (Williams et al. 1979). However, the results were very discouraging. The strong acid caused severe sand production into the wellbore.

In 1933, Jesse Russell Wilson of the Standard Oil Company filed a patent about the use of HF for treating sandstone formation (Wilson 1935). Many sandstone acidizing

treatments have been pumped since then without such understanding of purpose and potential.

Dowell introduced a mixture of 12% HCl-3% HF; called mud acid, in 1939. The purpose of mud acid was to remove drilling mud filter cake from the wellbore. However, the use was limited to wellbore treatment only. Mud acid represented a major breakthrough in well stimulation despite its unpopularity in early time. HCl in mud acid was found to be effective in removing carbonate deposits while HF was accounted for dissolving siliceous materials. This 12% HCl-3% HF mixture is known as a regular-strength mud acid.

In 1965, Smith and Hendrickson discussed the reactivity and kinetics of HF and the effects of common variable encountered in the field (Smith and Hendrickson 1965). They developed the tapered HF treatments, with HCl preflush and overflush, to inhibit deposition of plugging reaction products.

Numerous matrix acidizing treatments of sandstone formations have been conducted since the mid-1960s. A properly designed conventional treatment with HCl-HF mixtures will stimulate damaged sandstone formation. Risks associated with acidizing including fines migration, precipitation of reaction products, and rock deconsolidation can be minimized by use of proper volumes and concentration of acids.

Matrix acidizing is not capable of mitigating all formation damage; nevertheless, it is a valuable technique in removing acid-soluble damaging material. However, sulfate scales, paraffin, tar, water blocks, and the majority of emulsions are to a great extent unaffected by various types of mineral and organic acids. As a result, not all sources of

permeability damage are acid-soluble. To mitigate these complexities, special treatments are required instead of (or in addition to) matrix acidizing. Successful matrix acidizing depends on several factors including; but not limited to, good evaluation of candidate wells, proper design for the comprehensive coverage of all the plugged perforations, selection of compatible solvents, acids, and mineralogy to prevent or reduce fluid-fluid and fluid-rock incompatibilities (McLeod 1989). Moreover, a crucial factor in the success of any matrix acidizing treatment is proper acid placement so that the target zones are sufficiently contacted by adequate acid volumes.

In a heterogeneous reservoir, acid tends to flow through the path of least resistance flowing predominantly to higher permeability zones leaving lower permeability zones unacidized (Hill and Rossen 1994). Knowing how the formation will react to the acid designed and to anticipate the chemistry of the spent acid invading the lithology is crucial to acidizing success (McLeod 1984). Furthermore, the nature of the detrimental material and the knowledge of the depth at which the damage enters the formation are of vital importance to the success of the acid treatment. Well completion fluid systems design has always been a difficult challenge to engineers and researchers. Cost considerations, material incompatibilities, undesired chemical interactions, and physical limitations present immense complexities in matrix acidizing treatments (Chiu et al. 1993; Coulter and Jennings 1999; McLeod 1984, 1989; McLeod et al. 1983; Shaughnessy and Kunze 1981).

Sandstone acidizing consists of three key phases: (1) a preflush, typically of a weak HCl solution, (2) a mud acid stage of HCl and HF, and (3) a post-flush of HCl, ammonium

chloride or diesel oil. However, Gidley et al. (1996) suggested that many complications may occur during sandstone acidizing with mud acid. Those problems include, but are not limited to, the disintegration of clays in HCl, fluosilicates precipitation, carbonate presence in sandstone resulting in calcium fluorides precipitation, silica-gel formation and deposition.

Problems with Mud Acid Jobs

Despite the good performance in dissolving aluminosilicates (clay minerals, feldspars, and mica), several problems could occur during mud acid treatments. Quartz reacts slowly with HF compared to aluminosilicates (Li et al. 1998). Mud acid cannot be used in sandstone with high calcite concentration due to the reaction product (CaF_2) between $CaCO_3$ and HF as follows:

$$CaCO_3 + 2HF \rightarrow CaF_2 + H_2O + CO_2 \quad \ldots\ldots (1)$$

CaF_2 has very limited solubility. Preflushing near the wellbore with HCl can be the solution to minimize this problem. The reaction products of fluorosilicic acid are typically water soluble, but their potassium, sodium, and calcium salts are partially insoluble.

$$SiF_6^{2-} + 2K^+ \rightarrow K_2SiF_6 \quad \ldots\ldots (2)$$

$$SiF_6^{2-} + 2Na^+ \rightarrow Na_2SiF_6 \quad \ldots\ldots (3)$$

$$SiF_6^{2-} + Ca^{2+} \rightarrow CaSiF_6 \quad \ldots\ldots (4)$$

Therefore, formation water containing calcium chloride, potassium chloride, and sodium chloride should be avoided. Ammonium chloride (NH_4Cl) is considered the only compatible salt solution with HF. As soon as the acid spends and pH rises, ferric hydroxide

forms, $Fe(OH)_3$. The source of ferric iron is from minerals such as chlorite, siderite, hematite, and tubing rust. HF is primarily used to remove clays also capable of dissolving carbonate, feldspars, micas, and quartz. The reaction rate of HF with sand and clays depends on the volume of acid used in sandstone reservoirs to the ratio of the surface area of the rock.

Iron Precipitation Problems

The usual cause of iron precipitation is the formation of insoluble gelatinous ferric hydroxide as the pH rises in spent acid. Ferric hydroxide, $Fe(OH)_{3,}$ is the most damaging iron precipitant following an acid treatment (Smith et al. 1969). Both Fe(II) and Fe(III) can precipitate, but $Fe(OH)_3$ precipitates first from spent acid since it comes out of solution at a pH of 1 (Eq. 5). $Fe(OH)_2$ precipitates at pH values greater than 6, making it less of a problem when acidizing sweet wells because spent acid reaches a pH of only 5.5 (Eq. 6) (Taylor et al. 1999; Crowe 1986).

$$Fe^{+3} + 3OH^- \rightleftharpoons Fe(OH)_3 \,.\, mH_2O \downarrow \text{ Above pH 1} \quad \ldots\ldots(5)$$

$$Fe^{+2} + 2OH^- \rightleftharpoons Fe(OH)_2 \,.\, nH_2O \downarrow \text{ Above pH 6} \quad \ldots\ldots(6)$$

In sandstone acidizing, live acid returns are often observed after the treatment. However, this does not mean that there is no precipitation. Most of the acid around the wellbore does remain unspent; however, a zone of totally spent acid will be formed at the leading edge of the reaction front. In this area, potentially damaging iron (III) precipitation will occur.

Iron compounds that precipitate during acidizing can reduce reservoir permeability near wellbore area. Formation damage from fines and precipitated materials can be difficult to remove in subsequent remediation treatments (Taylor et al. 2001; Garzon et al. 2007).

HCl Application in Acidizing

In carbonate reservoirs, HCl has been comprehensively used as a stand-alone stimulating fluid to decrease skin damage and create optimized wormholes in carbonate reservoirs. Furthermore, carbonate and iron scales are removed by using HCl in strengths of 5 to 15%.

HCl is also used as a preflush for HCl/HF (mud) acid to remove drilling mud and to mitigate clay damage. HCl is used with HF at a strength of 1.5 to 3% (King 1986). The main function of preflush is to remove as much of the calcareous material as possible prior to injection of the mud acid. The preflush helps eliminate calcium fluoride and iron-related impairment problems. Conventionally, 5 wt% to 15 wt% HCl is used for preflush due to its low cost, high dissolving power, and soluble reaction products (Coulter and Jennings 1999). However, when illite and chlorite clays in sandstone are attacked by HCl, amorphous silica gel residue is formed (i.e. the aluminum layer extracted). Therefore, this reaction will weaken the clay structure and make it more sensitive to fluid flow, and, in turn, severe formation damage may occur (Thomas et al. 2001). The rapid and uncontrollable reaction rate between HCl and carbonate at high temperature also limits the penetration of HCl into the formation, especially at a low pumping rate, and can eventually

cause the undesired face dissolution pattern. Moreover, HCl is very corrosive to well tubulars.

HCl also has some other major drawbacks. Firstly, injection of HCl at low rates in stimulating shallow formations may cause face dissolution and potentially collapse weakly consolidated formations. Secondly, a high cost of inhibition is required. According to Tuttle (1987), the corrosion rate largely depends on "the susceptibility of the material under the environmental conditions to which it is exposed". Corrosion problems become more intensified at elevated temperatures, and special additives such as intensifiers are necessary to compensate for the corrosion inhibition loss at high bottom-hole temperatures (BHT) temperatures. The most efficient category of corrosion inhibitors are film-forming amines and their salts. However, they begin to decompose at 482˚F (Schauhoff and Kissel 2000).

The excessive addition of corrosion inhibitors may cause other problems, such as the adsorption of the corrosion inhibitor on the surface of the pay zone, wettability alteration or severe emulsion problems, particularly in low-permeability reservoirs (Schechter 1992). In extreme environments or less corrosion-resistant metallurgy, a higher loading of corrosion inhibitor intensifiers is required. Fluid incompatibility issues can occur when these inhibitors are combined with other additives present in the treatment fluid. Regarding the illitic-sandstone reservoirs, HCl-based fluids are not a viable option as when HCl directly contacts illite, it breaks down, induces fines migration, and results in a sharp decrease of permeability due to clogged formation pores (Mahmoud et al. 2011).

Clay and Mineral Reactions

Clays are layered silicates formed by the erosion and/or disintegration of rocks, caused by the chemical reactions of other rock-forming silicate minerals. The layers are composed of various combinations of two fundamental units:

1. Tetrahedral layers consisting of linked silicon-oxygen tetrahedral **(Fig. 1)**.

2. Octahedral layers in which hydroxyl ions fall in two planes, above and below a plane of magnesium or aluminum ions **(Fig. 2)**.

Sedimentary rocks are composed of clay minerals in the form of crystal packs. They are particularly tiny materials with a maximum dimension of a normal clay particle less than 0.005 mm.

The three main clay minerals in Berea and Bandera sandstone cores are kaolinite, illite, and chlorite. Kaolinite is composed of a two-layer structure, K^+ exchange cation with a negligible base exchange capacity. Kaolinite is a non-swelling clay, but will readily disperse and migrate. Kaolinite has the ability to adsorb water; which is held tightly to the clay surfaces. Conversely, illites are interlayered, thus, possess the poorest characteristics of the dispersible and swellable clays. Furthermore, illites are the most problematic to stabilize. Also, this type of clay can adsorb water, due to concentration imbalances between the ions found at the interchange locations on the clays and the solute content of the fluid in clay contact.

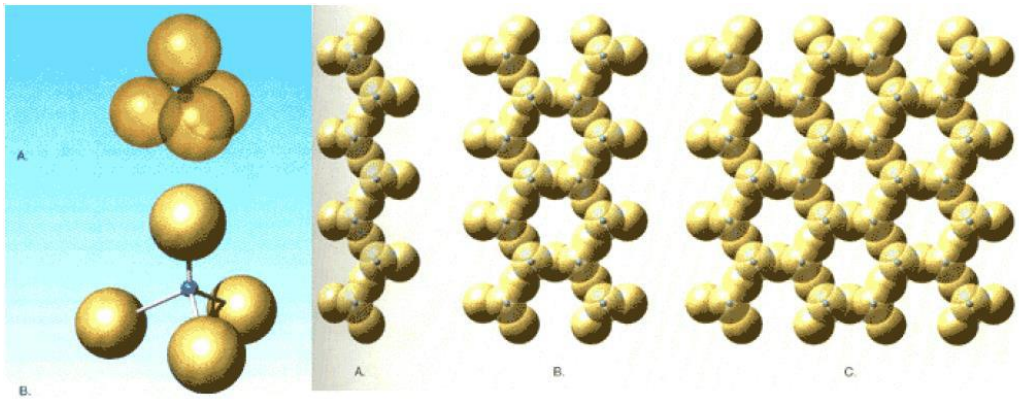

Fig. 1—Structure of the Tetrahedral Layer (geology.uprm.edu 2013).

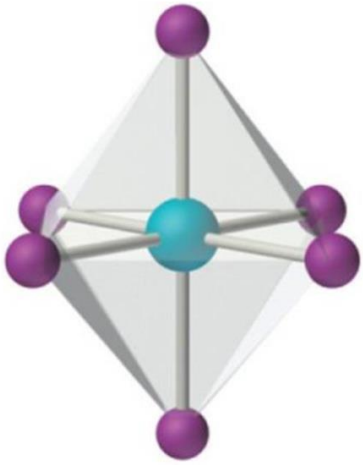

Fig. 2—Structure of the Octahedral Layer (Averill and Eldredge 2012).

Clay Instability

Simon and Anderson (1990) studied the stability of clays in HCl and their temperature limitations. Kalfayan and Metcalf (2000) modified McLeod's work to consider the effect of certain mineral sensitivities such as zeolites and the importance of using higher HCl:HF ratios to avoid precipitations. Walsh et al. (1982) presented guidelines to the minimum HCl requirement to prevent precipitations based on the concentration of HF and the remaining carbonates after the preflush.

Thomas et al. (2001) described that HCl has destabilized illite and chlorite in the investigated cores from producing sandstone formations. The degradation of illite and chlorite contributed to significant core damage.

Decomposition of clay minerals consumes HCl at elevated BHT. To avoid Fe precipitation, HCl acid should be avoided with chlorite content ranging from 0.5-2%. This is because when chlorite contacts HCl, it discharges iron and other clays and feldspars releases sodium or potassium. Silica gel forms, polymerizes, and creates colloidal particles inducing plugging problems. Literature shows that clays react to acetic acid in the same manner as it reacts to fresh water; however, it does not decompose clays. Also, it has been reported that acetic acid encouraged smectite and illite clays to swell. This issue can be solved by the addition of 5% NH_4Cl. This process helps prevent the disintegration and clay swelling after clay ion exchange completion. **Table 1** below shows the stability limit of clays in HCl.

Mineral Type	Temperature, °F
Zeolites	75
Chlorite	125
Illite	150
Smectite	150
Kaolinite	200

Table 1—Stability Limit of Clays in HCl (Coulter and Jennings 1999).

HCl Alternatives

Problems associated with HCl include, but are not limited to, formation damage caused by HCl-sensitive clays (e.g., illite) decomposition, the rapid rate of reaction and corrosion rates associated with high temperatures resulting in reaction products precipitation during secondary, and tertiary reactions. The following efforts have been made to overcome these problems.

Considering these problems, organic acids, such as formic and acetic, are the potentially attractive alternative for a preflush treatment. The advantages of using organic acids are their low corrosivity (Harris 1961) and lower reaction rate with the rock compared to HCl (Chang et al. 2008). However, they have the following limitations: (1) they cannot be used at high acid concentrations because they limit the solubility of their calcium salts. For example, acetic and formic acid are typically used at concentrations less than 13 and 9 wt%, respectively, to avoid precipitation of calcium acetate and calcium formate (Robert and Crowe 2000); (2) organic acids have a low dissociation constant that makes them not react at full capacity; (3) the degree of hydrogen ion generation decreases with increasing temperature (Chatelain et al. 1976; Williams et al. 1979); and (4) Organic acid cost is significantly higher than HCl for an equivalent mass of rock dissolved. In a further attempt to reduce the rate of acid-rock reactions, chelating agents such as EDTA (ethylene diamine tetra-acetic acid), HEDTA (hydroxyl ethylene diaminetriacetic acid), and GLDA (glutamic acid-N, N-diacetic acid) were evaluated. GLDA was found to be compatible with the sandstone mineralogy, having up to 18 wt% illite (Mahmoud et al. 2011). At 300˚F, GLDA, HEDTA, and EDTA were compatible with illitic-sandstone

cores. Moreover, the optimum ratio of GLDA/HF concentration was 20 wt% GLDA/1 wt% HF, giving a major increase in sandstone permeability. Nonetheless, Fernier et al. (2000) found that an EDTA in an acid solution has inadequate solubility at a pH lower than 4, and that EDTA is not typically biodegradable; while NTA has a lower stability constant for Fe and Ca, it was also found to be an animal carcinogen (Fernier et al. 2000; 2001; 2003).

To cope with these drawbacks associated with HCl and organic acids, urea-HCl, which is a new in-situ-generated acid system, is introduced in this study. Urea-HCl has a similar dissolution power compared to regular HCl, but its reaction rate is slower, resulting in deeper acid penetration into the formation before spending. In addition, it is less corrosive to well tubular, and the in-situ production generates NH_4Cl, thereby acting as a clay stabilizer. Finally, both urea and HCl are readily available and affordable.

The aim of this work is to investigate the performance of urea hydrochloride as an alternative to regular HCl in the dissolution of carbonate minerals in sandstone and dolomite cores. Second, to identify the effect of additives on the stimulation of Bandera sandstone cores, and finally to evaluate the effect of temperature on the outcome of the treatment.

Urea

Urea, or carbamide, is an organic compound with the chemical formula of $CO(NH_2)_2$. The urea molecule is composed of two amino ($-NH_2$) groups linked to a carbonyl ($C=O$) functional group. Urea has many distinctive characteristics; it is a white, odorless solid,

with high water solubility, and typically non-toxic when used in minute quantities. It also acts as a buffering medium for acid reactions. Urea has long been used since its synthetic discovery by Friedrich Wöhler in 1828 by treating silver cyanate with ammonium chloride using the following reaction:

$AgNCO + NH_4Cl \rightarrow (NH_2)_2CO + AgCl$ ……………………………..……..…(7)

Furthermore, in the laboratory, urea is formed when phosgene reacts with ammonia as shown by the following reaction:

$COCl_2 + 4\ NH_3 \rightarrow (NH_2)_2CO + 2\ NH_4Cl$ ………………………………....….(8)

The structure and appearance of urea can be seen as follows in **Fig. 3** and **Fig. 4**, respectively:

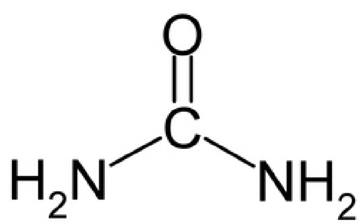

Fig. 3—Structures of Urea.

Fig. 4—Appearance of Urea.

In the oil and gas industry, urea is used to help isolate straight-chain and branched hydrocarbons in petroleum. Additionally, urea is extensively utilized in the production of many plastics and resins. Polyurea, on the other hand, is a unique product used to prevent corrosion and restore damaged surfaces of pipes and pipelines, tanks, and compressors. For industrial purposes, urea is manufactured from synthetic ammonia and carbon dioxide.

The properties of urea are shown in **Table 2**. The decomposition of urea was first presented by Wöhler (1829) and the understanding of its products, by-products, and reaction pathways have been the subject of several studies. The main decomposition products of urea are ammonia (NH_3), isocyanic acid (HNCO), and carbon dioxide (CO_2).

Chemical formula	CH_4N_2O
Molar mass	60.06 g·mol^{-1}
Appearance	White solid
Density at 25˚C (77˚F), 100 kPa	1.32 g/cm^3
Melting point	133 to 135°C (271 to 275°F)
Solubility in water	107.9 g/100 ml (20°C)

Table 2—Properties of Urea in the Urea-HCl solution including chemical formula, molecular weights, density, and solubility constants (Godfrey et al. 1997).

Urea decomposes into ammonium cyanate (Eq.10). Ammonium cyanate decomposes into ammonia and cyanic acid (Eq.11) followed by a second reaction where HNCO is hydrolyzed into carbon dioxide and ammonia (Eq.12).

For dry solid urea,

$$(NH_2)_2CO\ (s) \rightarrow NH_3\ (g) + HNCO\ (g) \quad \text{.....(9)}$$

For urea-water solutions,

$NH_2CONH_2 \rightarrow NH_4^+ + OCN^-$ ……..……...….(10)

Urea ammonium cyanate

$NH_4^+ + OCN^- \rightleftharpoons NH_3 + HOCN$ ……...…...……..... (11)

Ammonium cyanate ammonia Cyanic acid

$HOCN + H_2O + Heat \rightarrow NH_3 + CO_2$ ..... (12)

Cyanic acid water ammonia carbon dioxide

The decomposition reactions for urea are complex and dependent on various conditions such as temperature, heating rate, pressure, open or closed vessel, and mass and heat transfer limitations (Schaber et al. 2004). The following mechanisms are related to intramolecular and intermolecular proton exchange interactions involving both amino groups or the amino and the carbonyl groups (Estiu and Merz 2004).

Urea Hydrochloride

Urea Hydrochloride is an organic salt that hydrolyses in-situ bottomhole, releasing H^+ ions which react with earth-alkaline elements forming in-situ ammonium chloride (NH_4Cl), which acts as a clay stabilizer. Urea Hydrochloride is 71% as strong as HCl acid and twice as strong as phosphoric acid. A further aim of this work is to investigate the performance of the new package of urea-HCl as a comparable system to HCl in dissolving carbonates minerals (calcium and magnesium) in sandstone and carbonate cores and addressing the limitations with HCl including fast reaction rate and corrosion rate. Urea-HCl is given by the following formula CH_5ClN_2O and has a molecular weight of 96.5162 g/mol. The

structure and appearance of urea-HCl can be seen as follows in **Fig. 5** and **Fig. 6**, respectively:

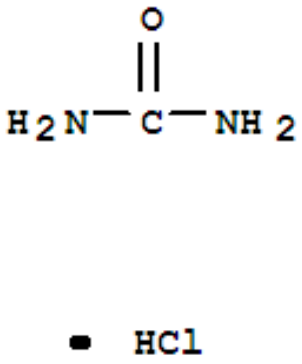

Fig. 5—Structures of Urea-HCl.

Fig. 6—Appearance of Urea-HCl.

Urea hydrochloride can be produced with any desired ratio of urea and HCl. A combination of 1:4 and 4:1 moles of urea with HCl can be formed to fit the desired

purpose. However, a typical ratio is between 0.5 moles of urea with 1 mole of HCl. An ideal composition contains at least roughly 1 mole of urea to one mole of HCl. The mixing of both components results in a slightly exothermic reaction (Sargent et al. 1997).

The molar ratio of the fixing agent (FA): HCl is provided to be 1.7. It is proposed that the adduction between HCl and urea via hydrogen bonding allowed for the dissolution of urea beyond the typical solubility limit. A proposed theory is that FA complexes with the HCl molecules to keep them in solution having higher concentration than 37 wt% (Jiang et al. 2013).

Applications

- Urea-HCl helps eliminate the accumulation of water-insoluble metal salts on surfaces such as Ca, Mg, Ba, Al, Sr, and Be.

- Urea-HCl also provides a method to reduce the solids content of industrial liquids containing water-insoluble metal salts.

- Urea-HCl helps remove carbonate scale from boilers.

- Urea-HCl is an affordable and useful agent in the dissolution of metal salt dispersions or suspensions, especially, calcium carbonate.

- Urea-HCl adjusts pH of dying baths and recreational waters, as well as, acting as a corrosion inhibitor and an anti-scaling agent.

- Urea-HCl can be used in ore reduction, food processing, pickling, industrial acidizing, and general cleaning.

Advantages

- Urea-HCl helps retard reaction rate and proved greater ability to get the acid deeper into the formation before spending.

- The acid is released in-situ; this leads to the reduction of CI loading, and as a result a reduction in the overall cost of the acid job.

- Urea hydrochloride is less corrosive to metal equipment, tubing, and smart completion.

- NH_4Cl is generated in-situ, thereby acting as a clay stabilizer.

- The HCl in the formula forms soluble reaction products so there is a lower chance to form insoluble precipitations.

- There is no need for Fe-control agents as the effluent pH is 0. The effluent samples generated contain live acid.

- Urea-HCl has a lower tendency to discharge hydrogen chloride gas.

- No fluoride leaches into the formulation, therefore, no risk of damaging the formation and creating insoluble precipitates (CaF_2, Na_2SiF_2, and K_2SiF_6).

- Urea-HCl provides the capacity to leave the formation water-wet and clean for optimum oil and gas production/injection.

- Both urea and HCl are readily available and affordable.

- Urea-HCl is environmentally friendly, as urea is biodegradable (93-98%) in a 24-hour cycle.

- The formulation has a pH reduction capability.

- The urea-HCl can act as a preflush before the mud acid treatment.

Hydrolysis of Urea Hydrochloride

According to Walker and Wood (1903), the salts of weak bases (urea) are incompletely disintegrated in aqueous solution into free acid and base, with a greater extent of hydrolysis as the base is weaker. Furthermore, the concentration of the free mineral acid in the aqueous solution is roughly proportional to the rate at which methyl acetate is transformed into methyl alcohol and acetic acid. It is, therefore, plausible to approximate the hydrolysis magnitude of the hydrochloride of the weak base by matching the rate at which a certain solution of methyl acetate is catalyzed under its impact with the rate at which the methyl acetate is catalyzed by a comparable solution of pure HCl. The rate of catalysis of methyl acetate by regular HCl was 0.00315; the rate of catalysis by regular urea hydrochloride under similar conditions was 0.00174. A standard solution of urea hydrochloride comprises less than half the quantity of urea hydrochloride. Consequently,

about 55% of the whole formulation is decomposed by water into free urea and HCl. The range of 77 to 104˚F (20 - 40˚C), has no effect on the hydrolysis of urea Hydrochloride. Moreover, the addition of NaCl slightly decreased the hydrolysis rate. The following equations propose the possible hydrolysis of urea-HCl in water.

$(NH_2)_2CO\ (s) + HCl \rightarrow NH_2CONH_3^+ .Cl^-$ ……..... (13)

$NH_2CONH_3^+ .Cl^- + H_2O \rightarrow (NH_2)_2CO + H_3O^+ + Cl^-$ ……..……...**.**(14)

The second suggested mechanism is advocated by Shaw and Bordeaux (1995) by employing the method of initial rates. Earlier works presented by Walker and Hambly (1895); Werner (1918, 1920); and Warner (1942) have studied the reaction of urea decomposition in the presence of acids and bases. The reaction of HCl with urea hydrochloride was found not to be catalyzed by the acid. Several of the works mentioned above agreed that ammonium cyanate is an intermediate in the decomposition of urea in aqueous solution.

The Nessler technique allowed the measurement of ammonium ion concentrations that corresponded to urea conversion to reaction products. The technique of initial rates was applied (i.e., $\Delta u / \Delta t$ can be set equal to du/dt, where u is the urea concentration and t is time). Product-time curves were generated and were found linear for all temperatures. In the reaction of water only; however, the curves displayed some departure from linearity. The effect was amplified with increasing urea conversion.

In acid, a rapid quantitative conversion of the cyanate ion to ammonium ion occurs and is shown in (Eq.18). If insufficient acid is available, it does not go to completion. However, if there is adequate acid, the cyanate ion is quantitatively converted to

ammonium ion. Cyanate forms ammonium ions, which in turn dissociate, releasing H^+ ions shown by (Eq. 19). This closed loop retards the rate of reaction as H^+ ions circulate between both reactions, allowing fewer available ions at any given time to attack the carbonate surface. This reaction, on the other hand, might not go to completion under certain conditions. But, the reaction is complete at room temperature in sufficiently concentrated acid solution, even though it is extremely slow. At pH of 1.4, the E_o for the reaction in the presence of acid is the same as in water alone, which is equivalent to 30.9 Kcal, the frequency factor corresponds to $5*10^{13}$ sec^{-1}. According to Warner (1942), the constant in acid has a slight tendency to be higher than that in water. Werner (1918, 1920) established the structure of urea in aqueous solution as **I** shown in (Eq. 16).

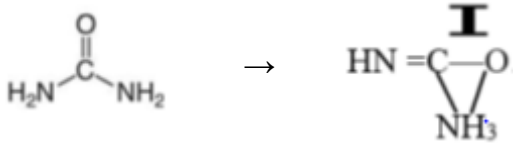

……..…...(15)

I $\xrightarrow{K_1}$ $HNCO + NH_3$. ……..……..(16)

$HNCO + NH_3 \rightarrow NH_4^+ + CNO^-$. ……..……(17)

$CNO^- + 2H^+ + 2H_2O \rightarrow NH_4^+ + H_2CO_3$. ……...…….…...…(18)

$NH_4^+ \rightarrow NH_3 + H^+$. ……...….(19)

$H^+ + CaCO_3 \rightleftharpoons Ca^{2+} + HCO_3^-$. …….(20)

$H_2CO_3 + CaCO_3 \rightleftharpoons Ca^{2+} + 2HCO_3^-$. ……(21)

$H_2O + CaCO_3 \rightleftharpoons Ca^{2+} + HCO_3^- + OH^-$. ……..….(22)

The reaction was observed to be a first order reaction with respect to urea over a wide range of concentration. This is displayed by Eq. 23:

Rate = $-\frac{du}{dt} = k_1.[u\ ]^1$ ……..…….…….……...….....(23)

$k_1 = k_o e^{-Ea/RT}$ …….…….....(24)

E_o= 30.9 Kcal

R= 1.986 Cal $mol^{-1}K^{-1}$

K_o= 5* 10^{13} @ 80˚C =176˚F=353 K

K= $5*10^{13}*\exp\left[\frac{-30.9*1000}{1.98*353}\right]$

The first-order rate constant was calculated based on data gathered by Warner (1942) using the Arrhenius (Eq. 24) and was found to be K= $3.15*10^{-16}$ sec^{-1}.

HCl in high-pressure/high-temperature (HP/HT) wells is problematic because of its rapid reactivity, resulting in face dissolution, corrosion, and associated increased inhibition costs. Moreover, HCl can attack clays in sandstone including illite, kaolinite, and chlorite forming amorphous silica gel, weaken the clay structure, and finally cause fine migration. To answer these challenges, the effectiveness of a new in-situ-generated HCl acid that will provide slower reaction rates and lower corrosion rates in high-temperature reservoirs will be investigated. The experimental techniques used in this study will be describes in the following chapter.

CHAPTER II

EXPERIMENTAL METHODS

The experimental techniques used in this study involved coreflooding experiment at 250 and 300˚F, Computed Tomography (CT) scan to see the porosity profile comparison in sandstone cores and wormhole propagation in carbonated cores, Inductively Coupled Plasma (ICP) to analyzed key cations in the core effluent samples. Furthermore density, pH, equivalent acid concentration of the core effluent samples were measured. Finally, Scanning Electron Microscope and Energy Dispersive X-Ray Spectrometer (SEM-EDS) were used to determine the nature of precipitates formed in the core effluent samples.

Materials

Three different types of cores were used in conducting the experiments: Grey Berea sandstone, Bandera sandstone, and Silurian dolomite. All the received cores were 1.5 in. diameter and 6 in. length. Concentrated hydrochloric acid solutions (36.46%) were obtained from Macron Fine Chemicals™ while 30 wt% urea-HCl and all the additives including corrosion inhibitor, non-emulsifier, intensifier, and iron-control agent were provided by a local service company. The brine used for all the experiments was 5 wt% KCl. The deionized water used throughout the experiments was obtained from a purification water system with a resistivity of 18.2 MΩ.cm at room temperature.

Treatment Fluid Characteristics

Acid treatment additives and characteristics are shown in **Table 3** and **Table 4**, respectively.

Composition	Concentration
Corrosion inhibitor	0.6 vol%
Non-emulsifier	3 gpt
Intensifier	4 vol%
Iron control agent	8 gpt

Table 3—Acid Treatment Additives.

Composition	Density, g/cm^3	Viscosity, cP	Equivalent HCl concentration, wt%	pH
30 wt% Urea-HCl	1.13	1.83	16.89	0
30 wt% Urea-HCl + additives	1.14	1.92	19.54	0
15 wt% HCl + additives	1.082	1.30	18.76	0

Table 4—Characteristics of Treatment Fluids Measured at 75°F.

Core Preparation

All types of the cores were oven-dried at 220˚F overnight. After that, the dry weight of each core was measured. The cores were then saturated with 5 wt% KCl under a vacuum pump for four hours, and the saturated cores were weighed to calculate the pore volume of each one. The difference between the dry weight and the weight of the saturated cores divided by the density of the brine used in the experiments was used to calculate the porosity of the cores (Eq. 25):

$$V_p = \frac{W_{wet} - W_{dry}}{\rho}$$,……..……..…(25)

where:

V_p = pore volume, cm^3,

W_{wet} = saturated volume, g,

W_{dry} = dry weight. G, and

P = brine density, g/cm^3.

Permeability was calculated from the stabilized pressure drop before and after the acid treatment at high temperature (250˚F and 300˚F) by injecting a 5 wt% KCl brine. Darcy's equation for the laminar flow was used for the permeability calculation (Eq. 26).

$$k = 122.8 \frac{qL\mu}{\Delta p\, d^2}$$,……...……(26)

where:

k = permeability, mD,

L = core length, inch,

d = core diameter. Inch,

q = flow rate, cm^3/min,

μ = dynamic viscosity, cp, and

Δp = pressure drop across the core, psia.

Coreflood

Fig. 7 shows the coreflood setup used in the experiments. A back pressure of 1200 psi was applied to all experiments to keep the CO_2, resulting from carbonate dissolution in solution. The overburden pressure applied was approximately 1500 psi. A low-pressure transducer of the range 0-300 psi was used for all experiments. A pressure transducer was linked to a computer to measure the pressure drop across the core during the whole set of experiments. The pressure drop across the core was plotted against time using the LabVIEW™ software. A Teledyne ISCO D500 precision syringe pump, having a maximum allowable pressure of 2000 psi, was used to inject the acid treatment into the core. The pressure drop across the samples was automatically recorded with time while injecting the treatment.

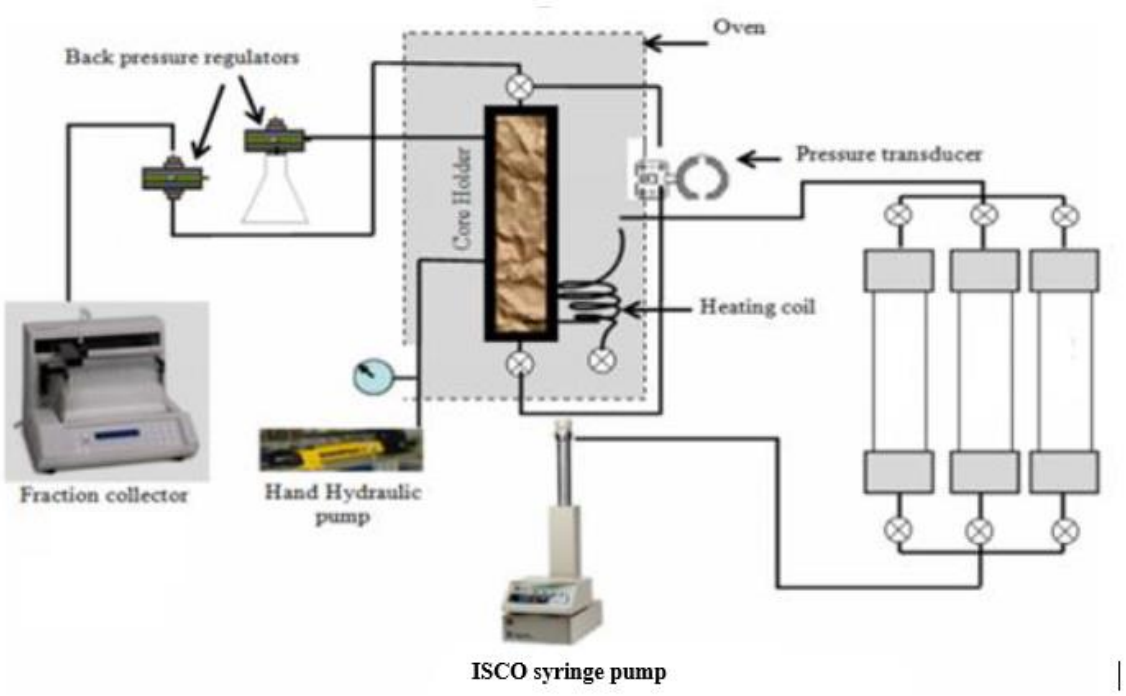

Fig. 7—A Schematic Diagram of the Coreflood Apparatus.

CT Scan

Computed tomography (CT) scanning is considered one of the best tools to pinpoint the damage in sandstone cores with high precision (Bartko et al. 1995)

CT scans were conducted on the cores before and after the treatment in both dry and saturated conditions to monitor changes in core porosity. The relationship between the CT number and the porosity can be described as follows (Eq. 27, Izgec et al. 2005):

$$Porosity = \frac{CT_{wt} - CT_{ar}}{CT_w - CT_a}, \quad \text{.....(27)}$$

where:

CT_{wt} is the CT number of the water-saturated rock,

CT_{ar} is the CT number of the air-saturated rock,

CT_w is the CT number of water = 0, and

CT_a is the CT number of air = -1,000.

The CT scanner was used to get CT numbers and generate porosity profiles for the sandstone cores utilized in the coreflood experiments. The cores were CT-scanned dried and then saturated with its inlet direction facing the entrance of the scanner. For the dolomite cores, CT scan was used to visualize wormhole propagation along the cores.

X-Ray Diffraction (XRD)

D8 DISCOVER, displayed in **Fig. 8,** is an analytical technique used to determine the atomic and molecular crystal structure of the sample, in which the crystalline atoms cause a beam of incident X-rays to diffract into various specific directions. A crystallographer can emit a 3D image of the electron density within the crystal by measuring the angles and

intensities of these diffracted beams. XRD specimens mechanically crushed to fine powder and put in a concave sample base. Clay-size portion samples are separated from the bulk sample on a glass slide. XRD provides semi-quantitative information on the relative abundance of bulk and clay minerals present in the samples examined. These percentages are crucial to effective stimulation treatment design.

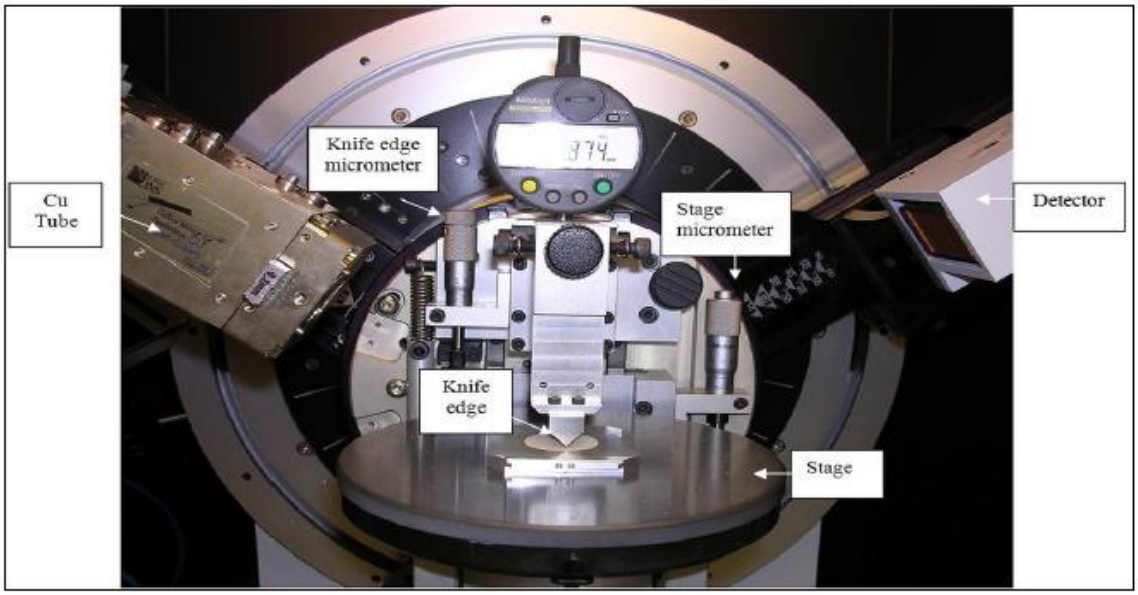

Fig. 8—X-ray Diffraction Device.

Inductively Coupled Plasma Optical Emission Spectrometry (ICP-OES)

Optical emission spectroscopy (OES) uses quantifiable measurement of the optical emission from excited atoms to measure cation concentration. Those atoms dissolved in solution are aspirated into the excitation region where they are dissolved and atomized by a plasma. Electrons can either be in their stable state or excited when they are given energy. Cation concentration is measured in the excited state. A photon of light is emitted

when an electron falls from its excited state to its ground state. Each element has a distinctive set of wavelengths that it can emit. A schematic is given in **Fig. 9.**

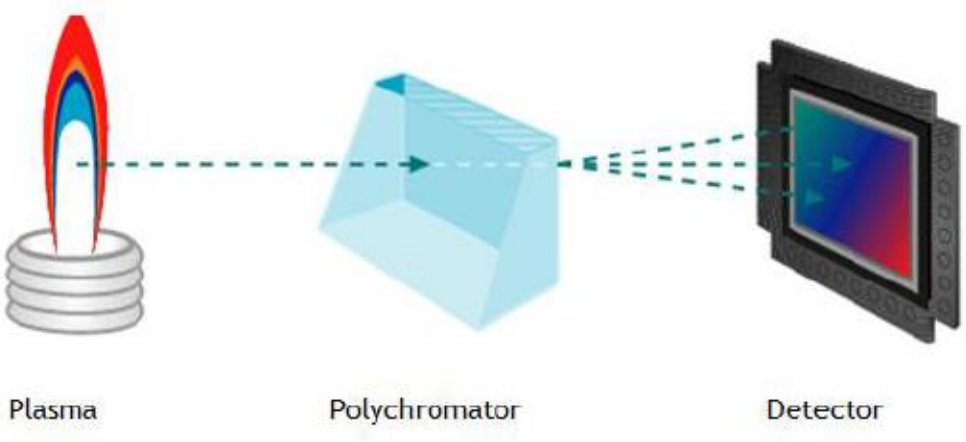

Fig. 9—An Illustration of ICP Theory.

An Optima 7000 ICP-OES Spectrometer was utilized in this research to investigate the core effluent samples collected for the iron, magnesium, silicon, aluminum, calcium and potassium concentrations.

Auto Titrator

The acid titration is based on the volumetric method for determining the acid concentration. The Titrando titrators from Metrohm utilized in this study is shown in **Fig. 10**. An auxiliary reagent (NaOH) of an identified concentration (1M and 5M) is applied to the pre-dose volume of titrant (acid solution). The auxiliary reagent was automatically added to the solution until it reaches equilibrium (pH = 7). Then the volume of the reagent

of a known molarity will be used for molarity calculations. The effluent sample acid concentrations is calculated using the flowing equation:

$M_{acid} \times V_{acid} = M_{base} \times V_{base}$, ……..(28)

where:

M_{acid} is the acid molarity,

V_{acid} is the acid volume,

M_{base} is the base molarity, and

V_{base} is the base volume.

Fig. 10—Auto-Titrator Device.

Viscosity and Density Measurements

The dynamic viscosity was measured at room temperature using an Ubbelohde capillary viscometer. The treatment fluid was poured into the capillary tube of the 0C type

viscometer. The viscosity timings were recorded by using a stopwatch. The viscosity was calculated by multiplying the timing in seconds with the constant value, C, of 0.003. The viscosity measured was then multiplied by the density of the treatment fluid to obtain the absolute viscosity.

The faster it takes for the fluid to pass between the two marks on the capillary tube, the lower the viscosity of the fluid. The kinematic viscosity is the proportion of the dynamic viscosity μ to the density of the fluid ρ. Kinematic viscosity was calculated using (Eq. 29):

$$\mathcal{V} = \mu \times \rho, \quad \text{.....(29)}$$

The density of both HCl and urea-HCl was measured at room temperature using the DMA 35 portable density meter.

SEM-EDS

A scanning electron microscope (SEM) is a type of electron microscope that produces images of a sample by scanning it with a focused beam of electrons. The electrons in the beam interact with electrons in the sample, producing various signals that can be detected and that contain information about the sample's surface topography and composition. SEM can achieve resolution better than a nanometer.

CHAPTER III

RESULTS AND DISCUSSION

To cope with the limitations from regular HCl in a preflush stage of sandstone acidizing, a new in-situ-generated acid system, i.e. urea-HCl, was introduced in this study due to its slower reaction rate resulting in deeper acid penetration into the formation before spending. Moreover, urea-HCl provides a similar dissolution power as HCl and less corrosive to well tubulars. In addition, in-situ generated NH_4Cl acts as a clay stabilizer, and both urea and HCl are readily available and affordable.

The acid injection rate for each coreflood experiment was fixed at 1 cm^3/min, and the temperature of 250 and 300°F was tested on two types of sandstone (Grey Berea and Bandera) and Silurian dolomite. The coreflood results were compared based on the final to initial permeability ratio. The effluent samples were collected after 0.5 PV of acid injection and every after 0.25 PV until the end of the coreflood experiment. After 5 PV of acid was injected, the flow was switched back to brine. The brine injection was stopped based on two scenarios:

1) The pressure drop stabilized, or

2) The effluent samples were colorless.

The effluent samples were diluted at 1,000 times for Grey Berea sandstone, 2,000 times for Bandera sandstone, and 5,000 times for Silurian dolomite to make sure that the concentration of each cation was below 30 mg/l. These samples were analyzed using inductively coupled plasma (ICP) using an Optima 7000 DV ICP-OES system and WinLab 32™ software. Ca, Mg, Al, Si, Fe and K cations were analyzed in the effluent

samples of sandstone corefloods, while only Ca, Mg and K cations were analyzed in the effluent samples of carbonate corefloods.

In sandstone cores, the CT scan technique was performed before and after the treatment in both dry and saturated conditions to determine their porosity profile before and after the treatment. For Silurian dolomite, the cores were scanned after the treatment to visualize wormhole propagation along the cores.

XRD was performed on both Grey Berea and Bandera sandstone, and on the Silurian dolomite cores to determine their carbonate and clay contents. Fluid analysis including density, pH measurements, and equivalent acid concentration for the coreflood effluent samples was carried out to study the reaction of urea-HCl with Grey Berea, Bandera sandstone, and Silurian dolomite cores.

Coreflood Studies

Coreflood experiments were run to further investigate the complex action of urea-HCl. The equipment was chosen to cover a range of experimental conditions, including the operating temperatures of the coreflood system and the temperature range for urea's decomposition. To ensure inert conditions, argon and nitrogen were used.

In this chapter, the performance of urea-HCl compared to regular HCl is discussed. Moreover, the effect of temperature and additives in the acidizing treatments were studied. Five sets of coreflood experiments were conducted on 6 in core Grey Berea Bandera sandstone, and Silurian dolomite up to 300˚F. The first set of experiments was performed with 30 wt% urea-HCl solutions with the addition of the four types of additives were used to study the effect of acidizing on each lithology. In the second set of experiments, 15 wt%

HCl solutions with the same additives were used. Results from this set of experiments were used as a base case to compare with urea-HCl performance at 250˚F. The third set of experiments involved the injection of 30 wt% urea-HCl with some additives modification on Bandera sandstone cores. The first experiment in this set included the increment of the corrosion inhibitor concentration, while the second experiment included the addition of silica inhibitor. This set of results represented the effect of additives on the stimulation of Bandera sandstone cores. In the fourth set of experiments, 30 wt% urea-HCl solutions with the same additives were injected into Grey Berea sandstone, Bandera sandstone, and Silurian dolomite cores to study the effect of acidizing on each lithology at 300°F. This set of experiments revealed the influence of temperature on the stimulation results. The fifth and last set of experiments involved the injection of 15 wt% HCl with the same additives into the cores at 300°F. This set of results was used to compare with the treatment by urea-HCl at 300°F.

All of the received cores were dried in the oven at 220˚F overnight, and the dry weights of the cores were measured. After that, all the cores were saturated with 5 wt% KCl brine using a vacuum pump for four hours and the saturated cores were weighed to calculate the pore volume of each core.

Initially, 5 wt% KCl brine was injected using the coreflood system in the production direction, while heating up the system to the desired temperature, and the pressure drop across the core was plotted against time using the LabVIEW™ software. The initial permeability was calculated using Darcy's equation when the pressure drop stabilized. The pressure drop then increased as the flow was switched from brine to acid

in the injection direction since the acid generally has a higher viscosity compared to 5 wt% KCl. After 5 PV of acid had been injected, the flow was switched back to brine. The brine was injected in the injection direction for 2 PV, and then it was switched to the production direction. The injection continued until the pressure drop stabilized and the effluent samples were colorless. As a result, final permeability can be determined from the stabilized pressure. This procedure was repeatedly done for all sets of experiments.

First Set of Experiments: 30 wt% Urea-HCl including Four Additives -250˚F at 1 cm^3/min.

For this set of experiments, Grey Berea sandstone, Bandera sandstone and Silurian dolomite cores were used. A flow rate of 1 cm^3/min was used throughout the total of six tests at 250˚F. 5 wt% KCl brine and 5 PV of treatment fluid were injected in the injection direction. The effluent samples from the coreflood experiments were collected after half PV of acid injection and every quarter PV until the end of experiment.

Grey Berea Sandstone (G-6-22) at 250˚F using Urea-HCl with Four Additives

Regarding the pressure drop profile of Grey Berea sandstone (G-6-22) in **Fig. 11**. The stabilized pressure drop after the treatment was lower than the stabilized pressure drop before the treatment. This can imply the enhancement in permeability resulted from the dissolution of the carbonate minerals in sandstone, which will be confirmed from Ca and Mg ions dissolved as shown in the next section. The calculated final permeability increased **159%** from the initial permeability.

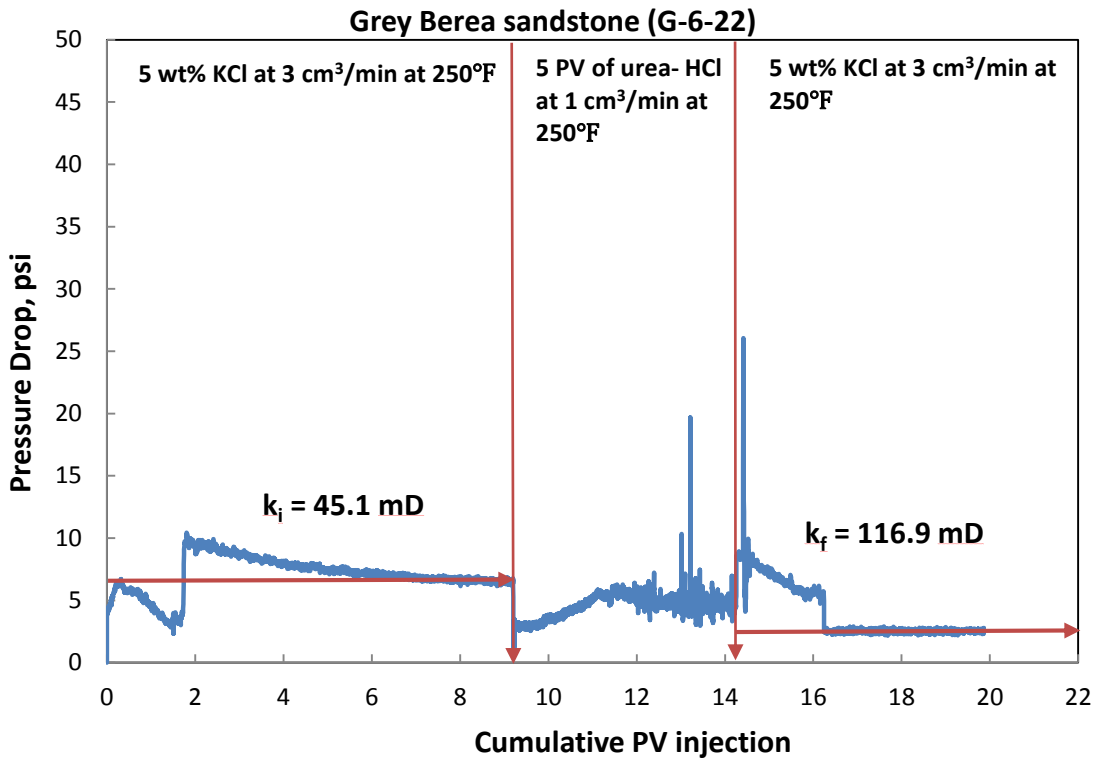

Fig. 11—Pressure Drop Profile Along the Berea-G-6-22 at 250°F (urea-HCl + 4 additives).

Some precipitates were observed in the effluent samples after 2.25 PV (pH = 3.32) acid injection **(Fig. 12)**. According to ICP results, high iron concentration (45,000 ppm) was observed in the core effluent samples **(Fig. 13)**. The high iron concentration was attributed to the dissolution of chlorite and illite clays in the sandstone, which was confirmed to exist in Berea-G-6-22 by XRD technique **(Fig. 14)**. The calcium and magnesium concentrations also increased after 2.25 PV of treatment confirming the dissolution by urea-HCl. Al^{3+} and Si^{4+} were present due to the dissolution of kaolinite and feldspars. K^{+} concentration from 5 wt% KCl brine also decreased during the reaction

interval of acid with the core. The injection face, production face, and side view of Berea-G-6-22 after acid treatment were shown in **Fig. 15**.

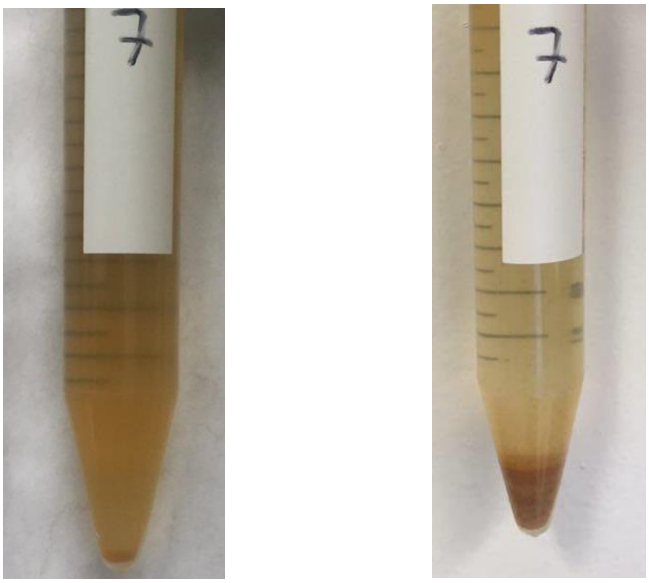

During coreflood **After 4 days**

Fig. 12—Precipitates from Effluent Samples of Berea-G-6-22.

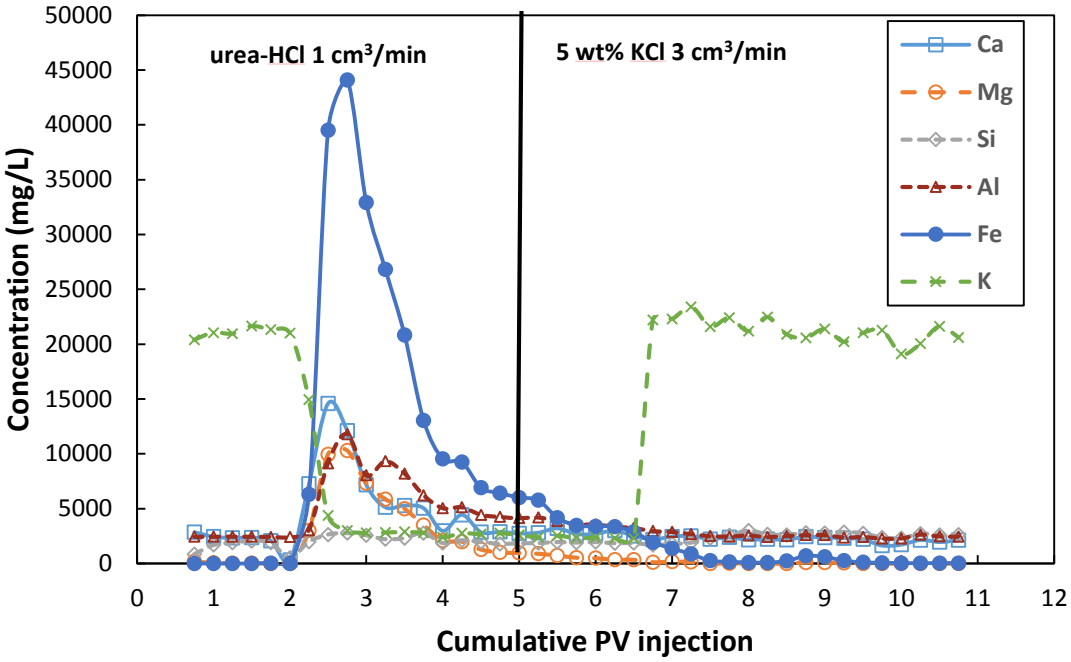

Fig. 13—ICP Analysis of 30 wt% Urea-HCl with Berea-G-6-22 at 250˚F.

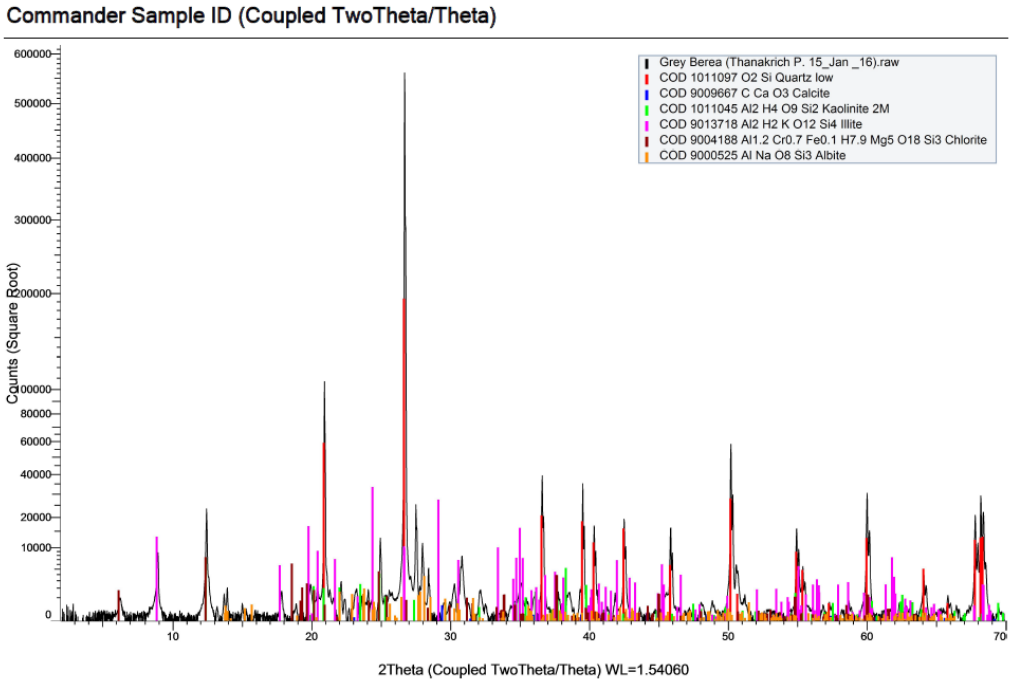

Fig. 14—Grey Berea XRD results.

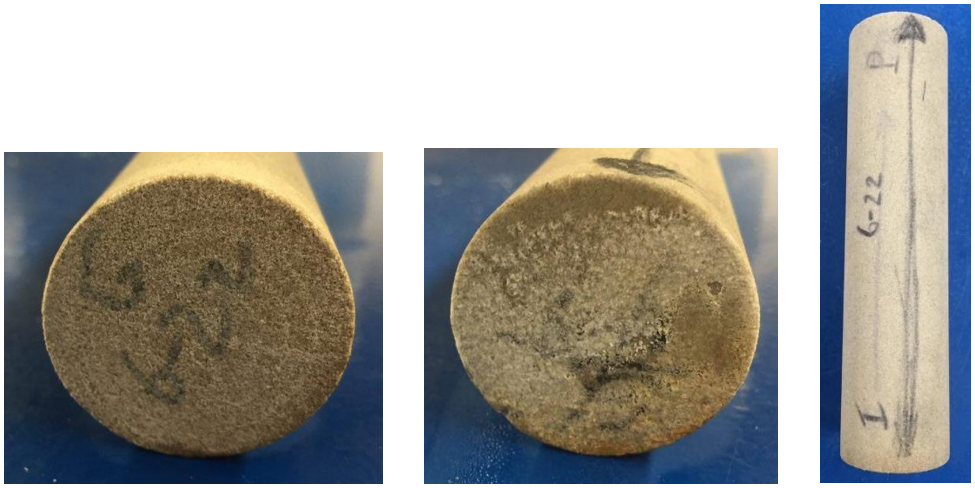

Fig. 15—Injection Face, Production Face, and Side View of Berea-G-6-22 After Acid Treatment.

The initial pH of the effluent samples containing 5 wt% KCl brine was approximately 8. The pH sharply decreased as the acid was injected to reach a pH of 0 (**Fig. 16**). This indicated that the effluent samples contained live acid and not all of the acid was spent to dissolve the carbonate minerals in the Grey Berea core. Subsequently, the pH rose as the core was flushed with brine.

The density of injected brine is around 1.029 g/cc. When the 5 PV of treatment fluid was injected, the density started to increase (after 2 PV injection) as the acid dissolved more Ca, Mg, Al, Si, and Fe. As the live acid became spent acid, less H^+ ions reacted with the carbonates resulting in fewer cations dissolution. Consequently, a gradual decrease in density was observed. When the flow was switched back to brine, the density returned back to its original value (**Fig. 16**).

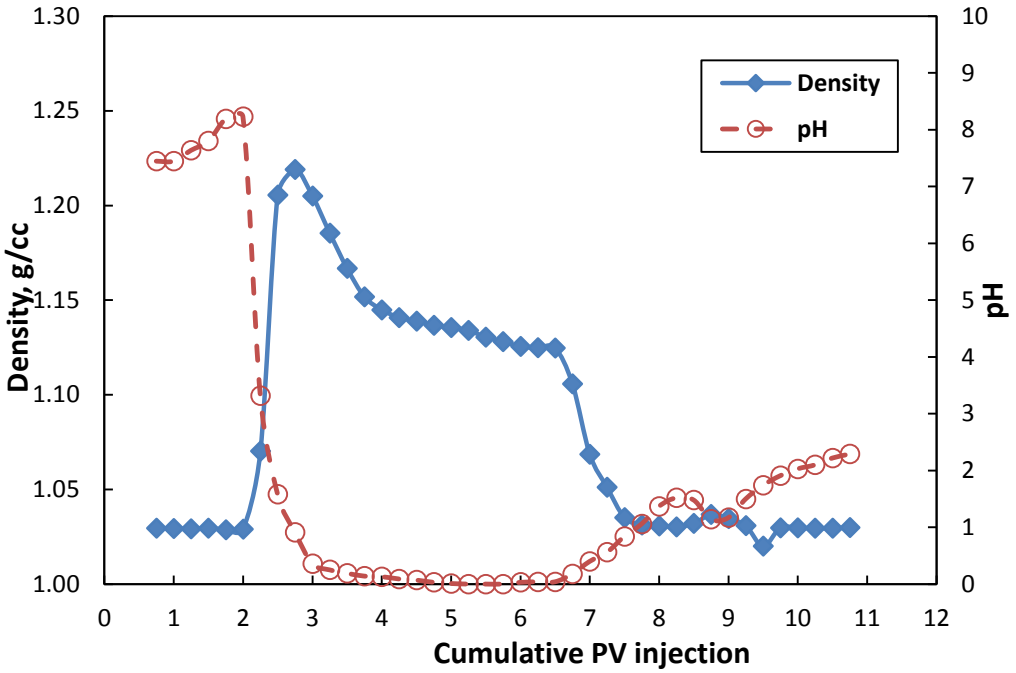

Fig. 16—Density and pH of Effluent Samples from Berea-G-6-22 at 250˚F.

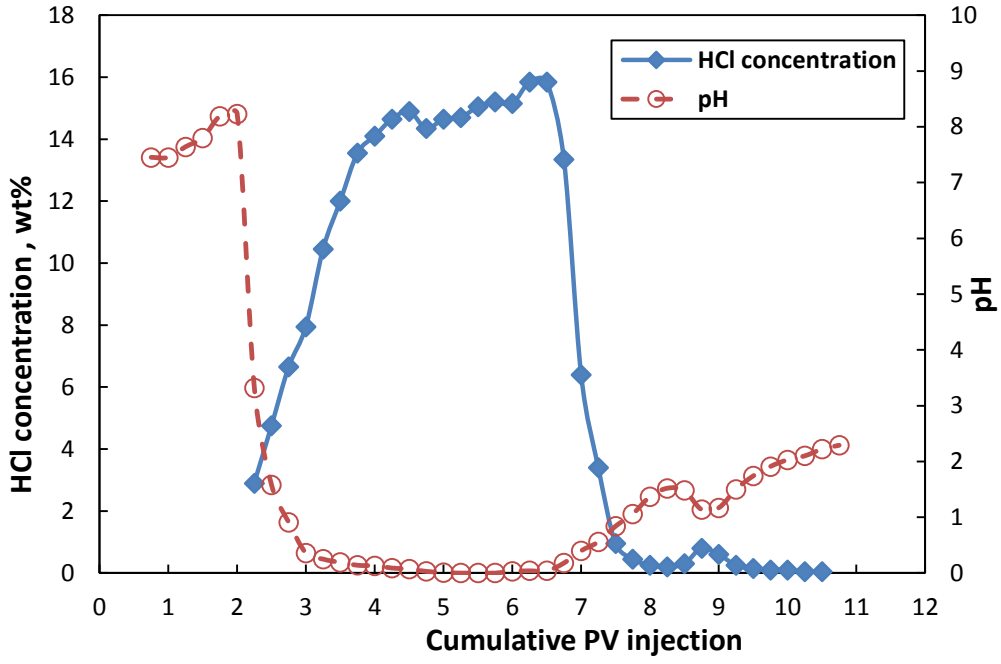

Fig. 17—HCl Concentration and pH of Effluent Samples from Berea-G-6-22 at 250˚F.

The titration was conducted to measure the equivalence of HCl in the effluent samples collected during the coreflood. The equivalent HCl concentration of the effluent samples of Grey Berea (G-6-22) increased sharply after 2 PV of acid was injected to the maximum value around 15.85 wt% HCl **(Fig. 17),** which was close to the equivalent HCl concentration of 30 wt% urea-HCl plus additives (19.54 %). After the flow had been switched back from acid to brine, HCl concentration decreased after around 2 PV of brine injection to 0 wt% HCl. This confirmed that all the acid was pushed out by the brine. These results were also consistent with the pH results (i.e. the higher acid concentration, the lower the pH value). High spent acid concentration suggests that lower live acid concentration can be used for cost-saving purposes.

CT scans were conducted on the Grey Berea core (G-6-22) before and after the treatment in both dry and saturated conditions to monitor change in core porosity. The results indicated an increase in the core porosity after the treatment, which meant the core was stimulated as the carbonate minerals were dissolved by the acid which was confirmed by the previous ICP results. The porosity profile **(Fig. 18)** showed significant improvement in porosity along the core after the treatment, especially the distance near the injection face.

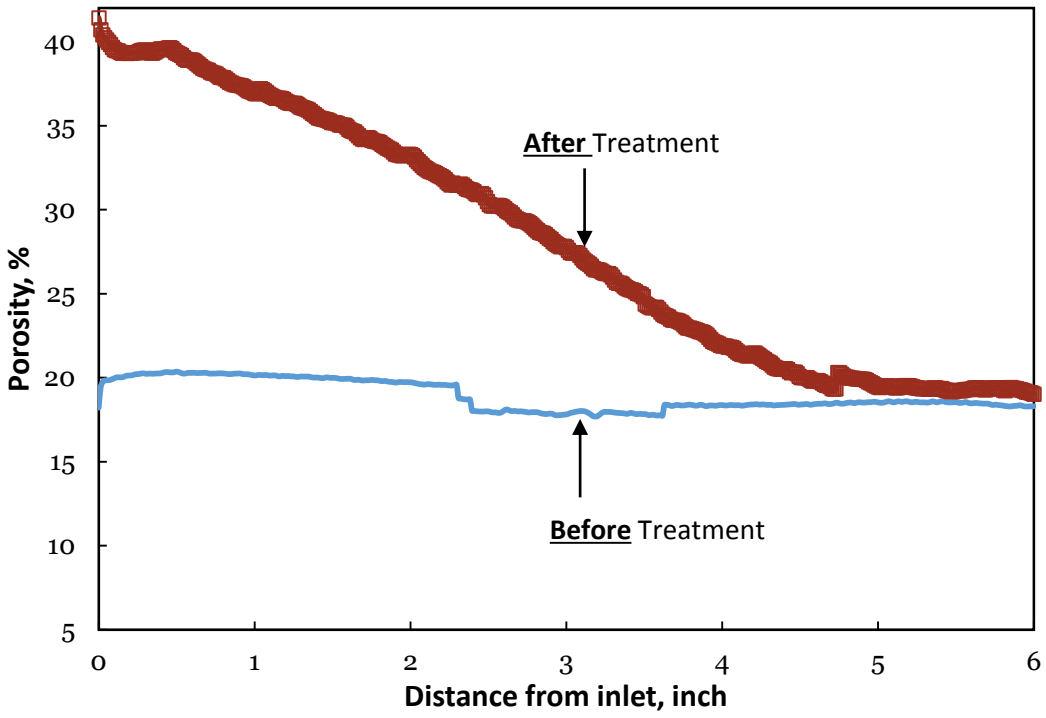

Fig. 18—Porosity Profile Before and after 30 wt% Urea-HCl Treatment for Berea-G-6-22.

Bandera Sandstone (BG-6-12) at 250˚F using Urea-HCl with Four Additives

According to the pressure drop profile of Bandera sandstone (BG-6-12) in **Fig. 19**. The stabilized pressure drop after the treatment was lower than the stabilized pressure drop before the treatment implying the enhancement in permeability from the dissolution of the carbonate minerals in sandstone. The calculated final permeability increased **72%** from the initial permeability.

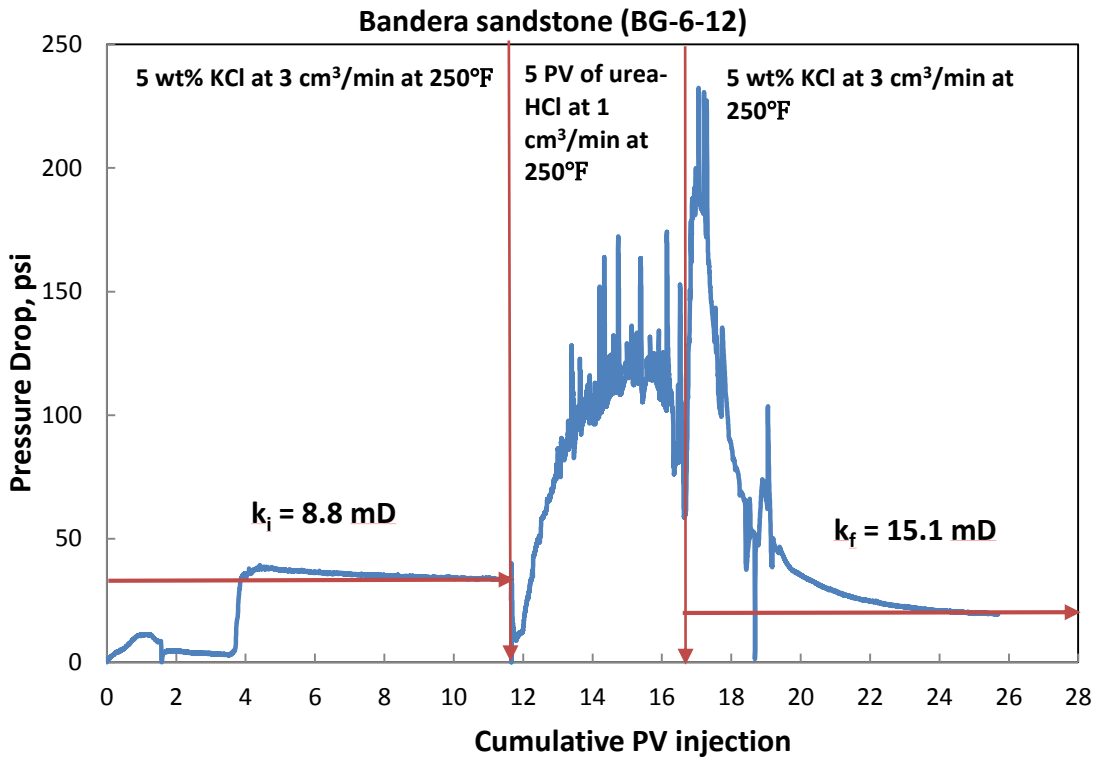

Fig. 19—Pressure Drop Profile Along the Bandera-BG-6-12 at 250˚F.

Some suspension and precipitates were also observed in the effluent samples after 1.25 PV (pH = 6.23) acid injection **(Fig. 20)**. According to ICP results, high iron concentration (40,000 ppm) was detected in the effluent samples **(Fig. 21)**. The high iron concentration was attributed to the dissolution of chlorite and illite clays in the sandstone which was confirmed to exist in Bandera-BG-6-12 by XRD technique **(Fig. 22)**. The calcium and magnesium concentrations also increased after 1.75 PV of treatment confirming the dissolution by urea-HCl. Al^{3+} and Si^{4+} were present due to the dissolution of kaolinite and feldspars. K^{+} concentration from 5 wt% KCl brine also decreased during the reaction interval of acid with the core. The injection face, production face and side

view of Bandera-BG-6-12 after acid treatment were shown in **Fig. 23.** The precipitates from effluent samples no. 6 to 10 were combined for SEM-EDS analysis. The samples were filtered through filter paper and clean with deionized water. After that they were dried in the oven at 60˚C overnight before performing SEM analysis **(Fig. 24).** The SEM images showed crystallization and could be divided into to two main parts which are flaky part **(Fig. 25)** and granular part **(Fig. 26)**. The EDS results in atomic percentage indicated mainly Fe, O, and Ca for flaky part **(Table 5)**. While, mainly Fe, O, and Ca were found in granular part **(Table 6)**. No amorphous part was found in the SEM sample which suggested no fines migration.

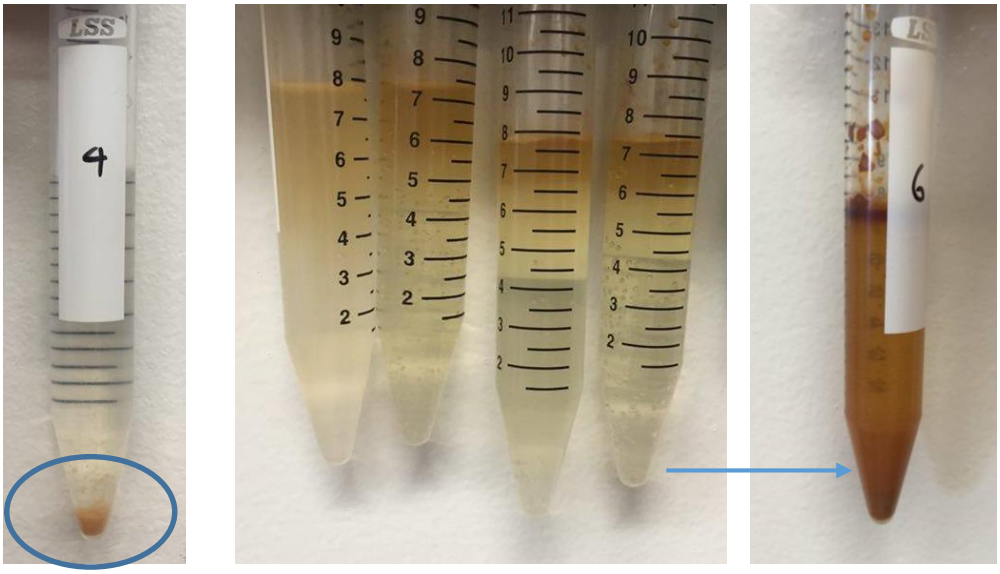

Fig. 20—Suspension and Precipitates of Bandera-BG-6-12.

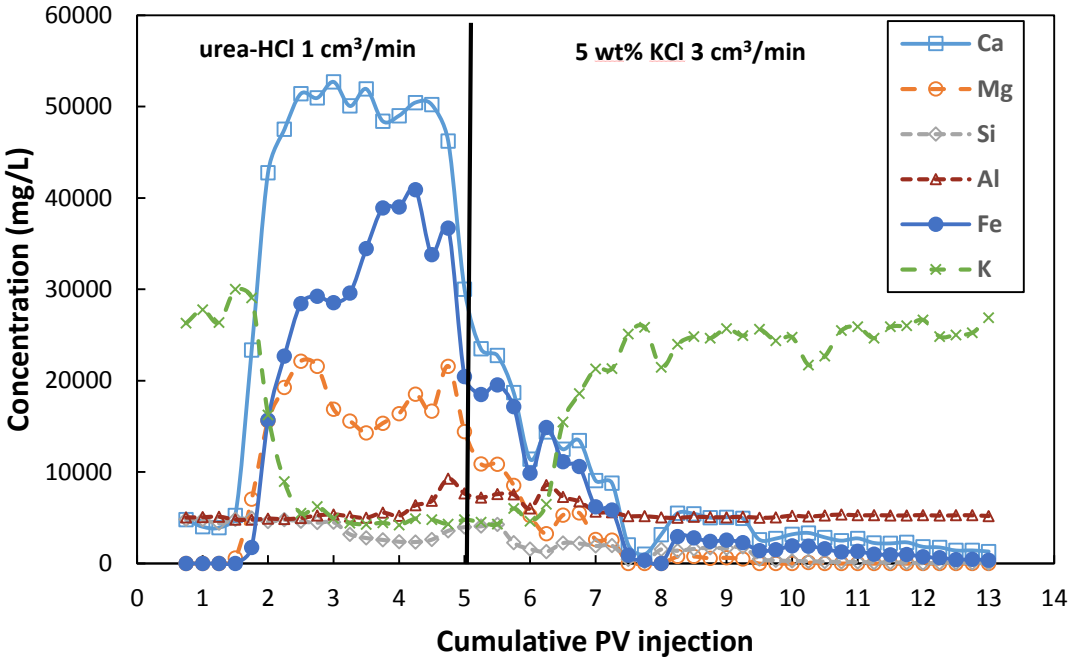

Fig. 21—ICP Analysis of the Effluent Samples- 30 wt% Urea-HCl with Bandera-BG-6-12 at 250˚F.

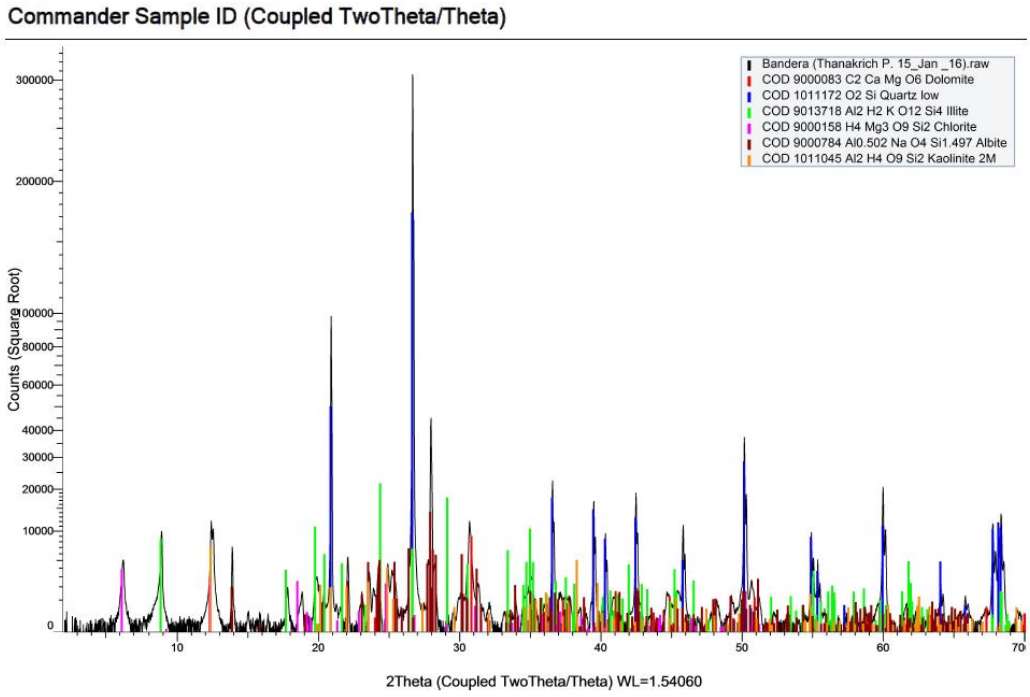

Fig. 22—Bandera XRD results.

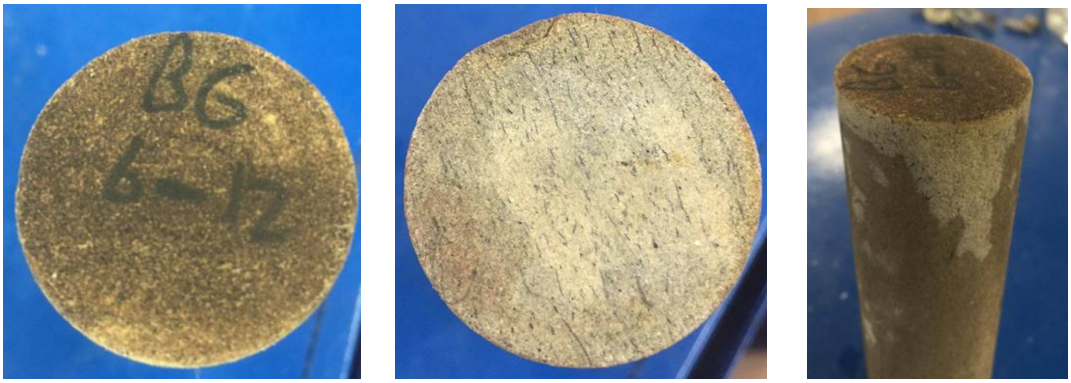

Fig. 23—Injection Face, Production Face, and Side View of Bandera-BG-6-12 After Acid Treatment.

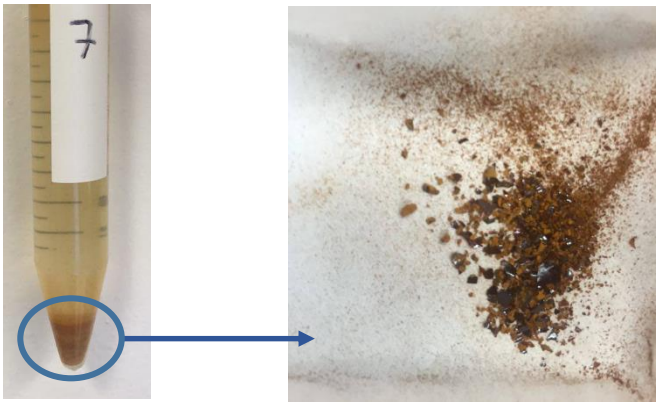

Fig. 24—Precipitates from BG-6-12 Effluent Samples.

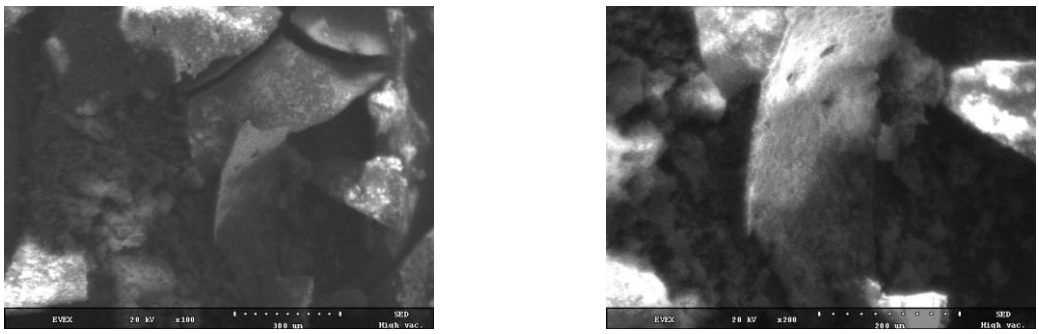

Magnification x100 **Magnification x200**

Fig. 25—SEM Images for BG-6-12 Precipitates (Flaky part).

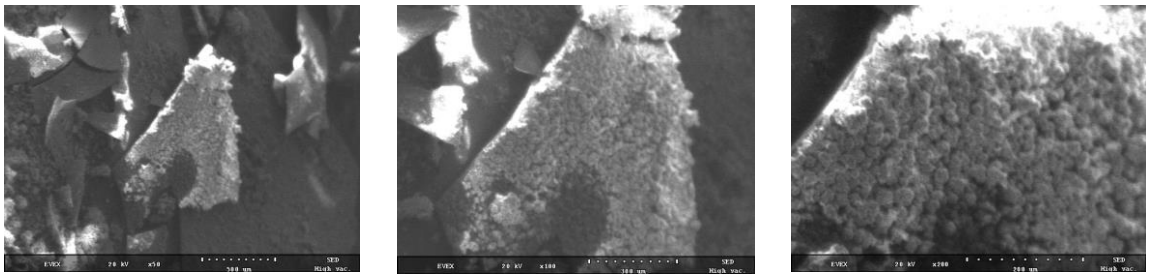

Magnification x500 **Magnification x100** **Magnification x200**

Fig. 26—SEM Images for BG-6-12 Precipitates (Granular part).

Element	Atomic (%)
Ca	17.27
O	71.24
Fe	10.49
Al	0.58
Cl	0.42

Table 5—EDS Results for Flaky Part of BG-6-12 Precipitates.

Element	Atomic (%)
Ca	29.5
O	56.42
Fe	10.44
Al	1.91
Au	1.35
Cl	0.28

Table 6—EDS Results for Granular Part of BG-6-12 Precipitates.

The initial pH of the effluent samples containing 5 wt% KCl brine was approximately 7. The pH sharply decreased as the acid was injected to reach the lowest pH of 0.11 **(Fig. 27)**. This indicated that the effluent samples contained live acid and not all of the acid was spent to dissolve the carbonate minerals in the core. Thereafter, the pH rose as the core was flushed with brine.

The density of injected brine is around 1.029 g/cc. When the 5 PV of treatment fluid was injected, the density started to increase (after 1.5 PV injection) as the acid dissolved more Ca, Mg, Si, Al, and Fe, which was consistent with the ICP results. As the live acid became spent acid, fewer H^+ ions reacted with the carbonates resulting in less cation dissolution. Consequently, a gradual decrease in density was observed. When the flow was switched back to brine, the density returned to its original value **(Fig. 27)**.

The HCl concentration increased sharply after 4 PV of treatment fluid injection to the maximum value around 9.5 wt% HCl **(Fig. 28)**. After the flow had been switched back from acid treatment to brine, HCl concentration decreased significantly after around 1.5 PV of brine injection to 0.4 wt% HCl. This confirmed that most of the acid were pushed out by the brine. High spent acid concentration suggested that lower live acid concentration can be used for cost saving purposes.

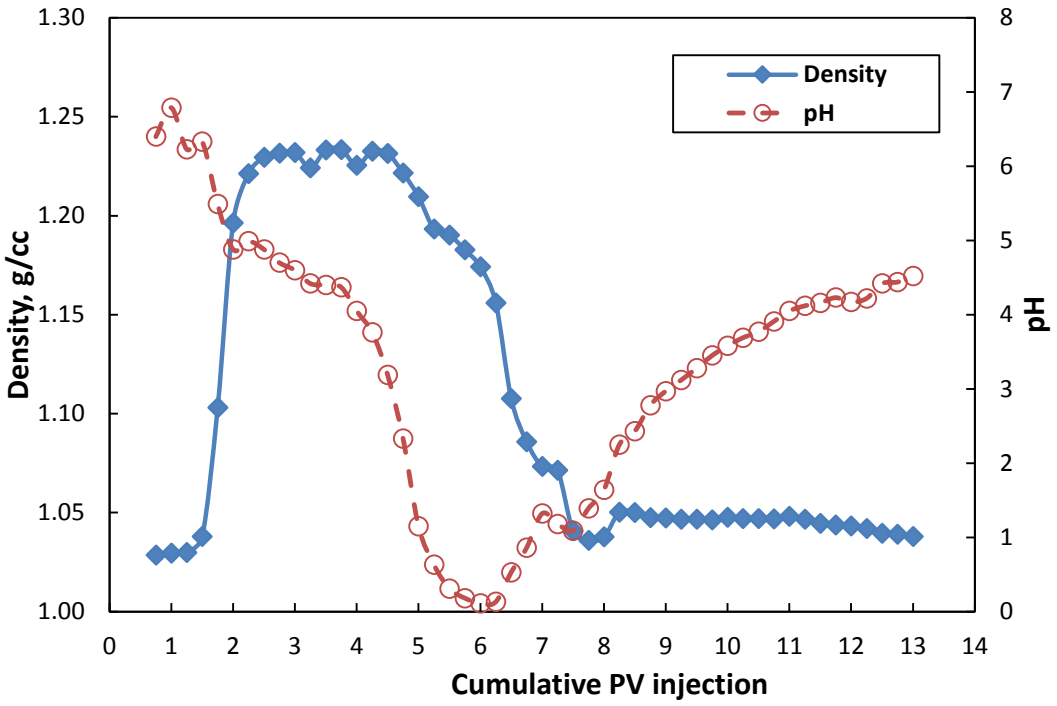

Fig. 27—Density and pH of Effluent Samples from Bandera-BG-6-12 at 250˚F.

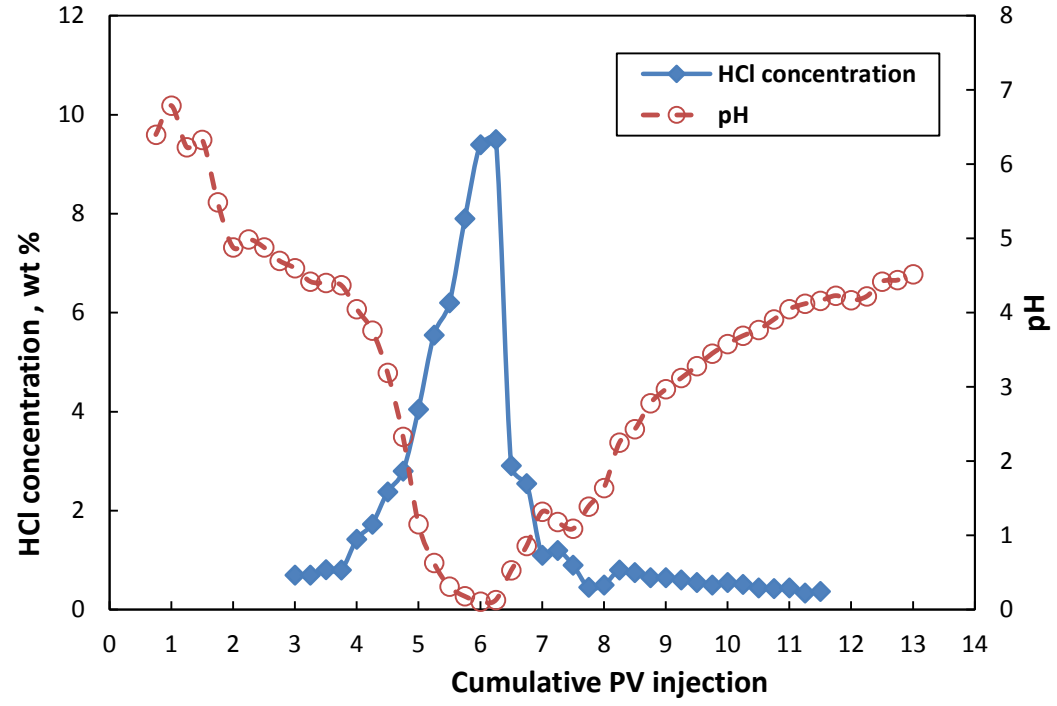

Fig. 28—HCl Concentration of Effluent Samples from Bandera-BG-6-12 at 250˚F.

CT scan results illustrated an increase in the core porosity after the treatment, which meant the core was stimulated as the carbonate minerals were dissolved by the urea-HCl which was confirmed by the previous ICP results. The porosity profile **(Fig. 29)** showed an improvement of porosity all the entire core.

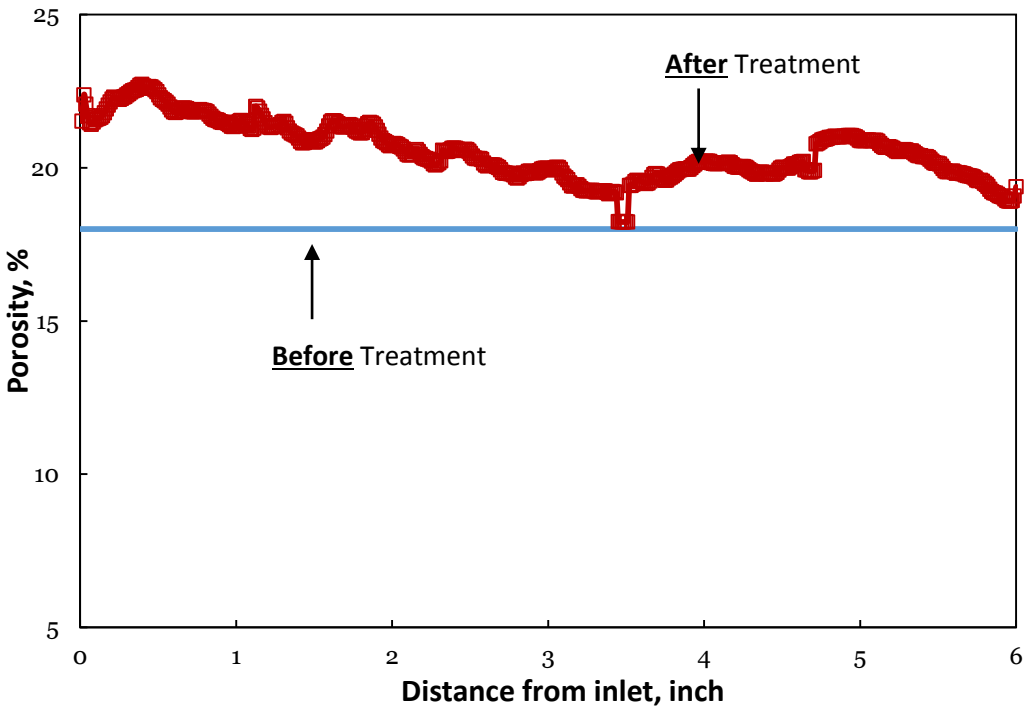

Fig. 29—Porosity Profile Before and After 30 wt% Urea-HCl Treatment for Bandera-BG-6-12.

Silurian Dolomite (SD-6-40) at 250˚F using Urea-HCl with Four Additives

At the beginning of the experiment, 5 wt% KCl brine was injected in the production direction while heating up the system to 250°F until the pressure drop was stabilized. The pressure drop then increased as the flow was switched from brine to acid in injection direction since the acid has a higher viscosity compared to 5 wt% KCl **(Fig. 30)**. After 3

PV of treatment, the pressure drop decreased to almost zero psi which signified acid breakthrough via the wormhole created by urea-HCl.

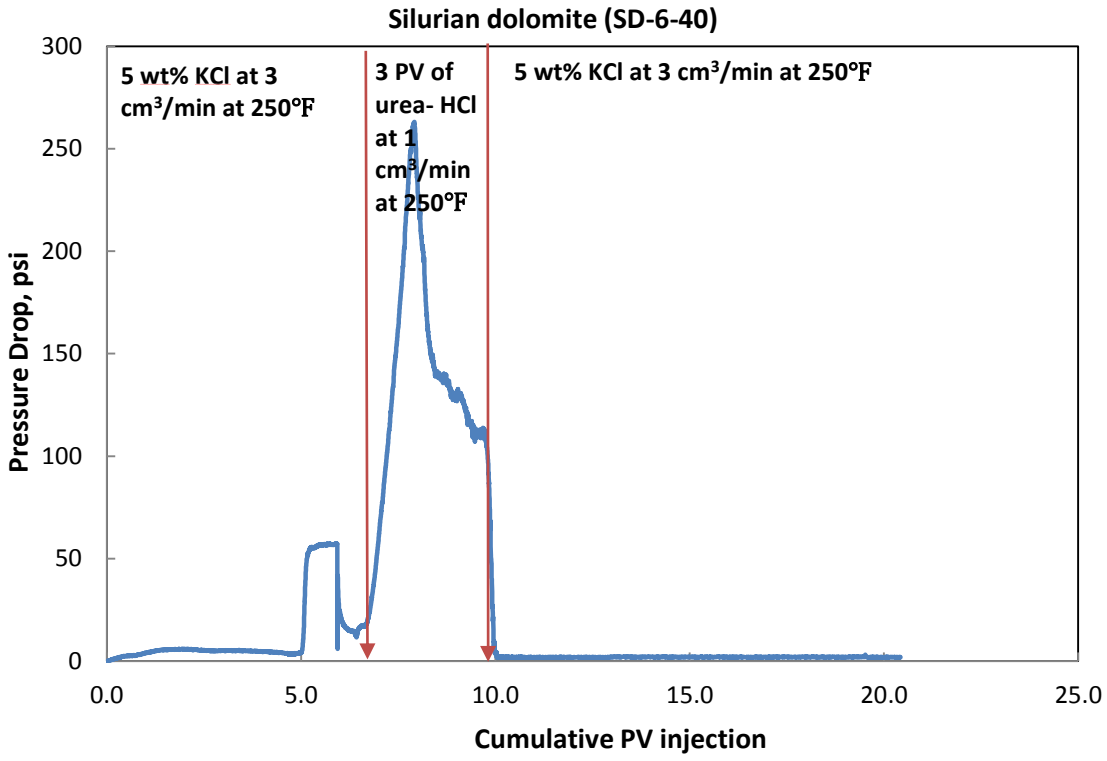

Fig. 30—Pressure Drop Profile Along the Silurian Dolomite SD-6-40 at 250°F.

Some suspension and precipitates from the dolomite dissolution were observed in the effluent samples after 2.25 PV (pH = 6.34) acid injection **(Fig. 31)**. The calcium and magnesium concentration from ICP **(Fig. 32)** also increased after 2.25 PV of treatment confirming the dissolution of dolomite by urea-HCl, which was consistent with the XRD techniques **(Fig. 33).** K^+ concentration from 5 wt% KCl brine also decreased during the

reaction interval of acid with the core. **Fig. 34** shows injection face, production face and side view of SD-6-40 after acid treatment.

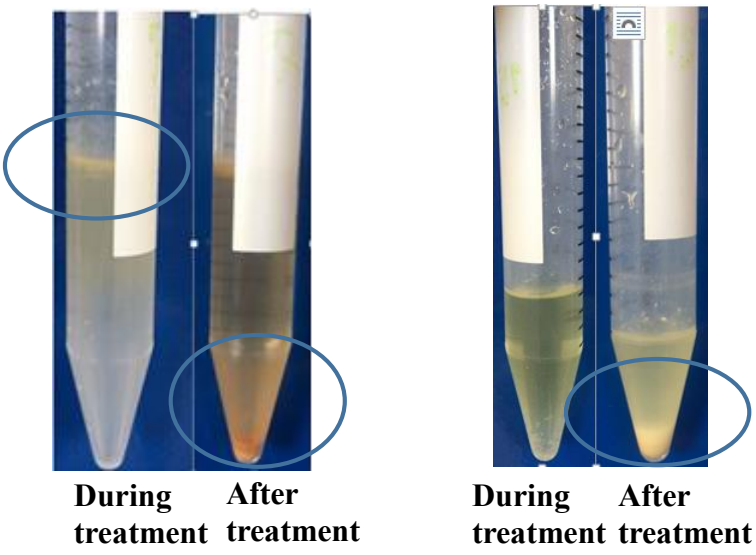

Fig. 31—Suspension and Precipitates of Silurian Dolomite SD-6-40.

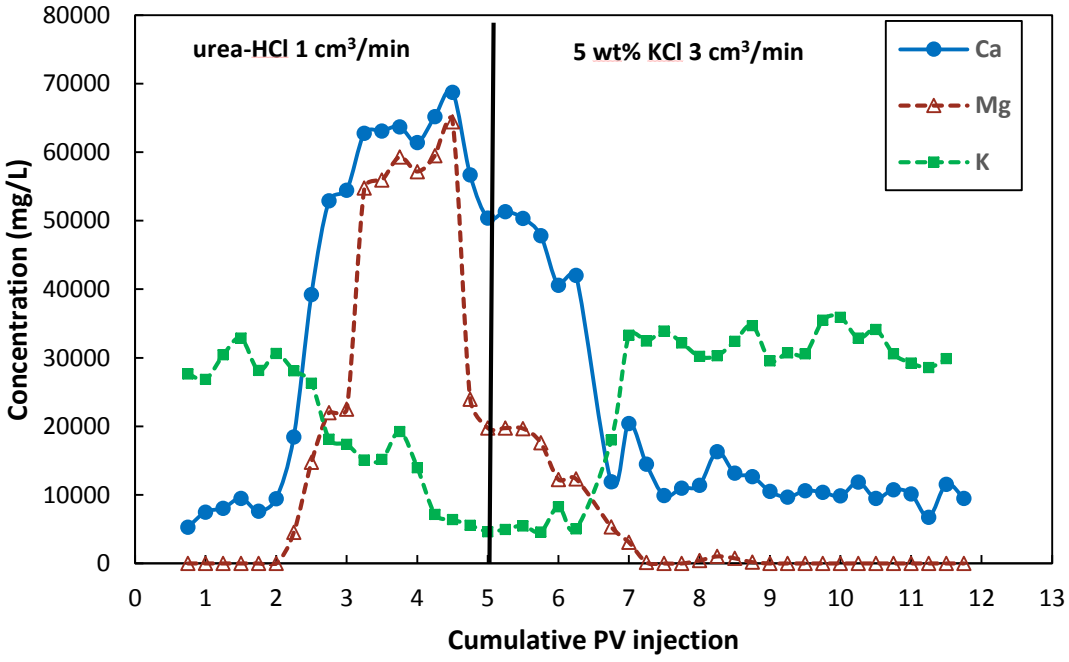

Fig. 32—ICP Analysis of the Effluent Samples- 30 wt% Urea-HCl with Silurian Dolomite SD-6-40 at 250˚F.

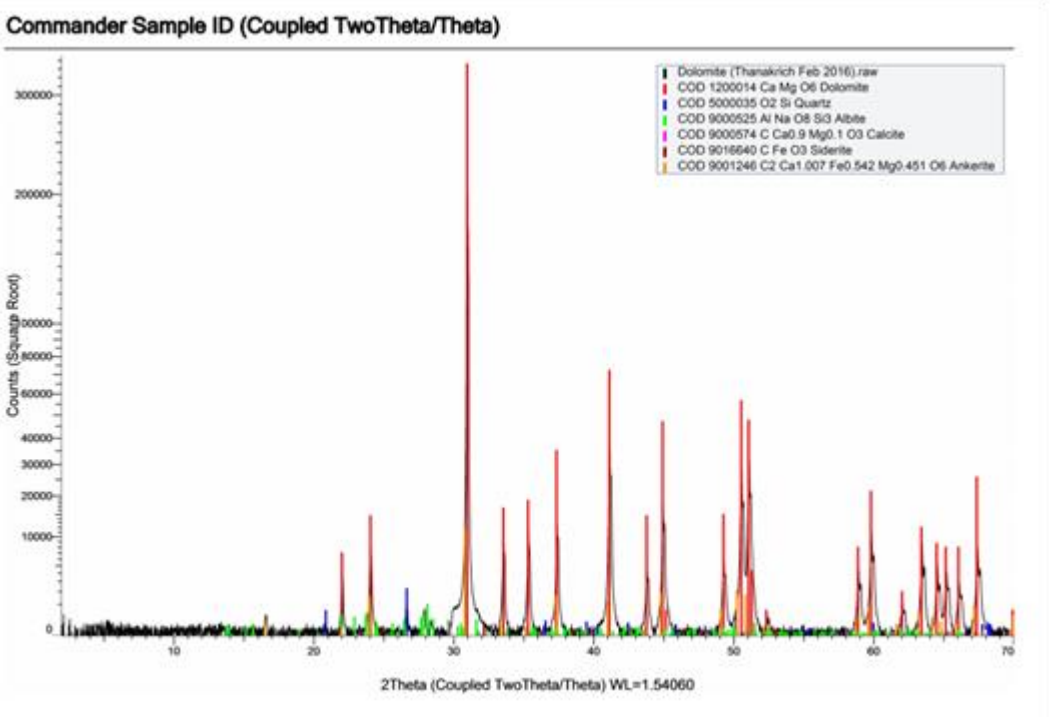

Fig. 33—Silurian Dolomite XRD results.

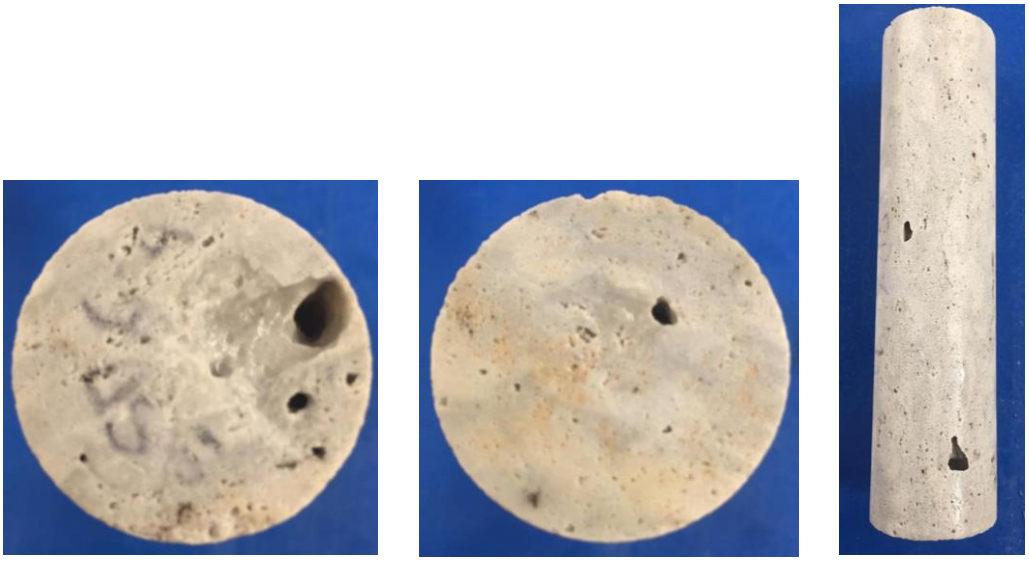

Fig. 34—Injection Face, Production Face, and Side View of Silurian Dolomite-SD-6-40 After Acid Treatment.

The initial pH of the effluent samples containing 5 wt% KCl brine was approximately 7. The pH sharply decreased as the acid was injected to reach the lowest pH of 0 **(Fig. 35).** This indicated that the effluent samples contained live acid and not all of the acid was spent to dissolve the carbonate minerals in the core. Subsequently, the pH rose as the core was flushed with brine.

The density of injected brine was around 1.029 g/cc. When the 3 PV of treatment fluid was injected, the density started to increase (after 2 PV injection) as the acid dissolved more Ca and Mg which was consistent with the ICP results. As the live acid became spent acid, less H^+ ions reacted with the carbonates resulting in less cation dissolution. Consequently, a gradual decrease in density was observed. When the flow was switched back to brine, the density returned to its original value **(Fig. 35).**

The titration was conducted to measure the equivalence of HCl in the effluent samples collected during the coreflood. The HCl concentration increased sharply after 4.5 PV of acid was injected to the maximum value around 10.6 wt% HCl **(Fig. 36)**. After the flow had been switched back from acid treatment to brine, HCl concentration decreased significantly after around 3.5 PV of brine injection to 0.4 wt% HCl. This confirmed that most of the acid were pushed out by the brine.

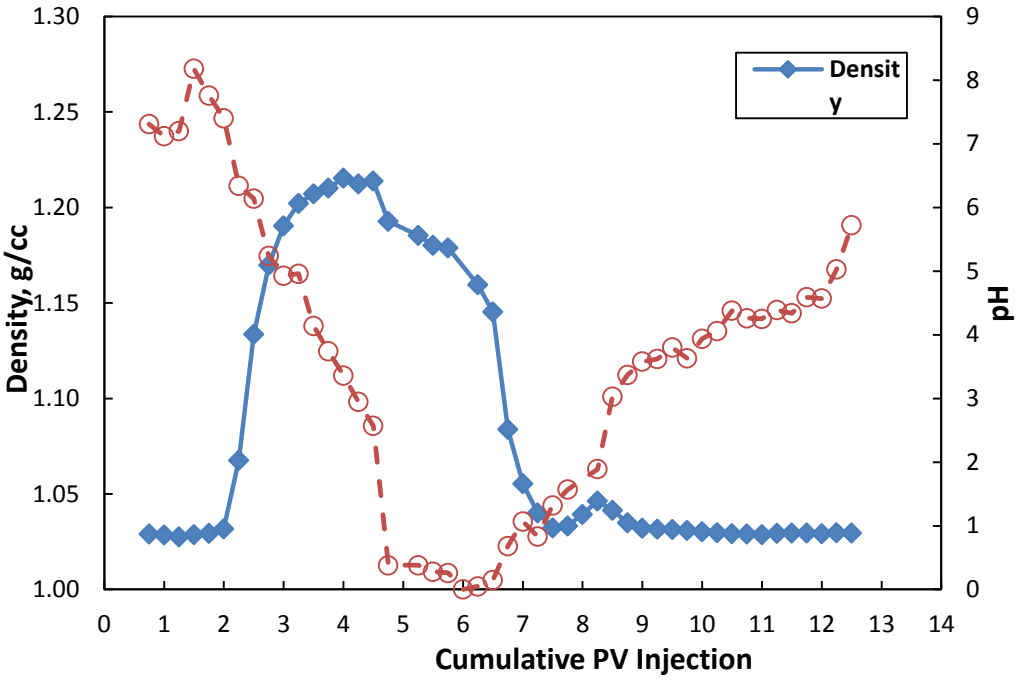

Fig. 35—Density and pH of Effluent samples from Silurian Dolomite SD-6-40 at 250˚F.

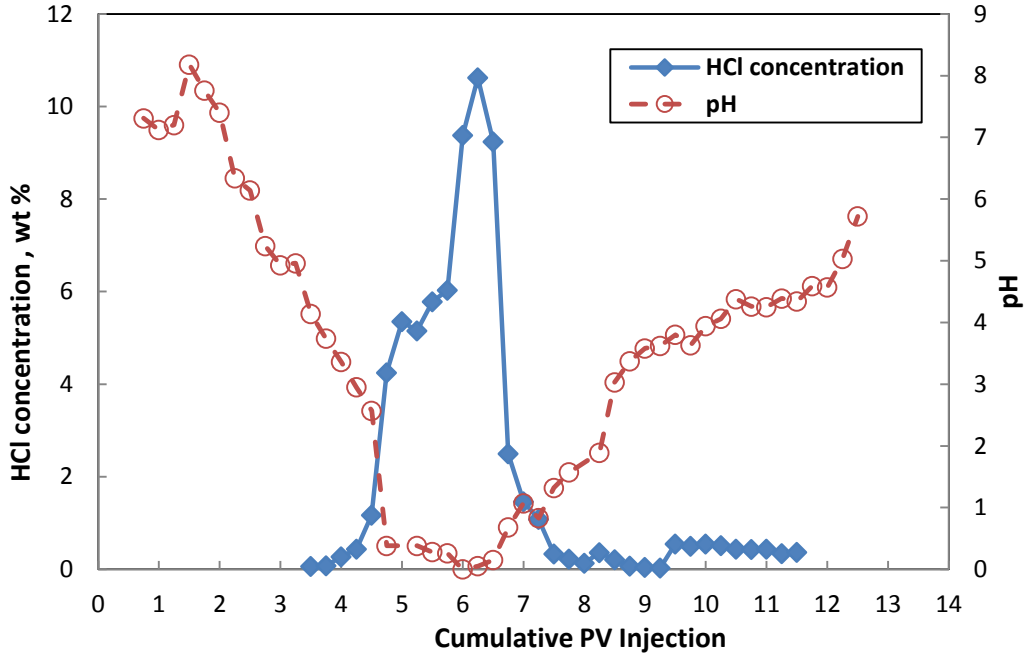

Fig. 36—HCl Concentration of Effluent Samples from Silurian Dolomite SD-6-40 at 250˚F.

Moreover, CT scans were conducted on the core after the treatment to visualize the wormhole propagation. The CT scan **(Fig. 37)** result showed the formation of one main wormhole along the core. No washout was observed at the injection face which was the major benefit of using urea-HCl as a treatment fluid compared to conventional HCl.

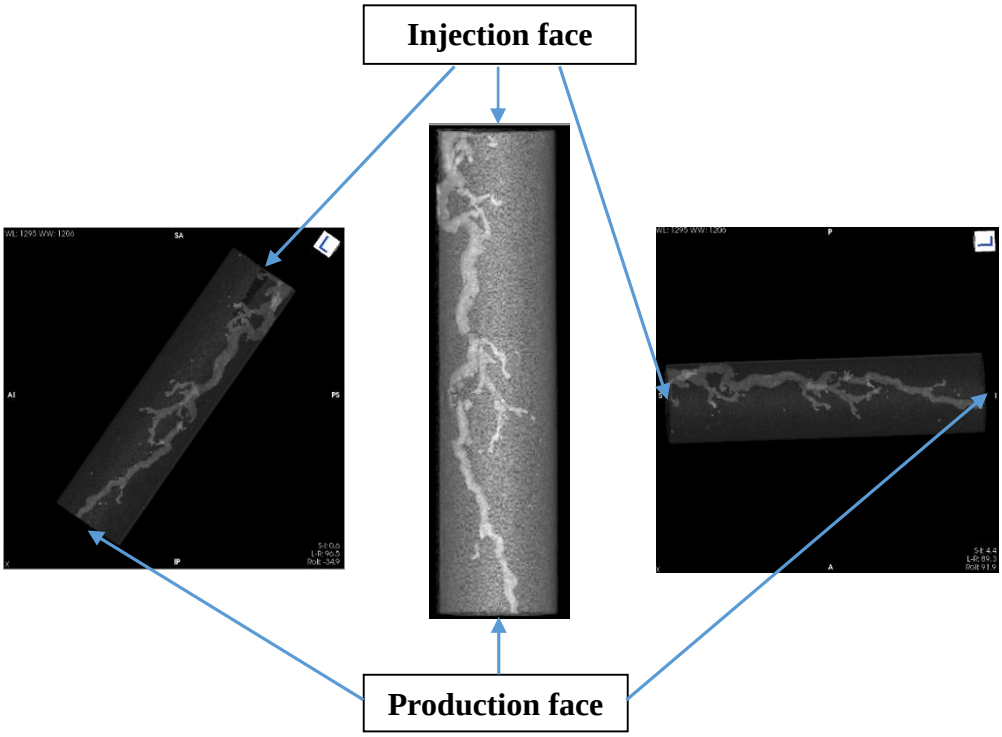

Fig. 37—Wormhole Propagation from CT Scan for Silurian Dolomite SD-6-40.

Second Set of Experiments: 15 wt% HCl Including Four Additives 250˚F at 1 cm^3/min.

The second set of experiments involved the injection of 15 wt% HCl with additives provided by a local service company into Grey Berea sandstone, Bandera sandstone, and Silurian dolomite cores to study the effect of acidizing on each lithology at 250°F. An acid injection rate of 1 cm^3/min was used throughout the experiments. 5 wt% KCl brine and 5 PV of treatment fluid were injected in the injection direction. The effluent samples from the coreflood experiments were collected after half PV of acid injection and every quarter PV until the end of each experiment. This set of experiments will be used as a base case to compare with urea-HCl performance.

Grey Berea Sandstone (G-6-27) at 250˚F using Urea-HCl with Four Additives

Regarding the pressure drop profile of Grey Berea sandstone (G-6-27) in **Fig. 38**, the stabilized pressure drop after the treatment was almost the same with the stabilized pressure drop before the treatment. This can imply that there is no stimulation or damage in permeability from the treatment.

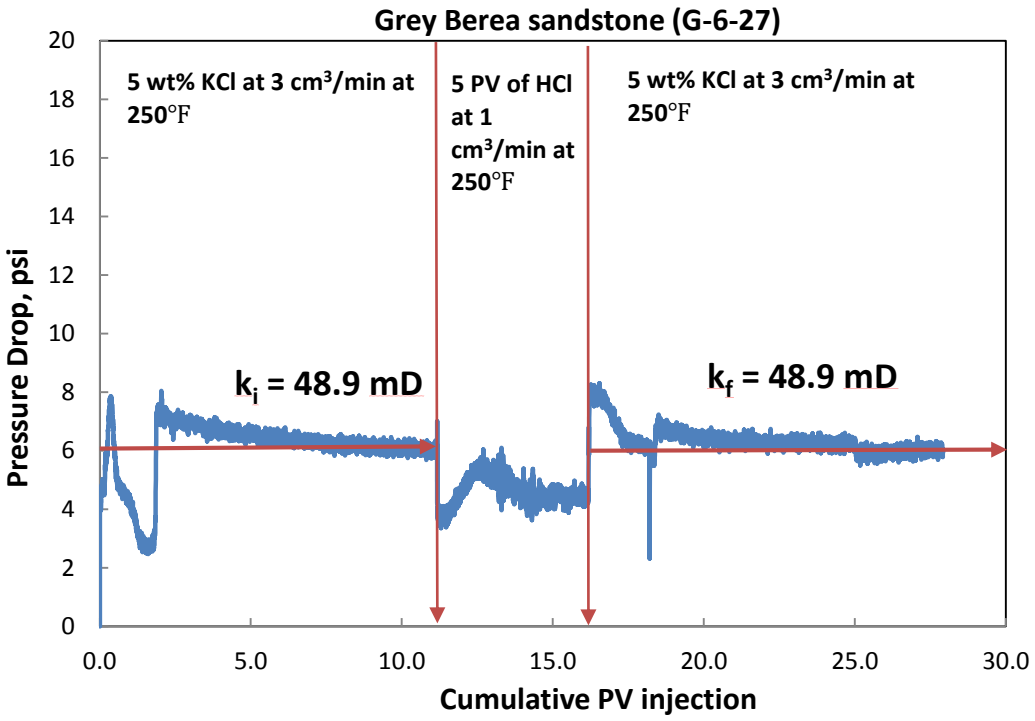

Fig. 38—Pressure Drop Profile Along the Berea-G-6-27 at 250°F (HCl + 4 additives).

Some precipitates were observed in the effluent samples after 2.25 PV (pH = 3.32) acid injection **(Fig. 39).** According to ICP results, a high iron concentration (47,000 ppm) was observed in the core effluent samples **(Fig. 40)**. The high iron concentration, which was in the same range with G-6-22 ICP results, was attributed to the dissolution of chlorite and illite clays in the sandstone. The calcium and magnesium concentrations also increased after 1.75 PV of treatment confirming the dissolution by HCl. Al^{3+} and Si^{4+} were present due to the dissolution of kaolinite and feldspars. More Al^{3+} was dissolved in HCl than urea-HCl, which resulted in clay instability (kaolinite) and fines migration at temperatures above 200°F in HCl (Coulter and Jennings 1999). **Fig. 41** shows the injection face, production face, and side view of Berea-G-6-27 after acid treatment.

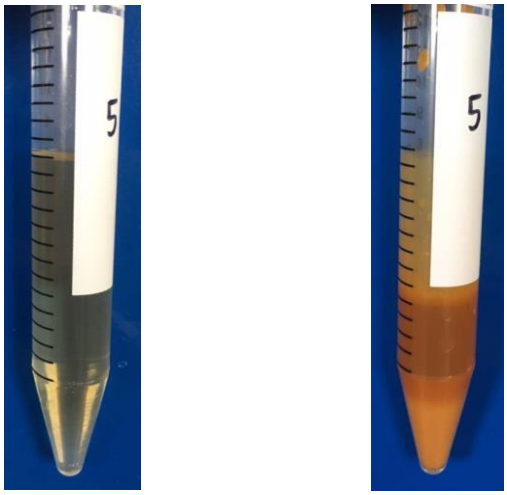

Fig. 39—Precipitates from Effluent Samples of Berea-G-6-27.

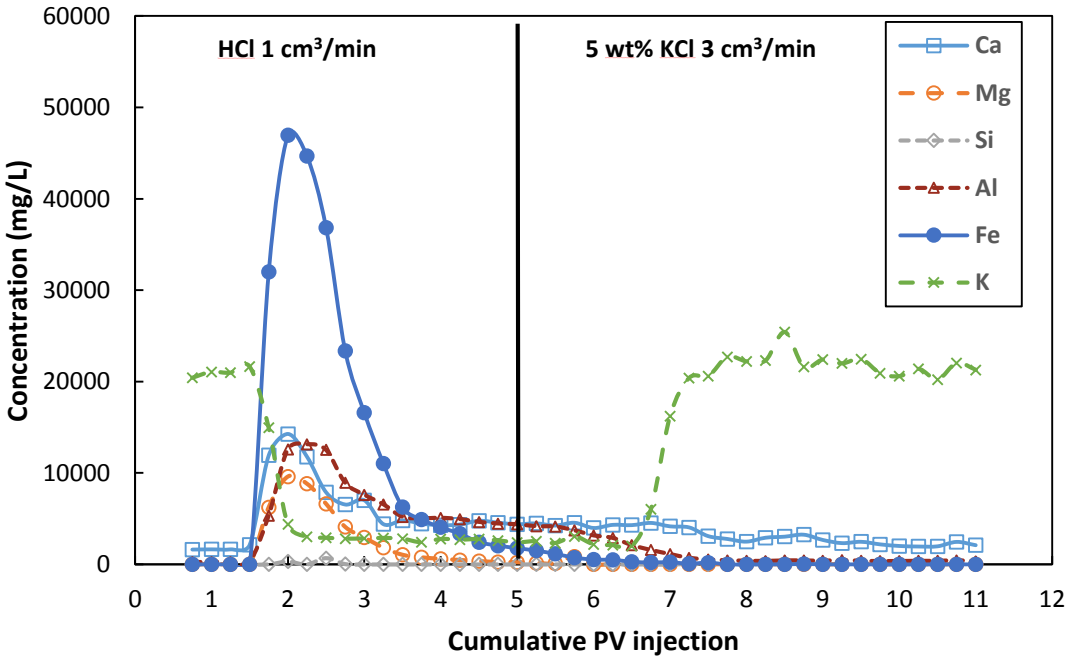

Fig. 40—ICP Analysis for 15 wt% HCl with Berea-G-6-27 at 250°F.

Fig. 41—Injection Face, Production Face, and Side View of Berea-G-6-27 After Acid Treatment.

The initial pH of the effluent samples containing 5 wt% KCl brine was approximately 8. The pH sharply decreased as the acid was injected to reach a pH of 0 **(Fig. 42)**. This indicated that the effluent samples contained live acid and not all of the acid was spent to dissolve the carbonate minerals in the Grey Berea core. Subsequently, the pH rose as the core was flushed with brine.

The density of injected brine is around 1.029 g/cc. When the 5 PV of treatment fluid was injected, the density started to increase (after 1.75 PV injection) as the acid dissolved more Ca, Mg, Al, Si and Fe. As the live acid became spent acid, fewer H^+ ions reacted with the carbonates resulting in fewer cations dissolution. Consequently, a gradual decrease in density was observed. When the flow was switched back to brine, the density returned to its original value **(Fig. 42)**. The peak of the density was about the same between the treatment by urea-HCl and HCl at 250˚F.

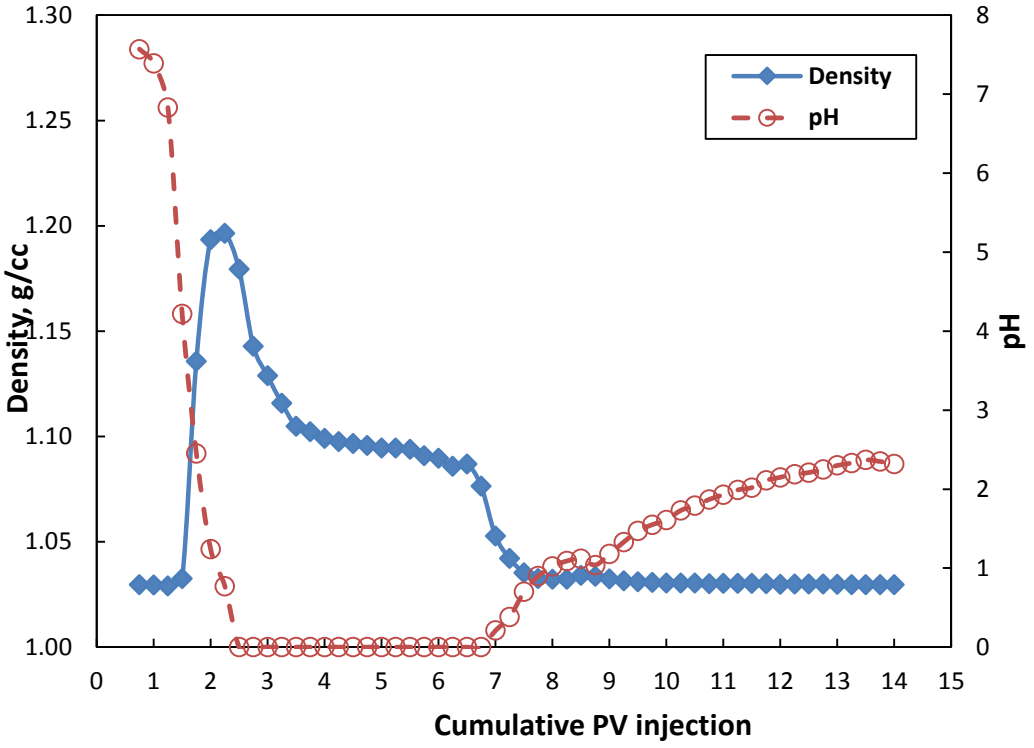

Fig. 42—Density and pH of Effluent Samples from Berea-G-6-27 at 250˚F.

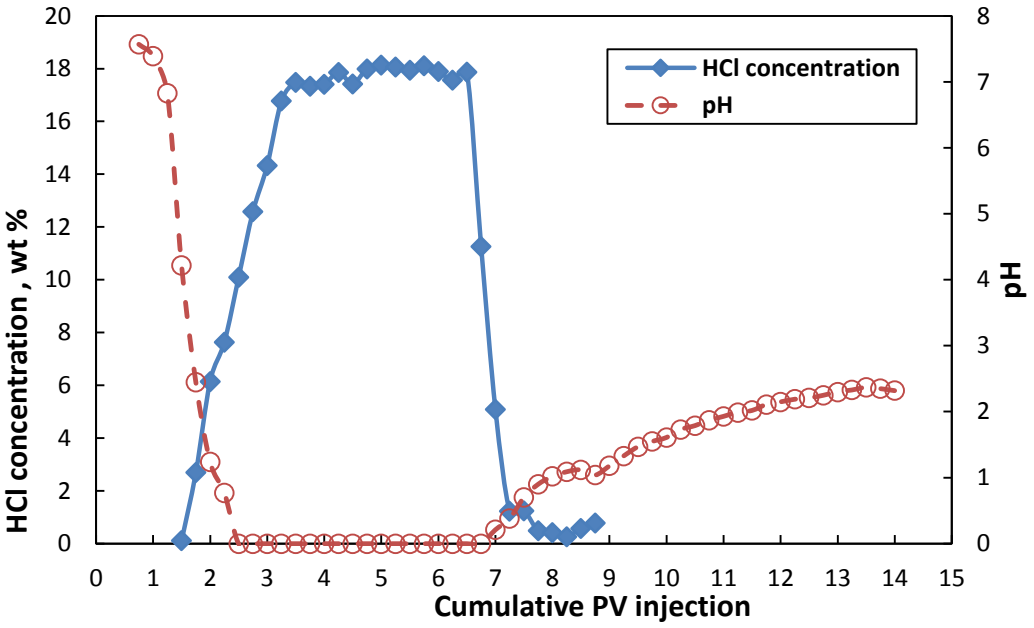

Fig. 43—HCl Concentration and pH of Effluent Samples from Berea-G-6-27 at 250˚F.

The HCl concentration of the effluent samples of Grey Berea (G-6-27) increased sharply after 1.75 PV of acid was injected to the maximum value around 18.14 wt% HCl **(Fig. 43)**, which was close to the equivalent HCl concentration of 15 wt% HCl and additives (18.76 %). The maximum acid concentration in HCl treatment was slightly higher compared to the treatment by urea-HCl. After the flow had been switched back from acid to brine, HCl concentration decreased from 18 wt% to 0.26 wt% after around 1.75 PV of brine injection. This confirmed that most of the acid were pushed out by the brine.

The results from the CT scan indicated a decrease in the core porosity after the treatment. The porosity profile **(Fig. 44)** showed reduction in porosity along the core after the treatment. The main reason behind this decrease was formation damage due to fines migration which can be observed by ICP results. **Table 7** gives the results comparison of urea-HCl and HCl at 250˚F.

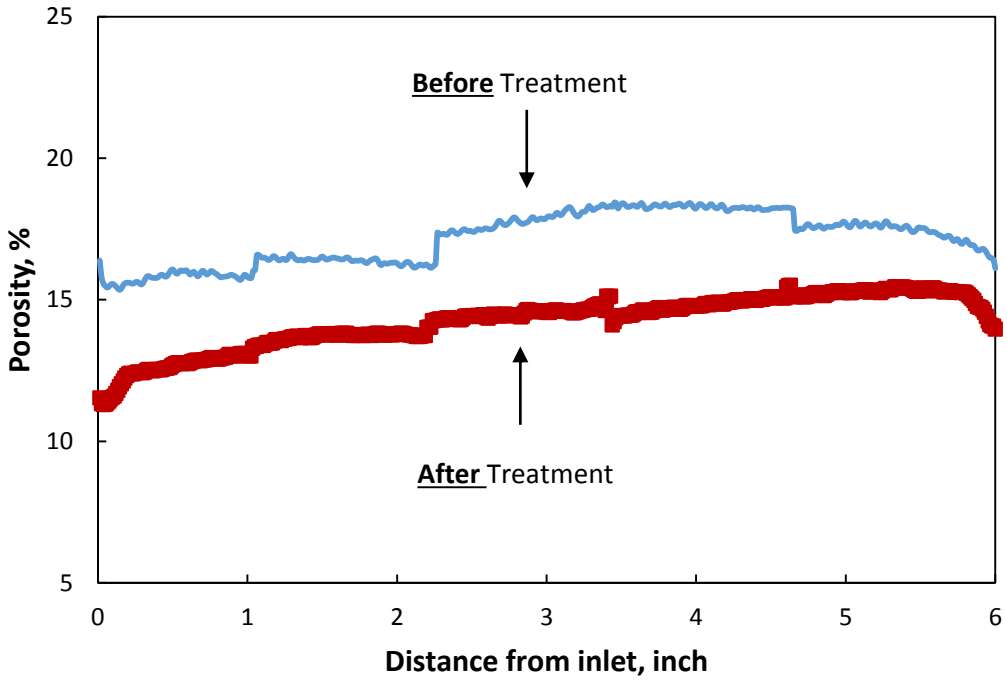

Fig. 44—Porosity Profile Before and After 15 wt% HCl Treatment for Berea-G-6-27.

Parameters		G-6-22 (UHC)	G-6-27 (HCl)
Permeability		+159 %	Not change
ICP (mg/L)	Ca^{2+}	15,000	15,000
	Mg^{2+}	10,000	10,000
	Fe^{2+}	45,000	49,000
	Al^{3+}	12,000	15,000
	Si^{4+}	3,000	0
pH		0	0
HCl concentration (%)		14-16	18
Density (g/cm^3)		1.21	1.2

Table 7—Results Comparison between G-6-22 and G-6-27 (urea-HCl vs. HCl at 250˚F).

Bandera Sandstone (BG-6-6) at 250˚F using 15 wt% HCl with Four Additives

Regarding the pressure drop profile of Bandera sandstone (BG-6-6) in **Fig. 45**. The stabilized pressure drop after the treatment was lower than the stabilized pressure drop before the treatment. This can imply the enhancement in permeability resulted from the dissolution of the carbonate minerals in sandstone which will be confirmed from Ca and Mg ions dissolved as shown in the next section. The calculated final permeability increased **111%** from the initial permeability.

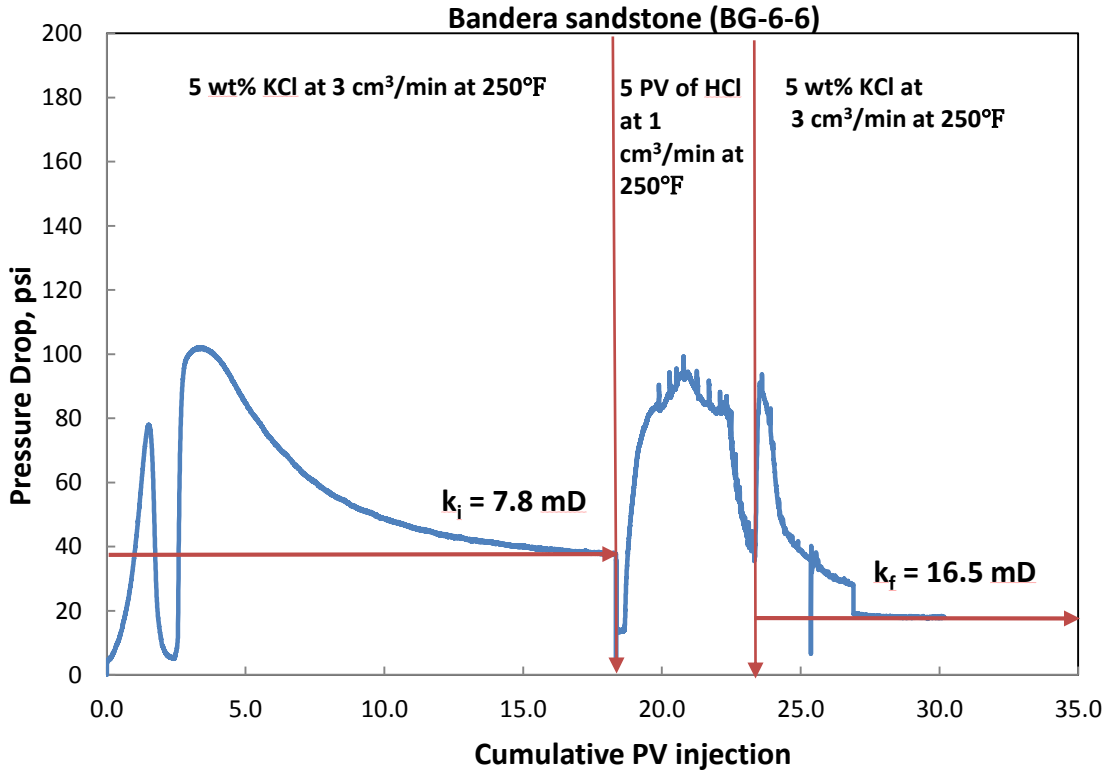

Fig. 45—Pressure Drop Profile Along the Bandera-BG-6-6 at 250˚F.

Some suspension and precipitates were observed in the effluent samples after 1.5 PV (pH = 5.44) acid injection **(Fig. 46)**. According to ICP results, high iron concentration (25,000 ppm) was found in the effluent samples **(Fig. 47)**. The calcium and magnesium concentrations also increased after 1.5 PV of treatment, confirming the dissolution by HCl. Al^{3+} was present due to the dissolution of kaolinite and feldspars, but in very small amount. K^{+} concentration from 5 wt% KCl brine was also decreased during the reaction interval of acid with the core. However, Si^{4+} was not present in this experiment. More Ca^{2+} was dissolved in HCl than urea-HCl, resulting in more porosity increase and permeability enhancement. However, iron dissolution was lower in HCl treatment which can cause more iron precipitation in the core (damage), but this effect was not dominant as Ca^{2+} dissolution. **Fig. 48** shows the injection face, production face, and side view of Bandera-BG-6-6 after acid treatment.

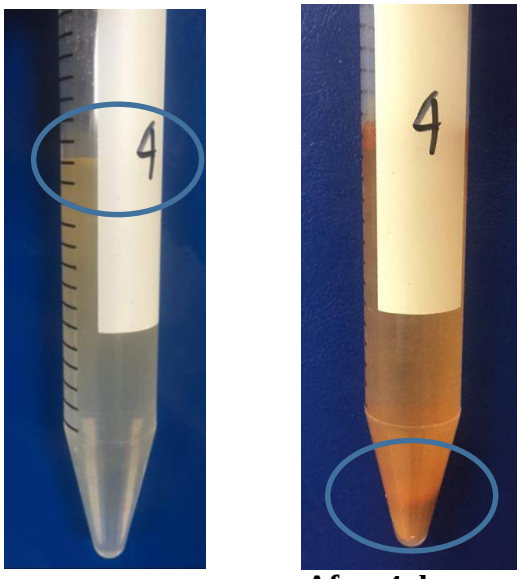

During coreflood **After 4 days**

Fig. 46—Suspension and Precipitates of Bandera-BG-6-6.

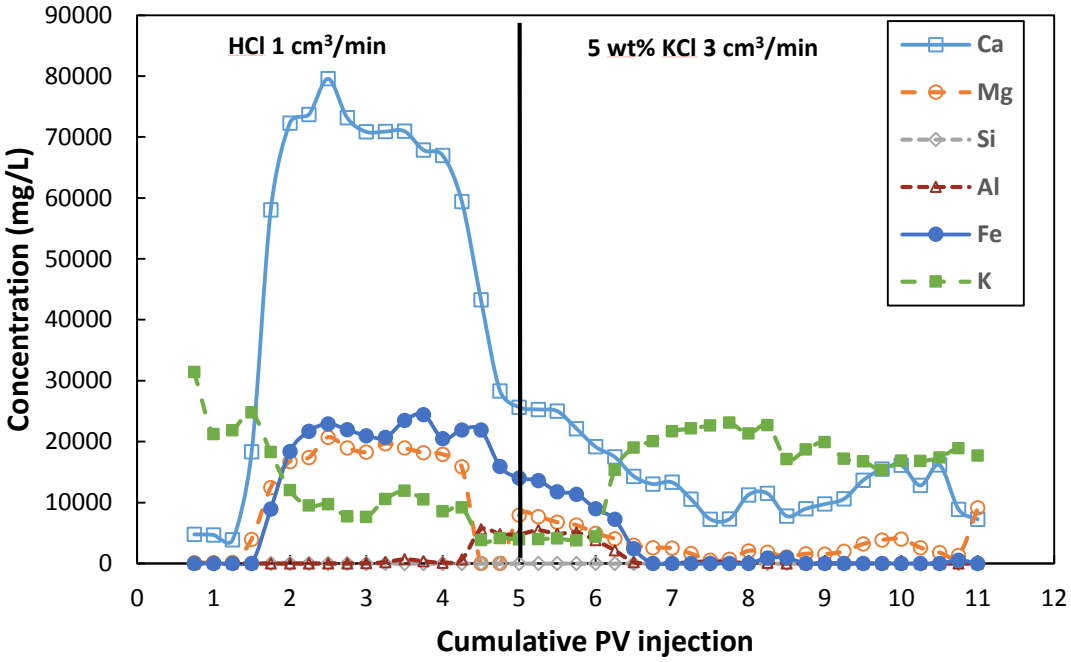

Fig. 47—ICP Analysis of the Effluent Samples- 15 wt% HCl with Bandera-BG-6-6 at 250˚F.

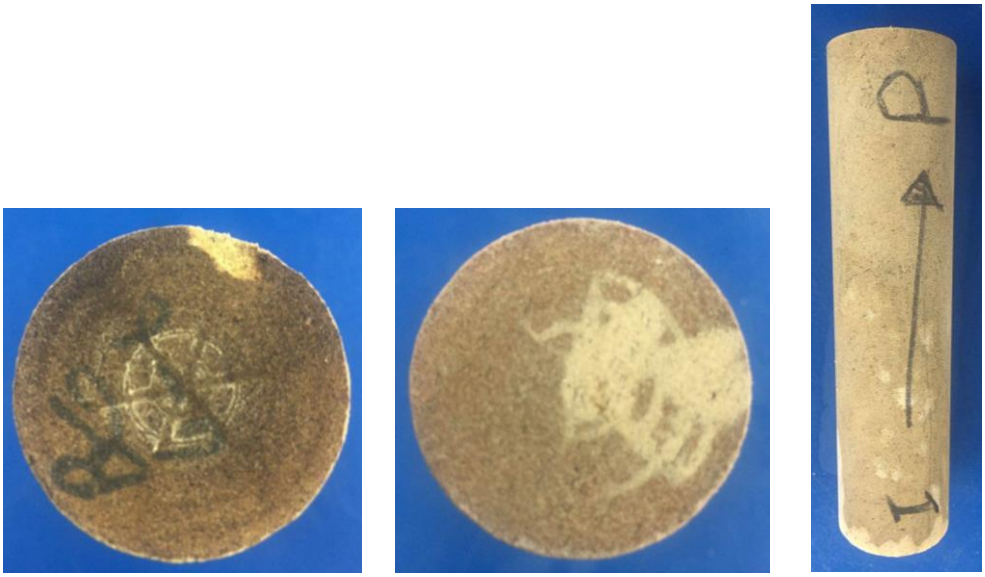

Fig. 48—Injection Face, Production Face, and Side View of Bandera-BG-6-6 After Acid Treatment.

The same procedure with BG-6-12 was applied for SEM-EDS analysis on BG-6-6 precipitates. The SEM images showed only amorphous structure and no crystallization **(Fig. 49 and Fig. 50)**, which suggested fines migration resulted from the treatment. The EDS results in atomic percentage indicated mainly Fe and O in amorphous part spot 1 **(Table 8 and Table 9)**.

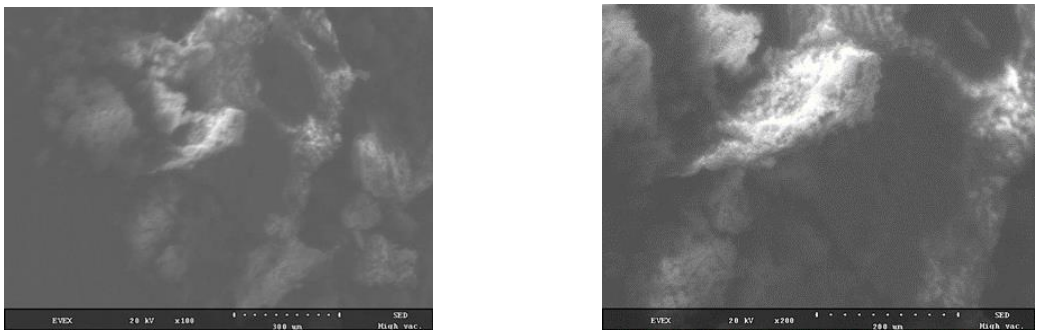

Magnification x100 **Magnification x200**

Fig. 49—SEM Images for BG-6-6 Precipitates (Amorphous spot 1).

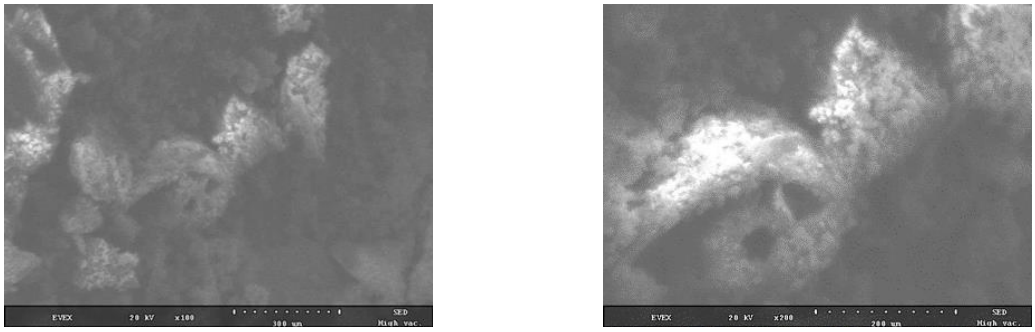

Magnification x100 **Magnification x200**

Fig. 50—SEM Images for BG-6-6 Precipitates (Amorphous spot 2).

Element	Atomic (%)
O	75.36
Fe	22.51
Al	0.83
Cl	1.3

Table 8—EDS Results for Amorphous Spot 1 of BG-6-6 Precipitates.

Element	Atomic (%)
Fe	10.58
O	46
Al	0.49
Cl	0.52

Table 9—EDS Results for Amorphous Spot 2 of BG-6-6 Precipitates.

The initial pH of the effluent samples containing 5 wt% KCl brine was approximately 8. The pH sharply decreased as the acid was injected to reach the lowest pH of 0 **(Fig. 51)**. This indicated that the effluent samples contained live acid and not all of the acid was spent to dissolve the carbonate minerals in the core. Thereafter, the pH rose as the core was flushed with brine.

The density of injected brine is around 1.029 g/cc. When the 5 PV of treatment fluid was injected, the density started to increase (after 1.5 PV injection) as the acid dissolved more Ca, Mg, Al, and Fe, which was consistent with the ICP results. As the live

acid became spent acid, less H^+ ions reacted with the carbonates, resulting in less cation dissolution. Consequently, a gradual decrease in density was observed. When the flow was switched back to brine, the density returned to its original value **(Fig. 51)**. The maximum density observed in this experiment was less than in BG-6-12 effluents due to less iron dissolution from ICP results.

The HCl concentration increased sharply after 4.5 PV of treatment fluid injection to the maximum value around 13.61 wt% HCl **(Fig. 52)**. After the flow had been switched back from acid treatment to brine, HCl concentration decreased significantly after around 1.25 PV of brine injection to 0.1 wt% HCl. This confirmed that most of the acid were pushed out by the brine.

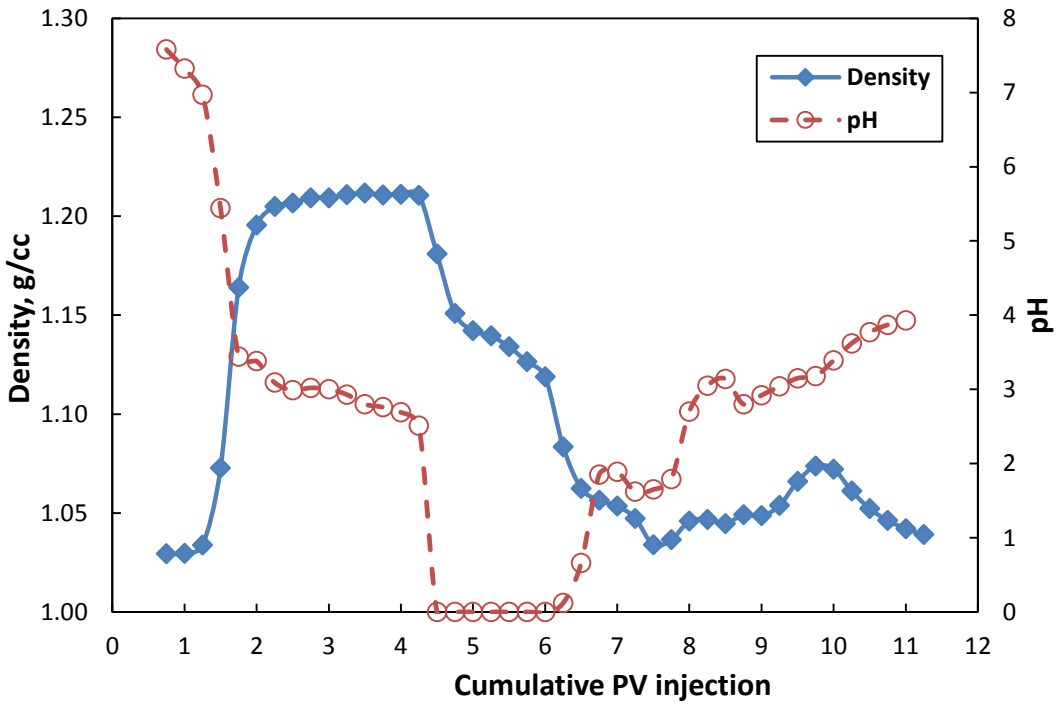

Fig. 51—Density and pH of Effluent Samples from Bandera-BG-6-6 at 250°F.

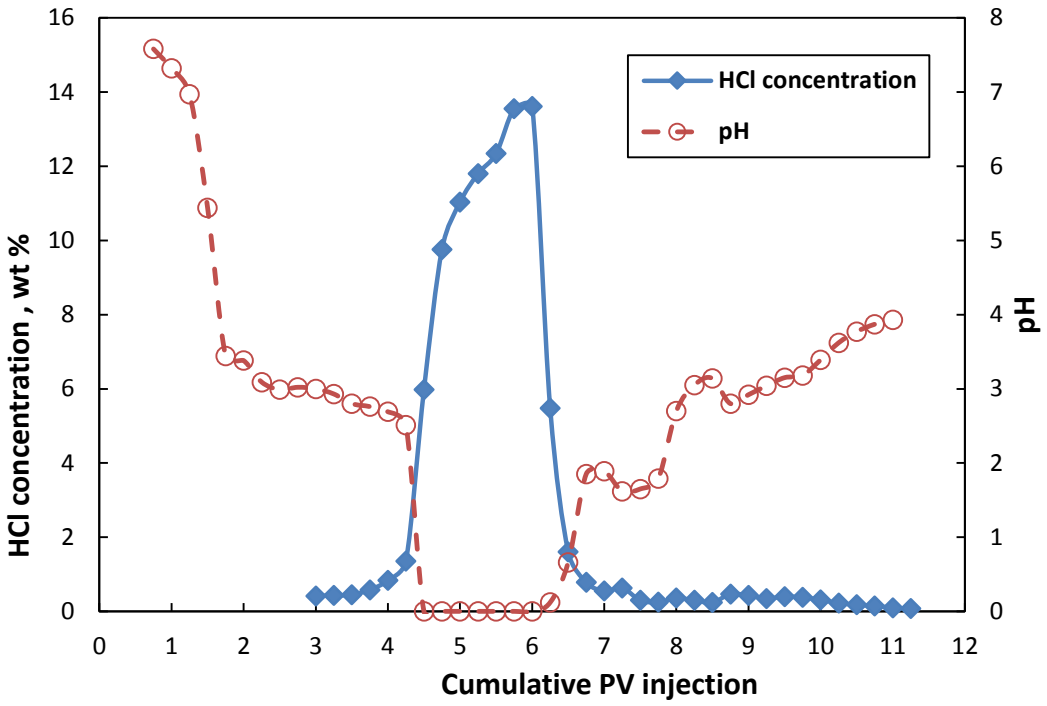

Fig. 52—HCl Concentration of Effluent Samples from Bandera-BG-6-6 at 250˚F.

CT scan results indicated an increase in the core porosity after the treatment which meant the cores were stimulated as the carbonate minerals were dissolved by the acid which was confirmed by the previous ICP results. The porosity profile **(Fig. 53)** showed significant improvement in porosity all the entire core. **Table 10** compares the results of urea-HCl and HCl at 250˚F on Bandera sandstone.

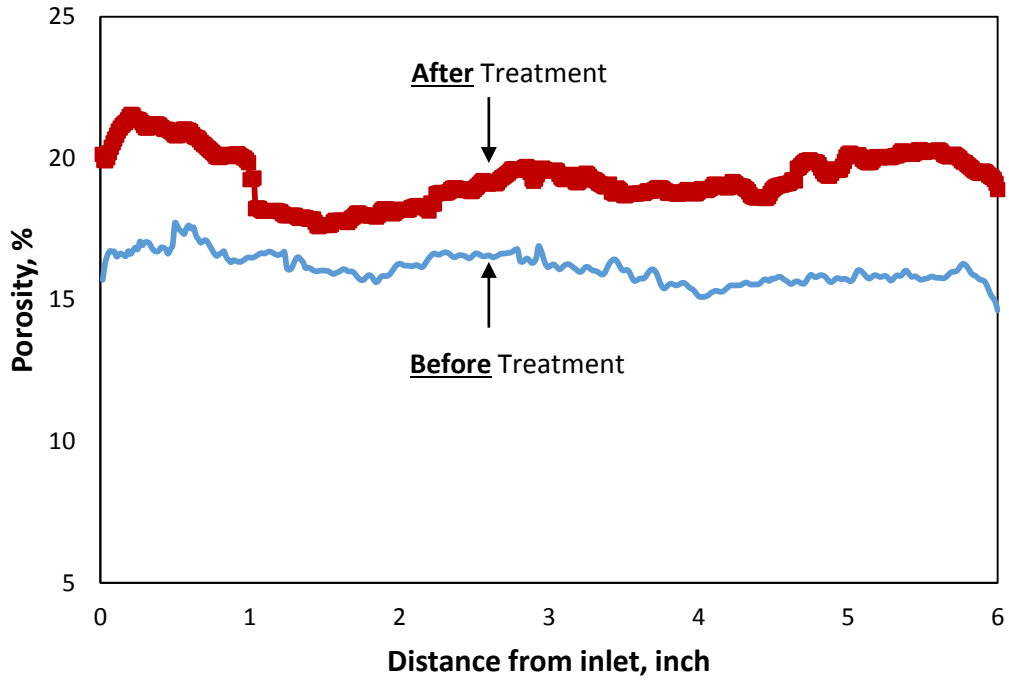

Fig. 53—Porosity Profile Before and After 15 wt% HCl Treatment for Bandera-BG-6-6.

Parameters		BG-6-12 (UHC)	BG-6-6 (HCl)
Permeability		+70 %	+111 %
ICP (mg/L)	Ca^{2+}	50,000	70,000-80,000
	Mg^{2+}	20,000	20,000
	Fe^{2+}	40,000	20,000-25,000
	Al^{3+}	5,000-10,000	5,000
	Si^{4+}	2,000-3,000	0
pH		0	0
HCl concentration (%)		9-10	12-14
Density (g/cm^3)		1.24	1.21

Table 10—Results Comparison between BG-6-12 and BG-6-6 (urea-HCl vs. HCl at 250˚F).

Silurian Dolomite (SD-6-42) at 250˚F using HCl with Four Additives

At first, 5 wt% KCl brine was injected in the production direction while heating the system to 250°F until the pressure drop was stabilized. The pressure drop then increased as the flow was switched from brine to acid in injection direction since the acid had a higher viscosity compared to 5 wt% KCl **(Fig. 54)**. After 5 PV of treatment, the stabilized pressure drop after the treatment was lower than the stabilized pressure drop before the treatment. However, the acid breakthrough which occurred in SD-6-40 (urea-HCl at 250°F) did not happen as in the case of HCl at 250°F.

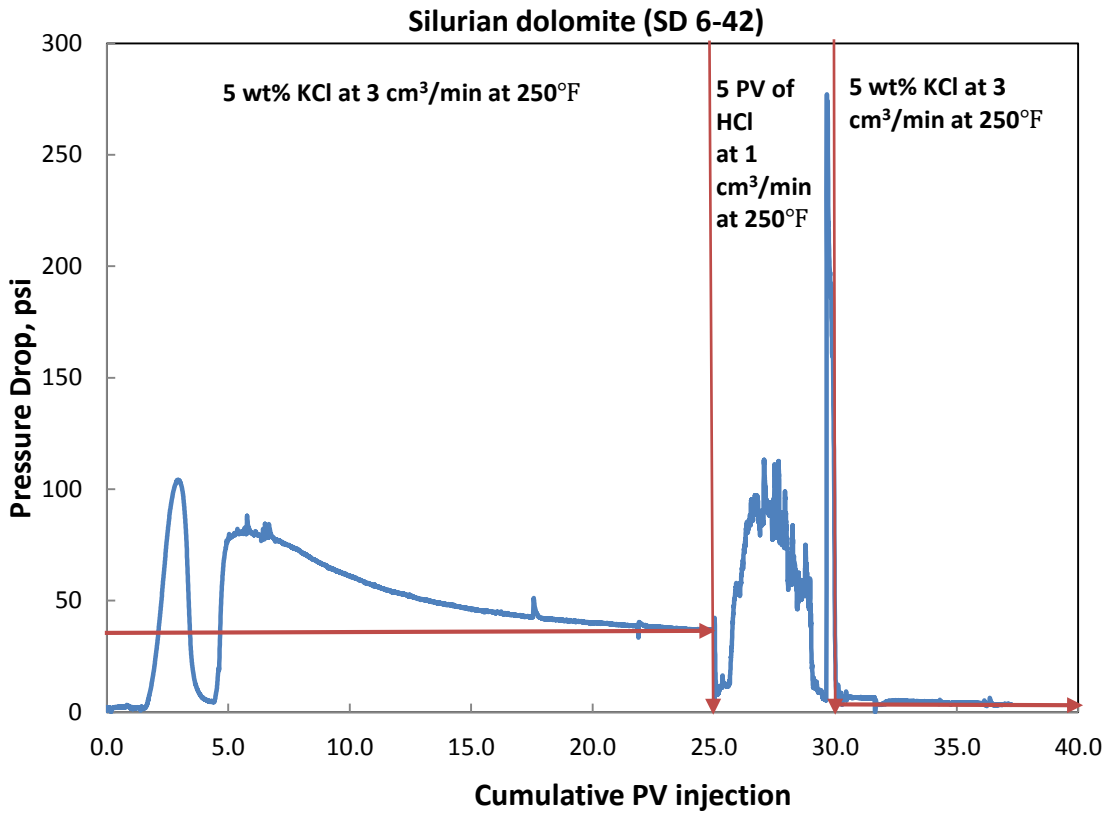

Fig. 54—Pressure Drop Profile Along the Silurian Dolomite SD-6-42 at 250˚F.

Some suspension and precipitates from the dolomite dissolution were observed in the effluent samples after 1.75 PV (pH = 4.15) acid injection **(Fig. 55)**. The calcium and magnesium concentration from ICP **(Fig. 56)** increased after 1.75 PV of treatment confirming the dissolution of dolomite by HCl. Ca^{2+} dissolution in this experiment was higher than the urea-HCl case at 250˚F, but the Mg^{2+} dissolution was higher. K^{+} concentration from 5 wt% KCl brine also decreased during the reaction interval of acid with the core. The injection face, production face, and side view of SD-6-42 after acid treatment were shown in **Fig. 57**. Face dissolution was observed at the injection face of the core.

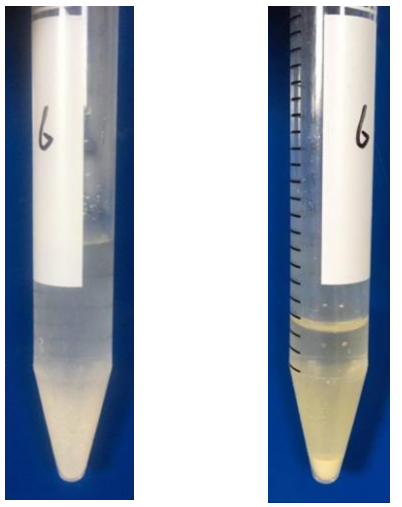

Fig. 55—Suspension and Precipitates of Silurian Dolomite SD-6-42.

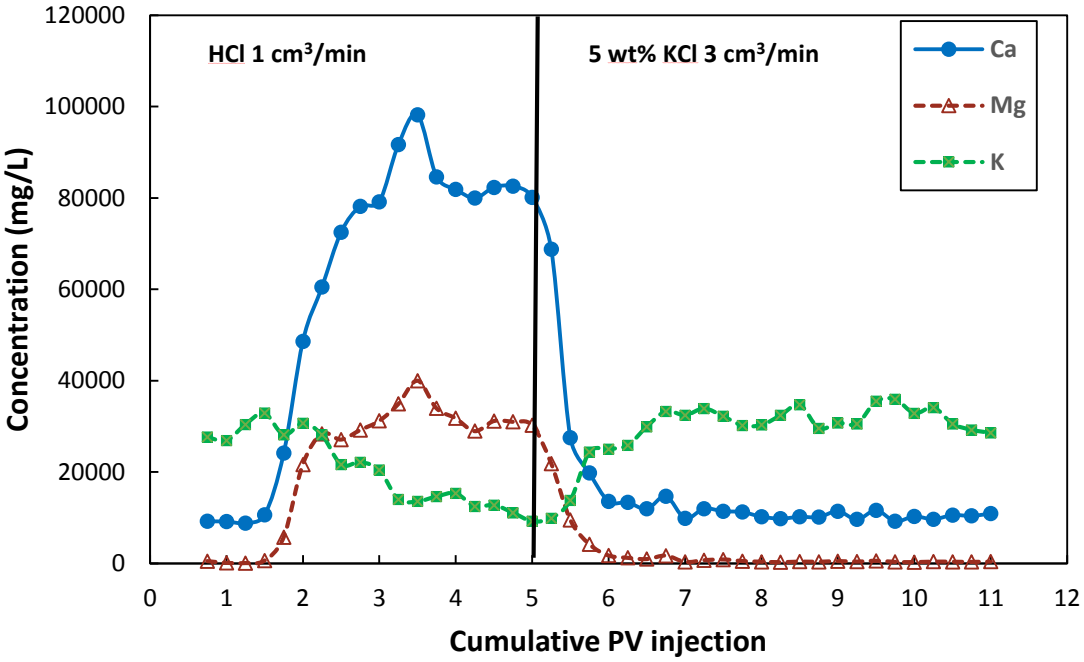

Fig. 56—ICP Analysis of the Effluent Samples- 15 wt% HCl with Silurian Dolomite SD-6-42 at 250˚F.

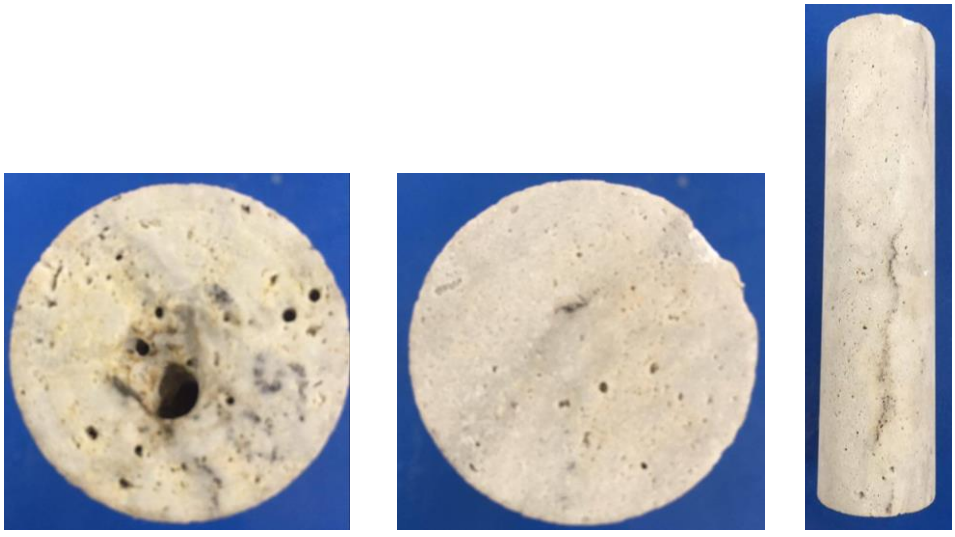

Fig. 57—Injection Face, Production Face, and Side View of Silurian Dolomite SD-6-42 After Acid Treatment.

The initial pH of the effluent samples containing 5 wt% KCl brine was approximately 7. The pH sharply decreased as the acid was injected to reach the lowest pH of 2.18, which was higher than the minimum pH of SD-6-40 **(Fig. 58)**. After that, the pH rose as the core was flushed with brine.

The density of injected brine is around 1.029 g/cc. When the 5 PV of treatment fluid was injected, the density started to increase (after 1.75 PV injection) as the acid dissolved more Ca and Mg which was consistent with the ICP results. As the live acid became spent acid, fewer H^+ ions reacted with the carbonates resulting in less cation dissolution. Consequently, a gradual decrease in density was observed. When the flow was switched back to brine, the density returned to its original value **(Fig. 58)**.

The HCl concentration increased after 4.5 PV of acid was injected to the maximum value around 1.55 wt% HCl which was very low compared to the treatment by urea-HCl **(Fig. 59)**. This meant the acid was spent more in HCl treatment, but still no breakthrough occurred. As a result, more face dissolution and less deep penetration with two wormhole formation occurred. After the flow had been switched back from acid treatment to brine, HCl concentration decreased significantly after around 0.5 PV of brine injection to 0.23 wt% HCl. This confirmed that most of the acid were pushed out by the brine.

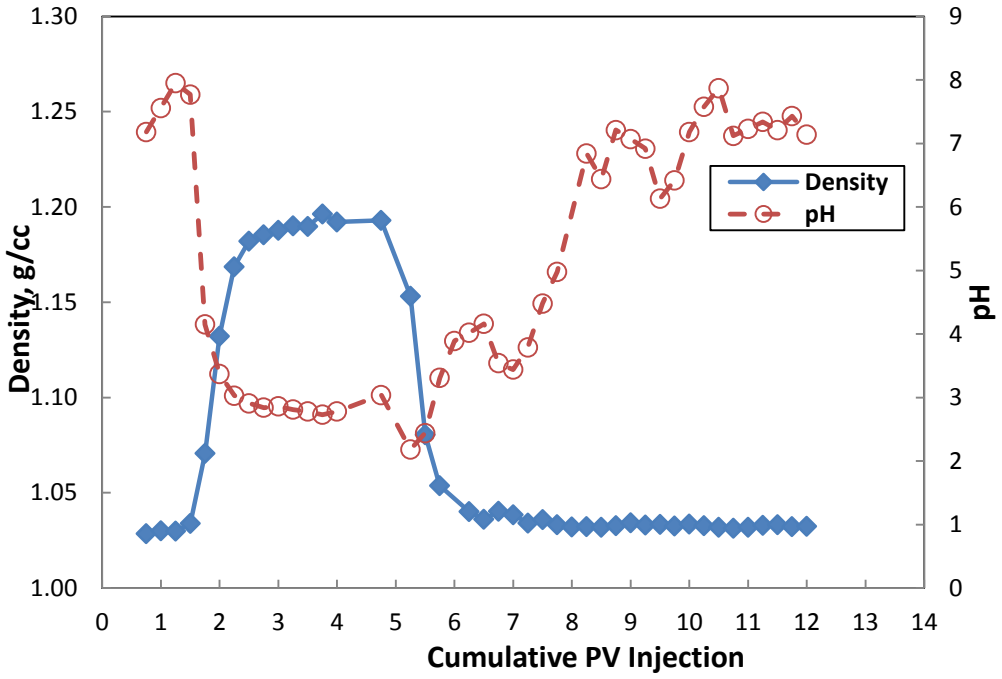

Fig. 58—Density and pH of Effluent Samples from Silurian Dolomite SD-6-42 at 250˚F.

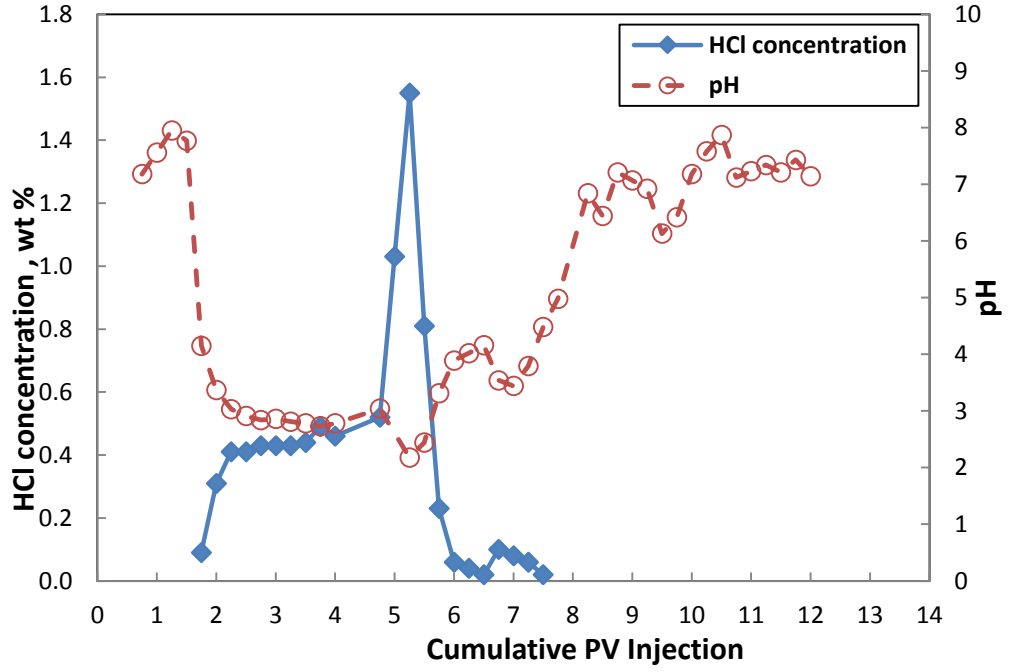

Fig. 59—HCl Concentration of Effluent Samples from Silurian Dolomite SD-6-42 at 250˚F.

The CT scan **(Fig. 60)** result showed the formation of two wormholes along the core. However, the breakthrough did not occur after 5 PV of the acid injection. Face dissolution was also observed from the CT scan at the injection face. **Table 11** gives the results comparison of urea-HCl and HCl at 250˚F on Silurian dolomite.

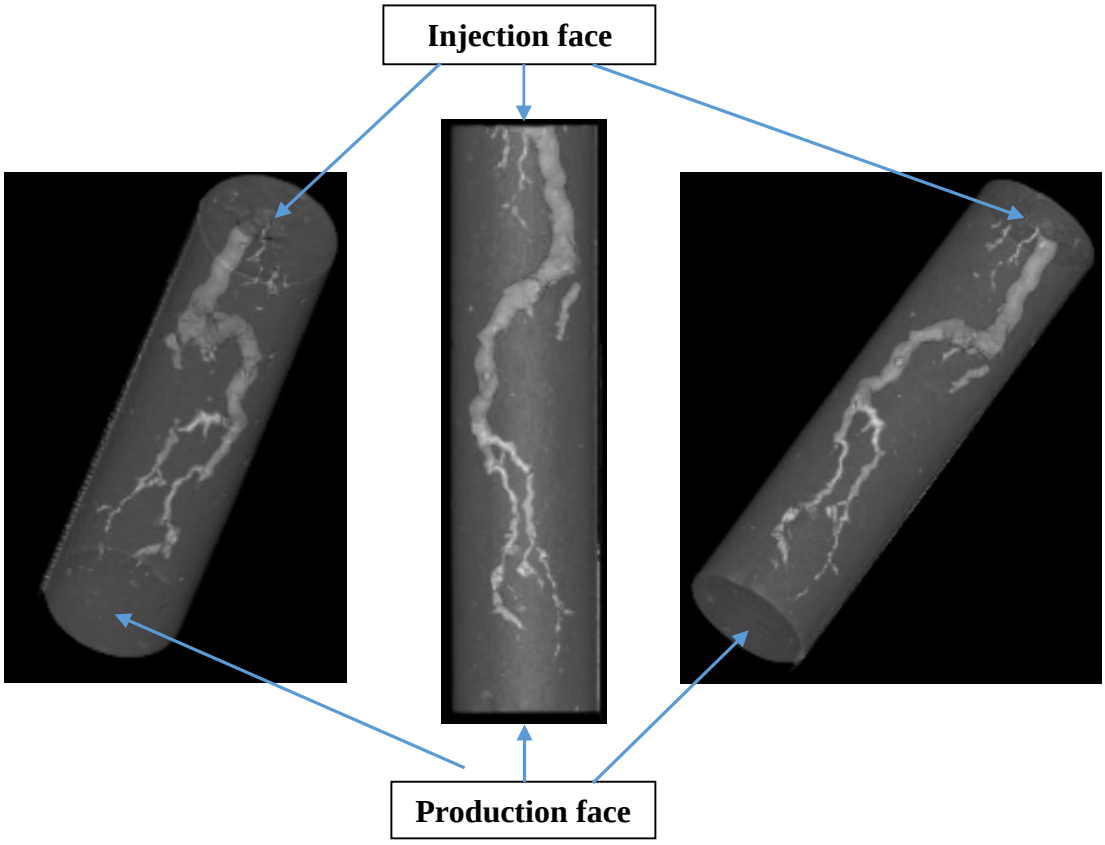

Fig. 60—Wormhole Propagation from CT Scan for Silurian Dolomite SD-6-42.

Parameters		SD-6-40 (UHC)	SD-6-42 (HCl)
Permeability		3	Not BT
ICP (mg/L)	Ca^{2+}	60,000-70,000	80,000-100,000
	Mg^{2+}	55,000-65,000	30,000-40,000
pH		0	2.2
HCl concentration (%)		9-11	1.6
Density (g/cm^3)		1.22	1.2

Table 11—Results Comparison between SD-6-40 and SD-6-42 (urea-HCl vs. HCl at 250˚F)

Third Set of Experiments: 30 wt% Urea-HCl Including Four Additives (with increment of corrosion inhibitor or addition of silica inhibitor) 250˚F at 1 cm^3/min.

The third set of experiments involved the injection of urea-HCl with additives provided by a local service company at 250°F. The experiments were conducted on two Bandera sandstone cores. The first experiment in this set included the incremental of the corrosion inhibitor concentration, while the second experiment included the addition of silica inhibitor. This set of experiments is representative of the effect of additives on the stimulation of Bandera sandstone cores.

Bandera Sandstone (BG-6-2) at 250˚F using Urea-HCl with Four Additives with Incremental of Corrosion Inhibitor Concentration

Regarding the pressure drop profile of Bandera sandstone (BG-6-2) in **Fig. 61**, the stabilized pressure drop after the treatment was lower than that before the treatment. This can imply the enhancement in permeability resulted from the dissolution of the carbonate

minerals in sandstone, which will be confirmed from Ca and Mg ions dissolved as shown in the next section. The calculated final permeability increased **87%** from the initial permeability.

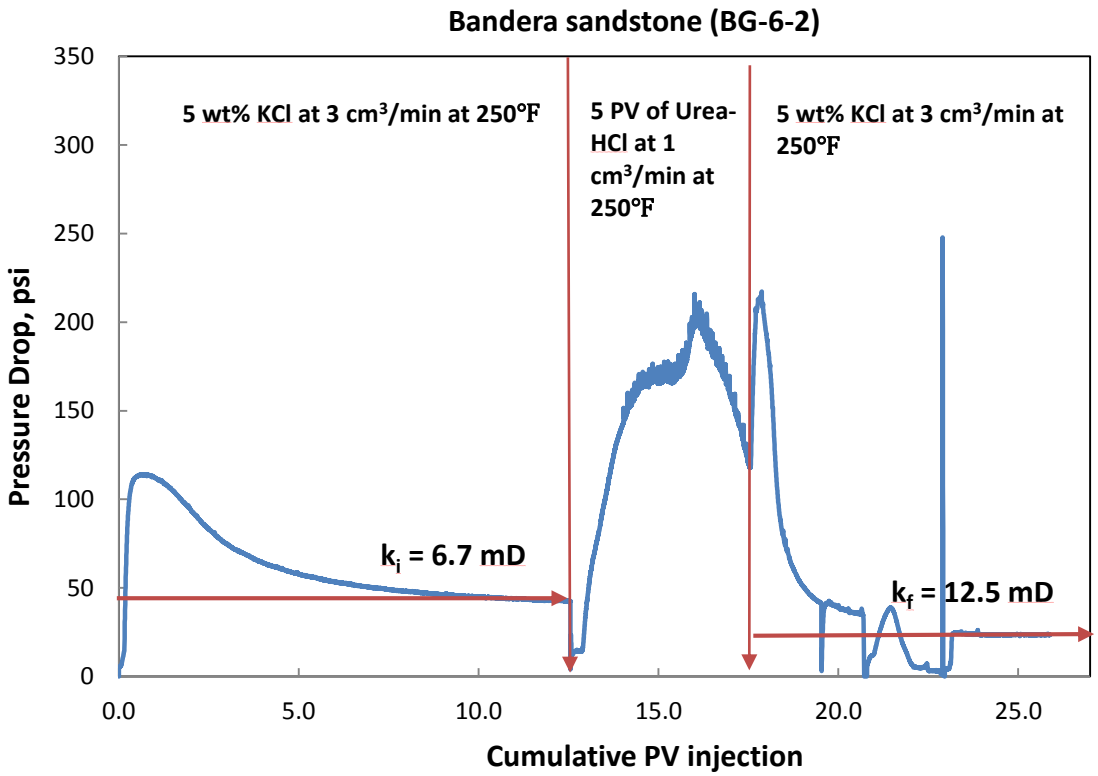

Fig. 61—Pressure Drop Profile Along the Bandera-BG-6-2 at 250˚F.

Some suspension and precipitates were also observed in the effluent samples after 1.75 PV (pH = 5.23) acid injection **(Fig. 62)**. According to ICP results, high iron concentration (35,000 ppm) was detected in the effluent samples **(Fig. 63)**. The calcium and magnesium concentrations also increased after 1.5 PV of treatment confirming the dissolution by urea-HCl. It can be observed that Ca^{2+} dissolution in this experiment

(increase CI load) was higher than BG-6-12. This was the reason for better stimulation results of BG-6-2 than BG-6-12. Al^{3+} and Si^{4+} were present due to the dissolution of kaolinite and feldspars but in very small amount. K^{+} concentration from 5 wt% KCl brine also decreased during the reaction interval of acid with the core. The injection face, production face, and side view of Bandera-BG-6-2 after acid treatment were shown in **Fig. 64.**

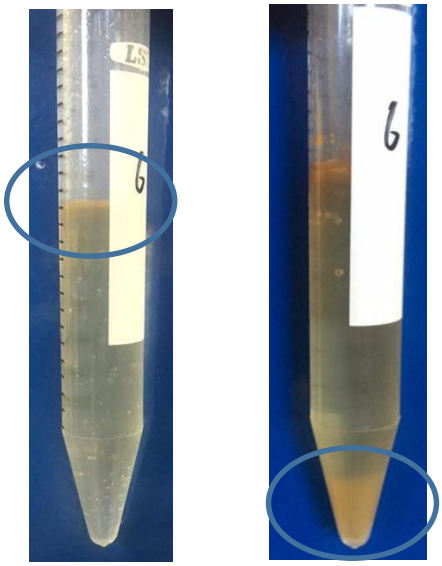

Fig. 62—Suspension and precipitates of Bandera-BG-6-2.

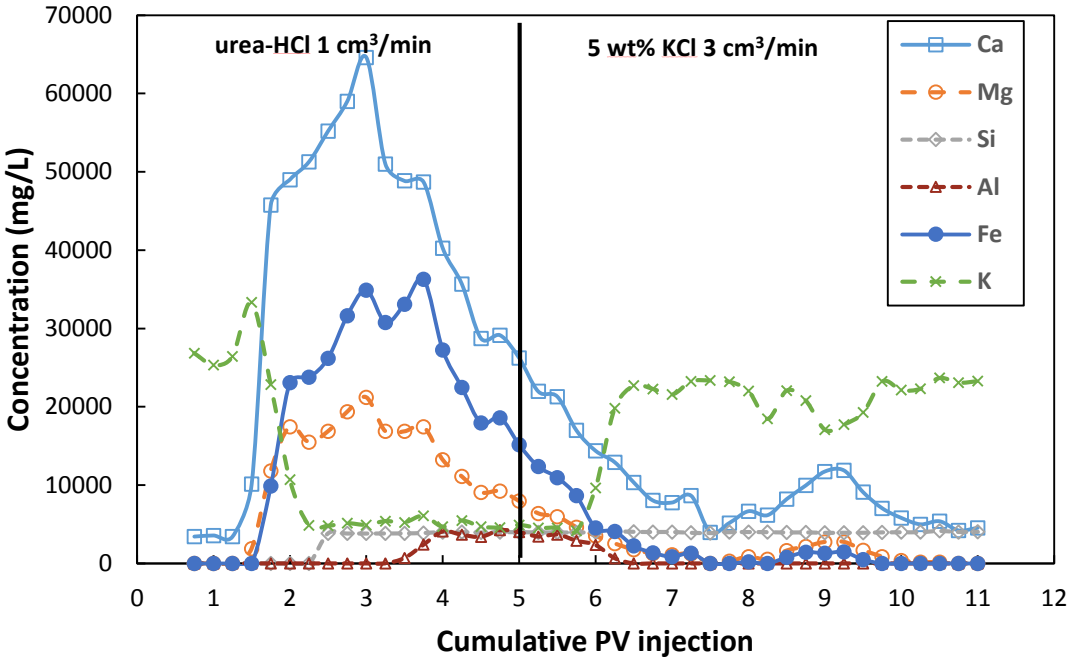

Fig. 63—ICP Analysis of the Effluent Samples- 30 wt% Urea-HCl with Bandera-BG-6-2 at 250˚F.

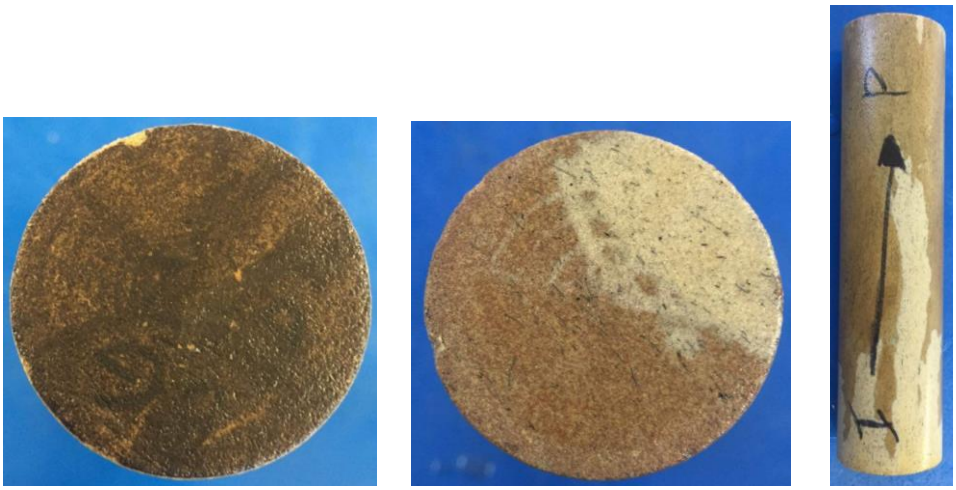

Fig. 64—Injection Face, Production Face, and Side View of Bandera-BG-6-2 After Acid Treatment.

The initial pH of the effluent samples containing 5 wt% KCl brine was approximately 8. The pH sharply decreased as the acid was injected to reach the lowest pH of 0 which was the same with BG-6-12 results **(Fig. 65)**. This indicated that the effluent samples contained live acid and not all of the acid was spent to dissolve the carbonate minerals in the core. Thereafter, the pH rose as the core was flushed with brine.

The density of injected brine was around 1.029 g/cc. When the 5 PV of treatment fluid was injected, the density started to increase (after 1.5 PV injection) as the acid dissolved more Ca, Mg, Si, Al, and Fe, which was consistent with the ICP results. As the live acid became spent acid, less H^+ ions reacted with the carbonates resulting in less cation dissolution. Consequently, a gradual decrease in density was observed. When the flow was switched back to brine, the density returned to its original value **(Fig. 65)**.

The titration was conducted to measure the equivalence of HCl in the effluent samples collected during the coreflood. The HCl concentration increased sharply after 4 PV of treatment fluid injection to the maximum value around 12.7 wt% HCl which was the same range with regular additive case **(Fig. 66)**. After the flow had been switched back from acid treatment to brine, HCl concentration decreased significantly after around 1.25 PV of brine injection to 0.13 wt% HCl. This confirmed that most of the acid were pushed out by the brine.

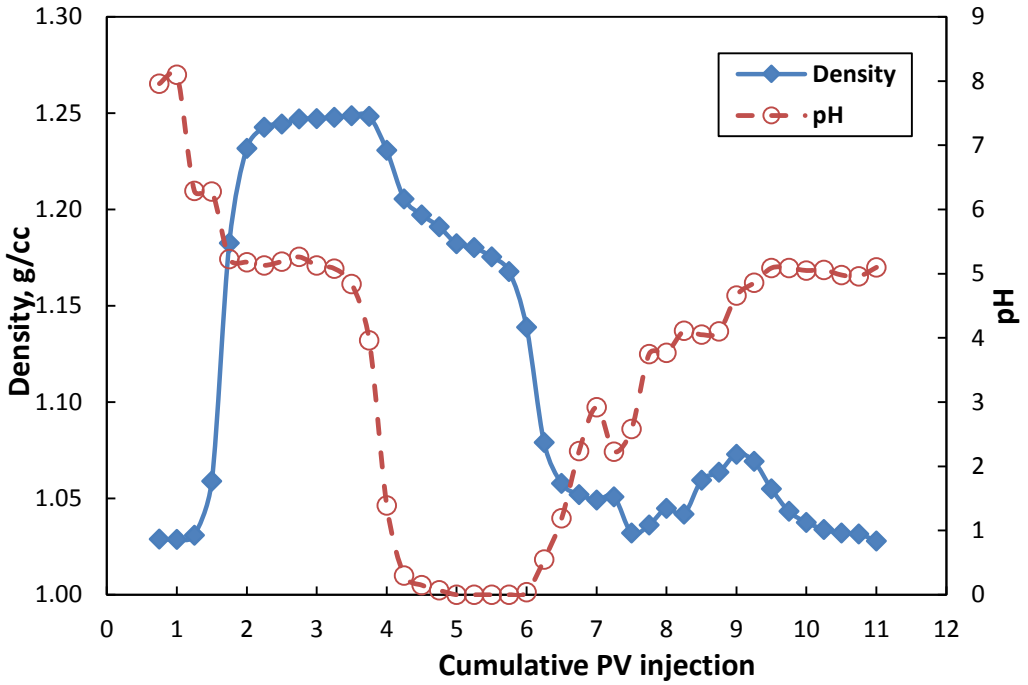

Fig. 65—Density and pH of Effluent Samples from Bandera-BG-6-2 at 250°F.

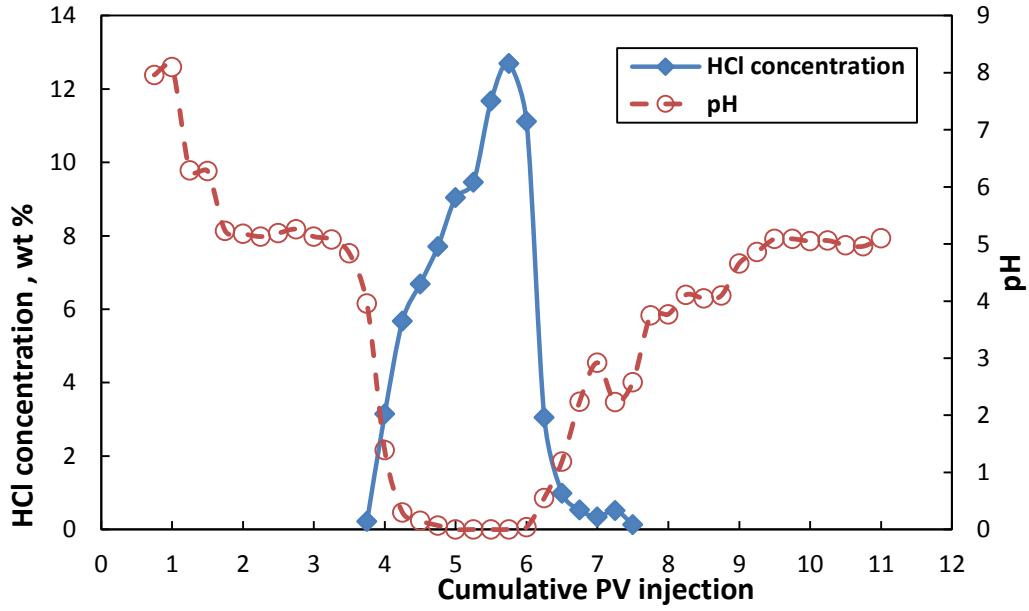

Fig. 66—HCl Concentration of Effluent Samples from Bandera-BG-6-2 at 250°F.

An increase in the core porosity after the treatment from CT scan meant that the core was stimulated as the carbonate minerals were dissolved by the acid which was confirmed by the previous ICP results. The porosity profile **(Fig. 67)** showed improvement in porosity along the entire core. The results comparison of increase CI case and normal case at 250˚F on Bandera sandstone was depicted in **Table 12**.

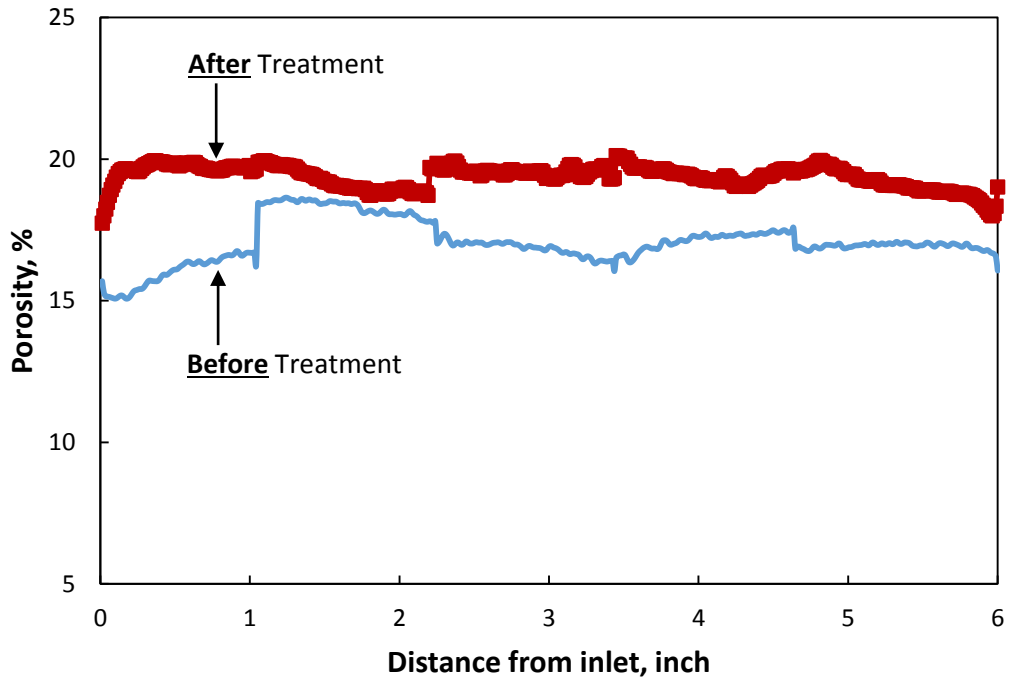

Fig. 67—Porosity Profile Before and After 30 wt% Urea-HCl Treatment for Bandera-BG-6-2.

Parameters		BG-6-12 (UHC)	BG-6-2 (UHC with increase Cl)
Permeability		+70 %	+87 %
ICP (mg/L)	Ca^{2+}	50,000	65,000
	Mg^{2+}	20,000	20,000
	Fe^{2+}	40,000	35,000
	Al^{3+}	5,000-10,000	4,000
	Si^{4+}	2,000-3,000	4,000
pH		0	0
HCl concentration (%)		9-10	11-13
Density (g/cm^3)		1.24	1.25

Table 12—Results Comparison between BG-6-12 and BG-6-2 (urea-HCl with normal additives vs. urea-HCl with increase CI at 250˚F).

Bandera Sandstone (BG-6-9) at 250˚F using Urea-HCl with Four Additives with Addition of Silica Inhibitor

Regarding the pressure drop profile of Bandera sandstone (BG-6-9) in **Fig. 68**. The stabilized pressure drop after the treatment was lower than the stabilized pressure drop before the treatment. This can imply the enhancement in permeability resulted from the dissolution of the carbonate minerals in sandstone which will be confirmed from Ca and Mg ions dissolved as shown in the next section. The calculated final permeability increased **49%** from the initial permeability.

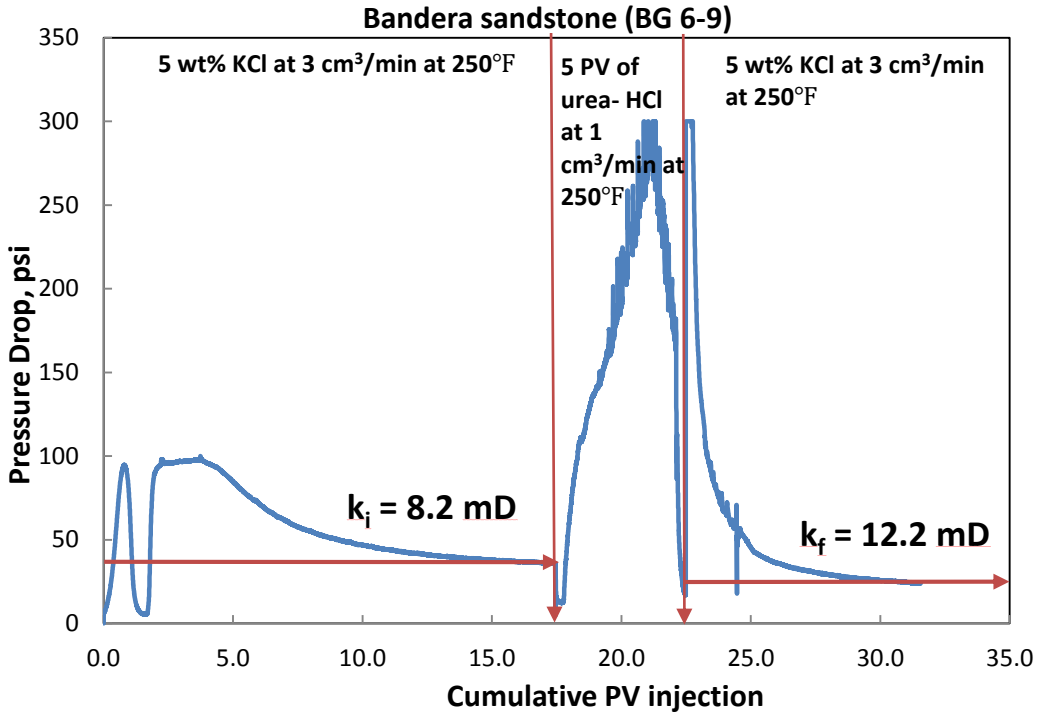

Fig. 68—Pressure Drop Profile Along the Bandera-BG-6-9 at 250˚F.

Some suspension and precipitates were also observed in the effluent samples after 1.75 PV (pH = 3.82) acid injection **(Fig. 69)**. According to ICP results, lower iron concentration (20,000 ppm) compared to normal additive case was detected in the effluent samples **(Fig. 70)**. This might cause some iron precipitation in the core resulting in lower stimulation. The calcium and magnesium concentrations also increased after 1.75 PV of treatment confirming the dissolution by urea-HCl. It can be observed that Ca^{2+} dissolution in this experiment was higher compared to urea-HCl with normal additive, but the Mg^{2+} dissolution was lower. Al^{3+} was present due to the dissolution of kaolinite and feldspars but in very small amount. Si^{4+} was not present due to the effect of silica inhibitor. K^{+} concentration from 5 wt% KCl brine was also decreased during the reaction interval of

acid with the core. The injection face, production face, and side view of Bandera-BG-6-9 after acid treatment were shown in **Fig. 71**.

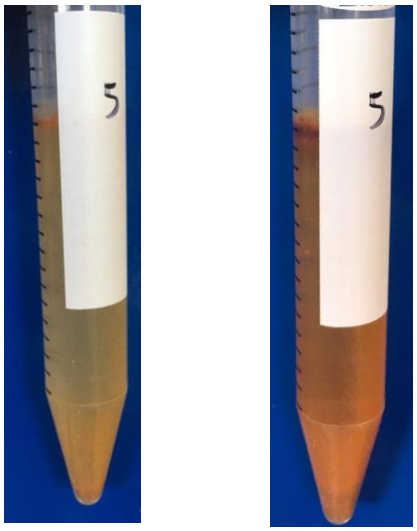

Fig. 69—Suspension and Precipitates of Bandera-BG-6-9.

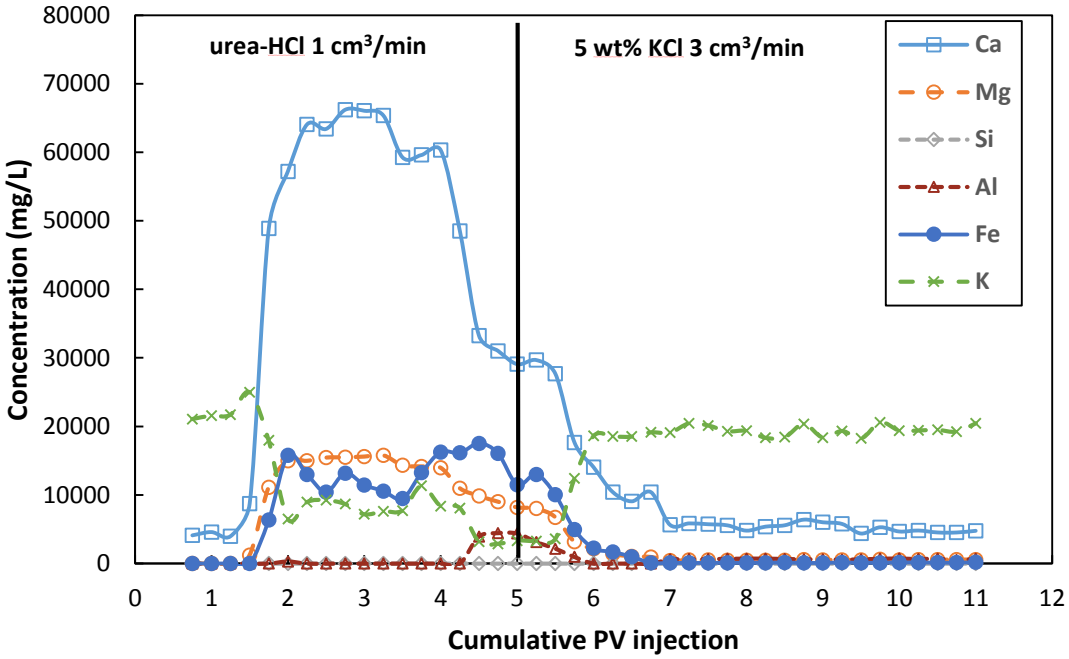

Fig. 70—ICP Analysis of the Effluent Samples- 30 wt% Urea-HCl with Bandera-BG-6-9 at 250˚F.

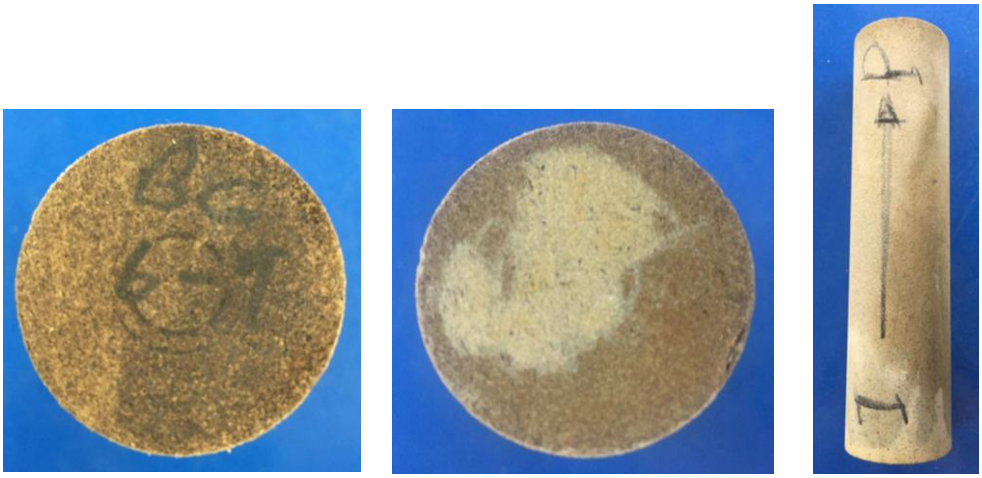

Fig. 71—Injection Face, Production Face, and Side View of Bandera-BG-6-9 After Acid Treatment.

The initial pH of the effluent samples containing 5 wt% KCl brine was approximately 8. The pH sharply decreased as the acid was injected to reach the lowest pH of 0.12 **(Fig. 72)**. This indicated that the effluent samples contained live acid and not all of the acid was spent to dissolve the carbonate minerals in the core. Thereafter, the pH rose as the core was flushed with brine.

The density of injected brine is around 1.029 g/cc. When the 5 PV of treatment fluid was injected, the density started to increase (after 1.5 PV injection) as the acid dissolved more Ca, Mg, Al, and Fe, which was consistent with the ICP results. As the live acid became spent acid, less H^+ ions reacted with the carbonates resulting in less cation dissolution. Consequently, a gradual decrease in density was observed. When the flow was switched back to brine, the density returned to its original value **(Fig. 72)**.

The HCl concentration increased sharply after 4 PV of treatment fluid injection to the maximum value around 8.59 wt% HCl which was in the same range with BG-6-12 **(Fig. 73)**. After the flow had been switched back from acid treatment to brine, HCl concentration decreased significantly after around 0.75 PV of brine injection to 0.11 wt% HCl. This confirmed that most of the acid were pushed out by the brine.

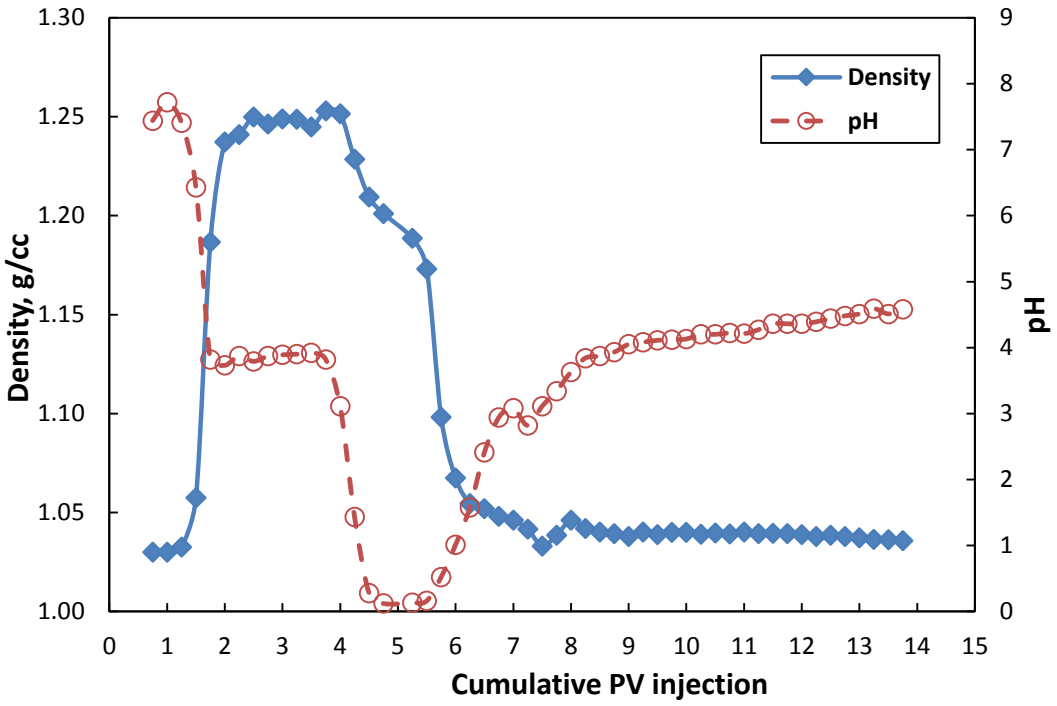

Fig. 72—Density and pH of Effluent Samples from Bandera-BG-6-9 at 250°F.

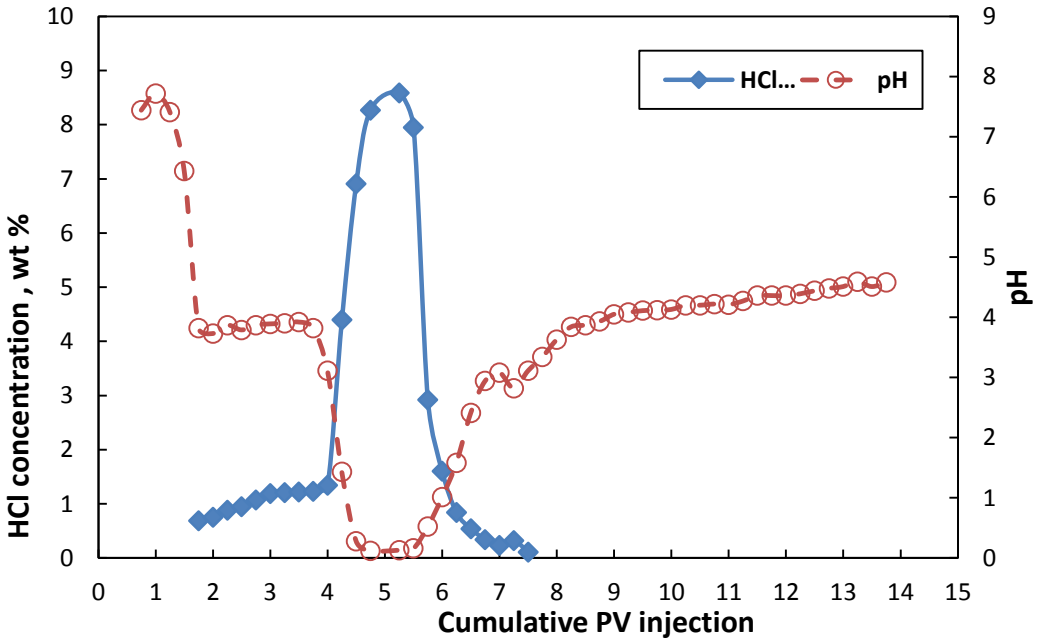

Fig. 73—HCl Concentration of Effluent Samples from Bandera-BG-6-9 at 250°F.

The porosity profile from CT scan results **(Fig. 74)** showed almost the same result between before and after treatment. The possible explanation was some iron precipitation in the core due to less iron dissolution compared to BG-6-12. **Table 13** gives the results comparison of addition of silica inhibitor case and the normal case at 250˚F on Bandera sandstone.

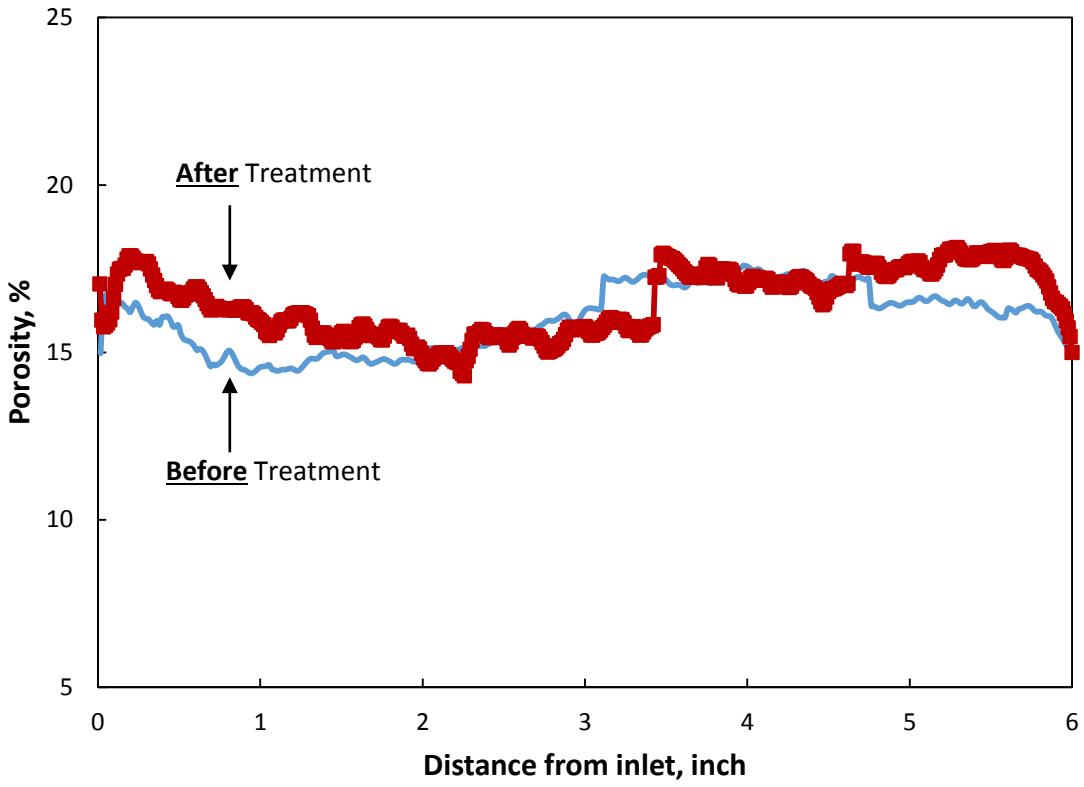

Fig. 74—Porosity Profile Before and After 30 wt% Urea-HCl Treatment for Bandera-BG-6-9.

Parameters		BG-6-12 (UHC)	BG-6-9 (UHC with Silica Inhibitor)
Permeability		+70 %	+49 %
ICP (mg/L)	Ca^{2+}	50,000	50,000
	Mg^{2+}	20,000	20,000
	Fe^{2+}	40,000	40,000
	Al^{3+}	5,000-10,000	5,000-8,000
	Si^{4+}	2,000-3,000	2,000-3,000
pH		0	0
HCl concentration (%)		9-10	8-9
Density (g/cm^3)		1.24	1.25

Table 13—Results Comparison between BG-6-12 and BG-6-2 (urea-HCl with normal additives vs. urea-HCl with addition of silica inhibitor at 250˚F).

Fourth Set of Experiments: 30 wt% Urea-HCl Including Four Additives -300˚F at 1 cm^3/min.

The fourth set of experiments involved the injection of 30 wt% urea-HCl with additives provided by a local company into Grey Berea sandstone, Bandera sandstone, and Silurian dolomite cores to study the effect of acidizing on each lithology at 300°F. This set of experiments will show the effect of temperature on the stimulation results.

Grey Berea Sandstone (G-6-21) at 300˚F using Urea-HCl with Four Additives

Regarding the pressure drop profile of Grey Berea sandstone (G-6-21) in **Fig. 75**. The stabilized pressure drop after the treatment was higher than the stabilized pressure drop

before the treatment. This can imply the damage in permeability from treatment. The calculated final permeability decreased **13%** from the initial permeability.

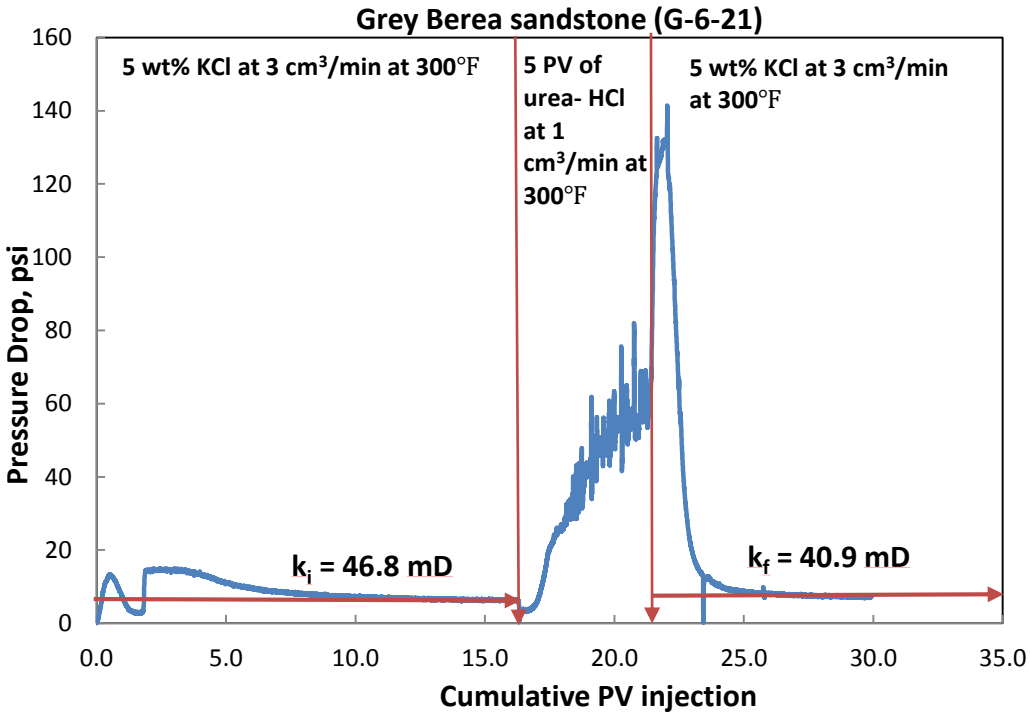

Fig. 75—Pressure Drop Profile Along the Berea-G-6-21 at 300˚F (urea-HCl + 4 additives)

Some precipitates were observed in the effluent samples after 1.5 PV (pH = 4.14) acid injection **(Fig. 76)**. According to ICP results, high iron concentration (20,000 ppm) was observed in the core effluent samples **(Fig. 77)**. The high iron concentration was attributed to the dissolution of chlorite and illite clays in the sandstone. However, the iron concentration was about 45% of the iron concentration found in G-6-22 (urea-HCl at 250˚F). The calcium and magnesium concentrations also increased after 1.5 PV of treatment confirming the dissolution by urea-HCl at high temperature. The peak

concentration of Ca^{2+} was about the same with G-6-22, while the peak concentration of Mg^{2+} was about half of G-6-22. Al^{3+} was present due to the dissolution of kaolinite and feldspars but in very low concentration. The lower Mg^{2+} and Fe^{2+} dissolutions in this experiment (urea-HCl at 300˚F) compared to urea-HCl treatment at 250˚F were the reasons for damage in permeability of G-6-21. The injection, production face, and side view of Berea-G-6-21 after acid treatment were shown in **Fig. 78**.

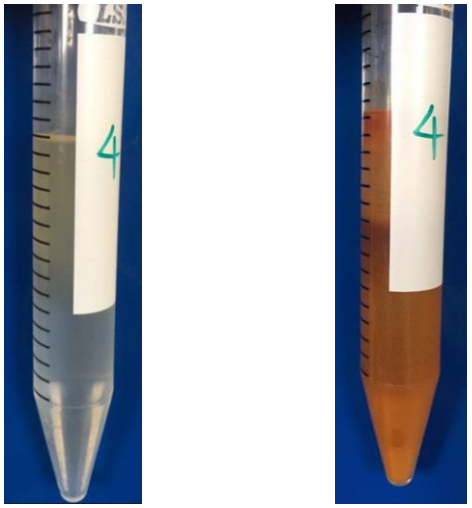

During coreflood **After 4 days**

Fig. 76—Precipitates from Effluent Samples of Berea-G-6-21.

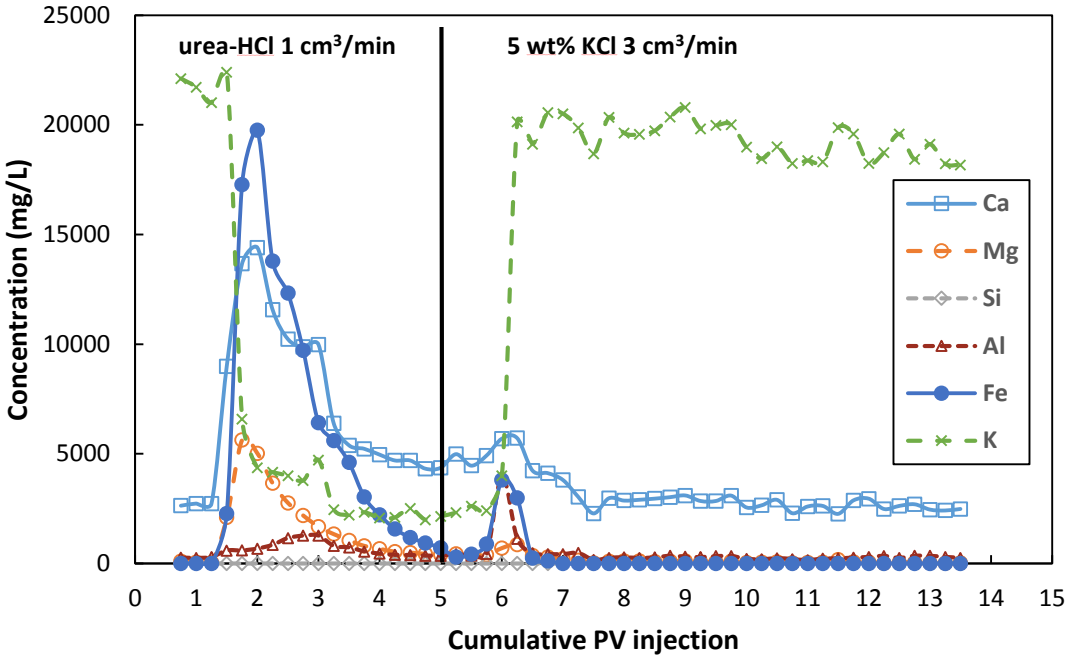

Fig. 77—ICP Analysis of 30 wt% Urea-HCl with Berea-G-6-21 at 300˚F.

Fig. 78—Injection Face, Production Face, and Side View of Berea-G-6-21 After Acid Treatment.

The initial pH of the effluent samples containing 5 wt% KCl brine was approximately 6.5. The pH sharply decreased as the acid was injected to reach a pH of 3.3 **(Fig. 79)**. The high pH of spent acid along with low iron dissolution from ICP indicated formation damage due to the iron precipitation in the core at pH >2 (Taylor et al. 1999; Crowe 1986).

The density of injected brine is around 1.029 g/cc. When the 5 PV of treatment fluid was injected, the density started to increase (after 1.5 PV injection) as the acid dissolved more Ca, Mg, Al, and Fe. As the live acid became spent acid, fewer H^+ ions reacted with the carbonates resulting in fewer cations dissolution. Consequently, a gradual decrease in density was observed. When the flow was switched back to brine, the density returned to its original value **(Fig. 79)**. The peak density of this experiment was lower than G-6-22 effluent samples was due to less iron dissolution from the ICP results.

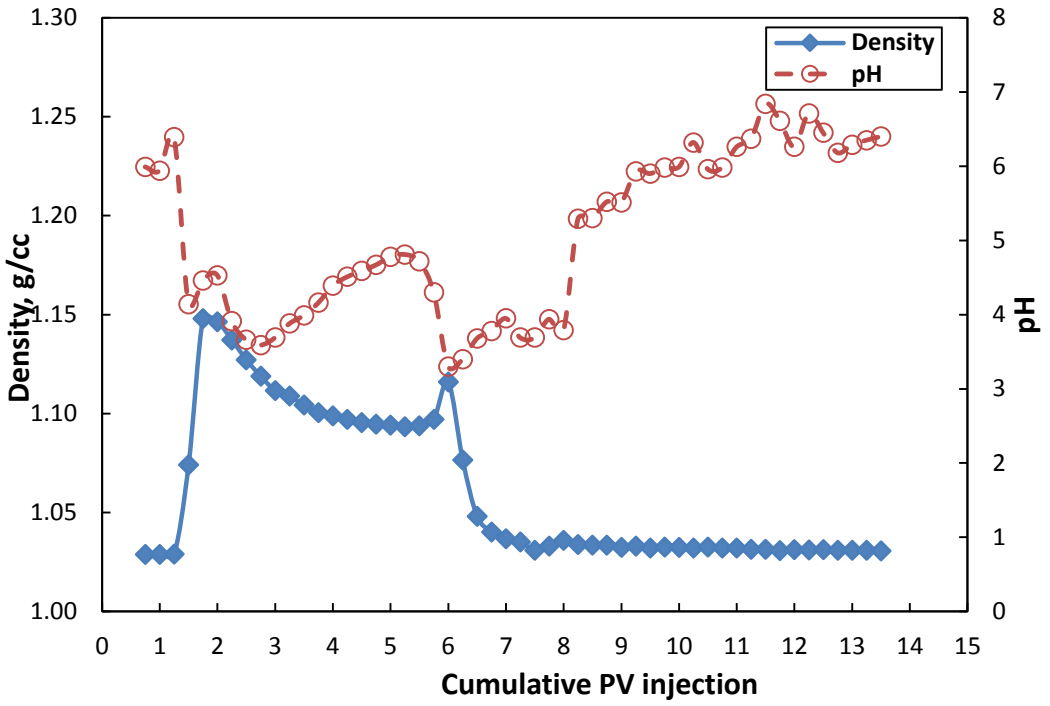

Fig. 79—Density and pH of Effluent Samples from Berea-G-6-21 at 300˚F.

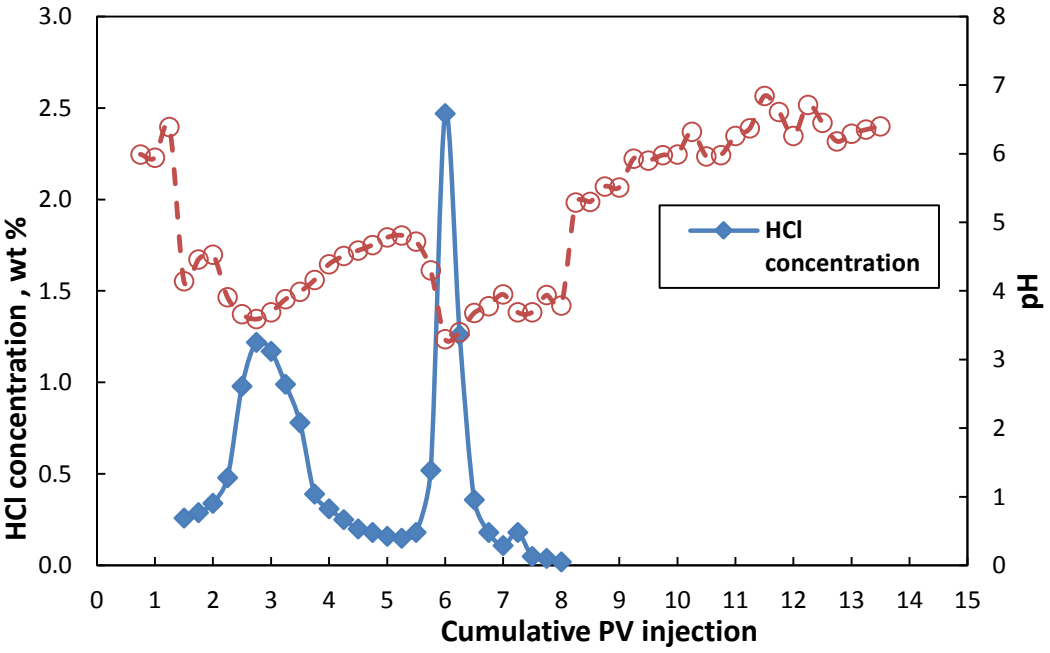

Fig. 80—HCl Concentration and pH of Effluent Samples from Berea-G-6-21 at 300˚F.

The HCl concentration of the effluent samples of Grey Berea (G-6-21) increased after 2.25 PV and decreased after 3 PV of acid injection. It was again increased after 5.5 PV of acid injection to the maximum value around 2.47 wt% HCl **(Fig. 80)**, which was quite low compared to the results of G-6-22. After the flow had been switched back from acid to brine, HCl concentration decreased significantly after around 1.25 PV of brine injection to 0.02 wt% HCl. This confirmed that all the acid was pushed out by the brine.

The CT scan results indicated a decrease in porosity on the first inch of the core from the injection face and then it increased after passed the 1-inch distance until the end of the core **(Fig. 81)**. Table 14 gives the results comparison of urea-HCl at 250 and 300˚F.

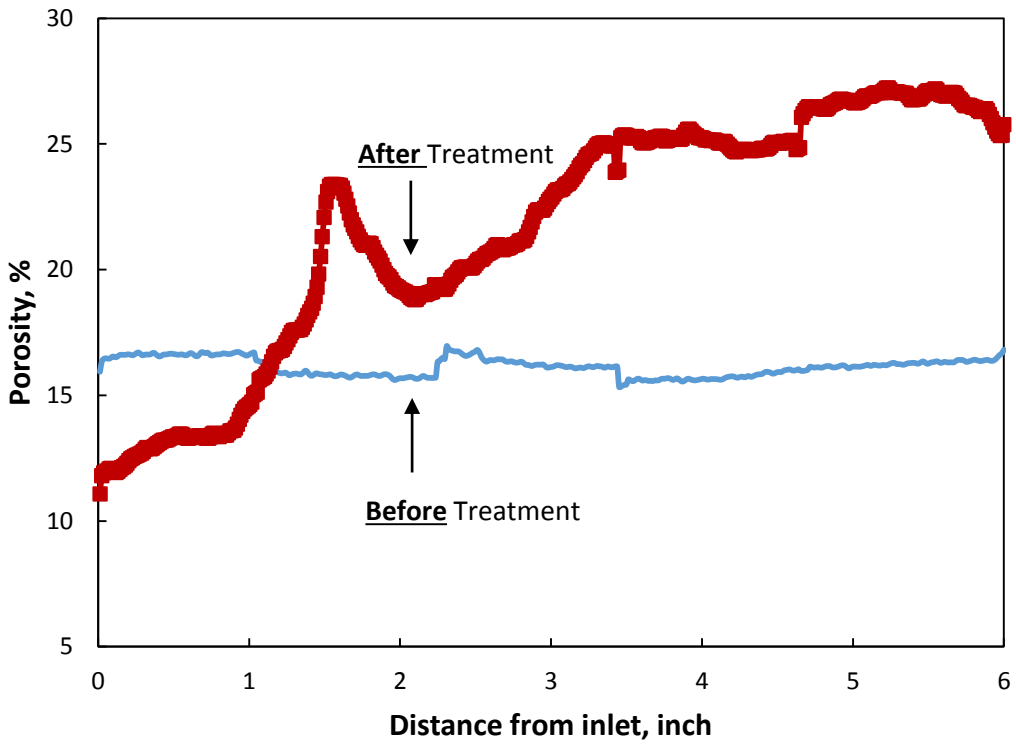

Fig. 81—Porosity Profile Before and After 30 wt% Urea-HCl Treatment for Berea-G-6-21.

Parameters		G-6-22 (250°F)	G-6-21 (300°F)
Permeability		+159 %	-13 %
ICP (mg/L)	Ca^{2+}	15000	15,000
	Mg^{2+}	10000	6,000
	Fe^{2+}	45000	20,000
	Al^{3+}	12000	2,000
	Si^{4+}	3000	0
pH		0	2.5-3.5
HCl concentration (%)		14-16	1-2.5
Density (g/cm^3)		1.21	1.15

Table 14—Results Comparison between G-6-22 and G-6-21 (urea-HCl at 250 vs. 300˚F).

Bandera Sandstone (BG-6-7) at 300˚F using Urea-HCl with Four Additives

According to the pressure drop profile of Bandera sandstone (BG-6-7) in **Fig. 82**. The stabilized pressure drop after the treatment was almost the same with the stabilized pressure drop before the treatment implying no enhancement or damage in permeability. The calculated final permeability decreased **2%** from the initial permeability.

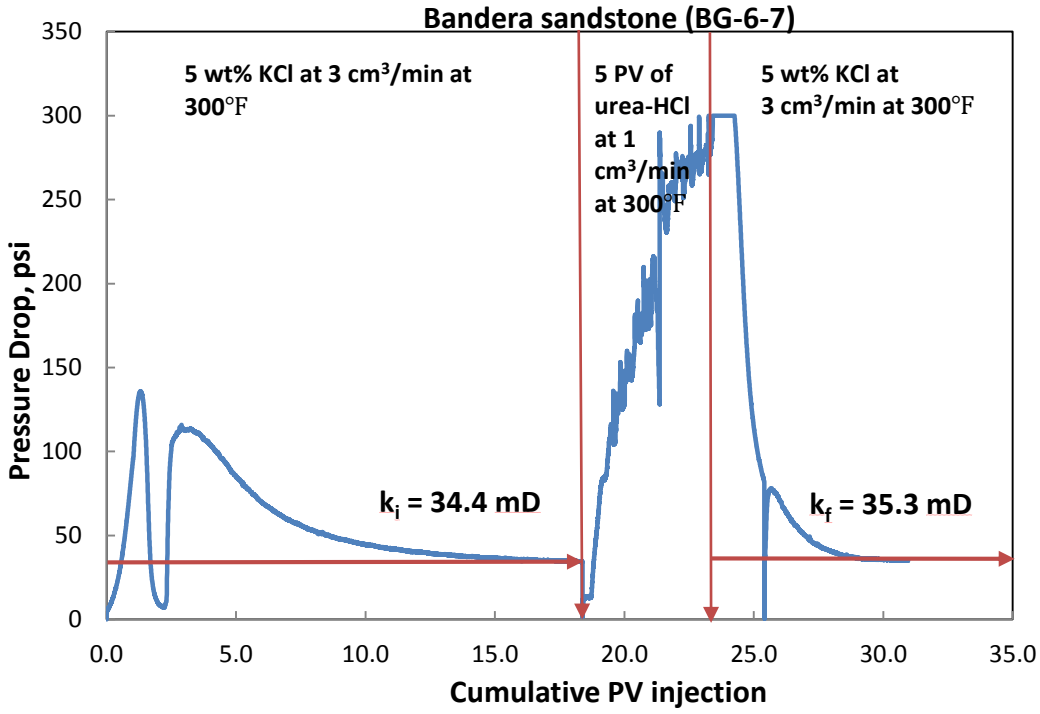

Fig. 82—Pressure Drop Profile Along the Bandera-BG-6-7 at 300˚F.

Some suspension and precipitates were also observed in the effluent samples after 1.75 PV (pH = 6.07) acid injection **(Fig. 83)**. According to ICP results **(Fig. 84)**, the iron concentration was relatively small (2000-5000 ppm) compared to the previous experiments. The low iron concentration can be the cause of iron precipitation in the core, which reflected in no stimulation. The calcium and magnesium concentrations also increased after 1.5 PV of treatment confirming the dissolution by urea-HCl. The dissolutions of Ca^{2+} and Mg^{2+} of this experiment were also less than BG-6-12 (urea-HCl at 250˚F). Al^{3+} was present due to the dissolution of kaolinite and feldspars. K^{+} concentration from 5 wt% KCl brine was also decreased during the reaction interval of

acid with the core. The injection face, production face, and side view of Bandera-BG-6-7 after acid treatment were shown in **Fig. 85**.

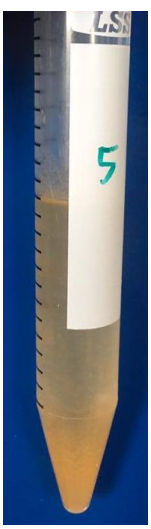

During coreflood

After 4 days

Fig. 83—Suspension and Precipitates of Bandera-BG-6-7.

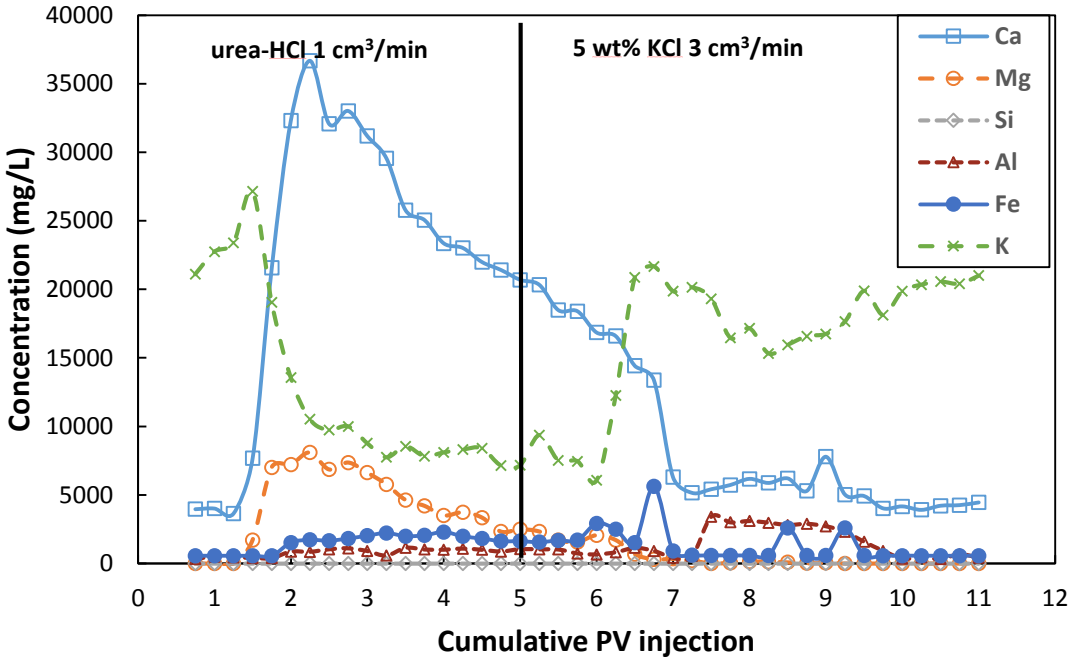

Fig. 84—ICP Analysis of the Effluent Samples- 30 wt% Urea-HCl with Bandera-BG-6-7 at 300˚F.

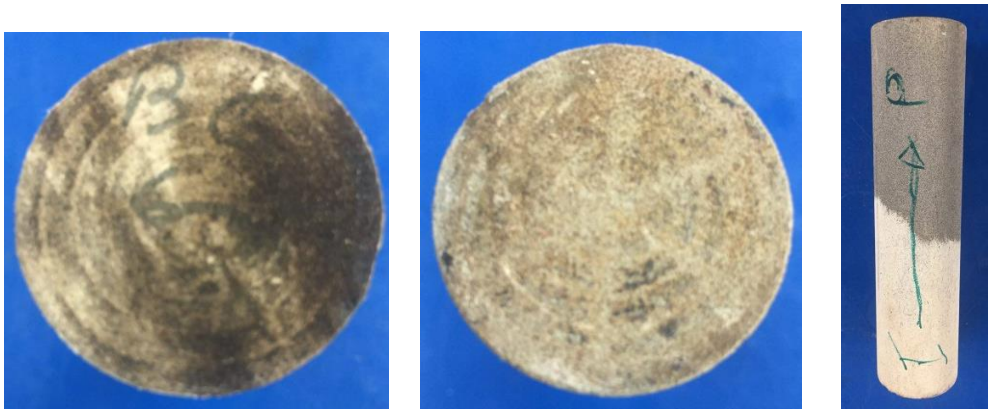

Fig. 85—Injection Face, Production Face, and Side View of Bandera-BG-6-7 After Acid Treatment.

The same procedure with BG-6-12 was applied for SEM-EDS analysis on BG-6-7 precipitates. The SEM images showed both granular (crystallization) and amorphous structures **(Fig. 86 and Fig. 87)**, which suggested some fines migration resulted from the

treatment. The EDS results of both granular and amorphous parts in atomic percentage indicated mainly Fe and O (**Table 15 and Table 16**).

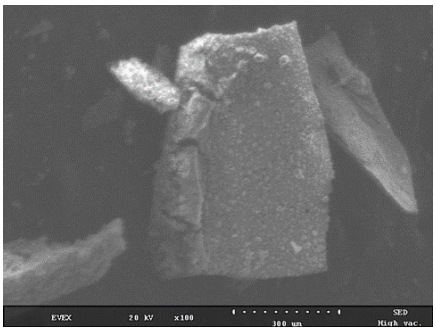

Magnification x100

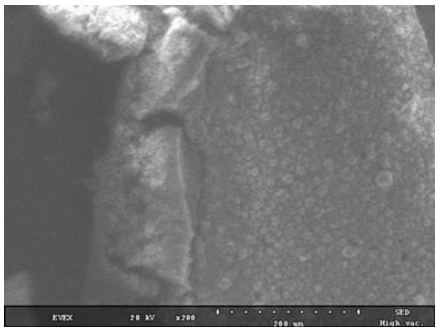

Magnification x200

Fig. 86—SEM Images for BG-6-7 Precipitates (Granular part).

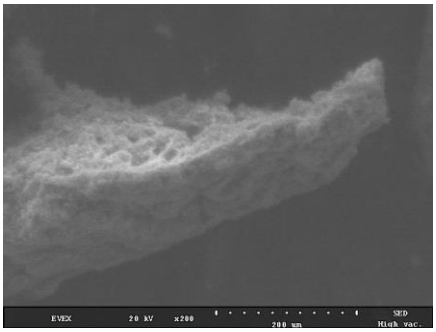

Magnification x100

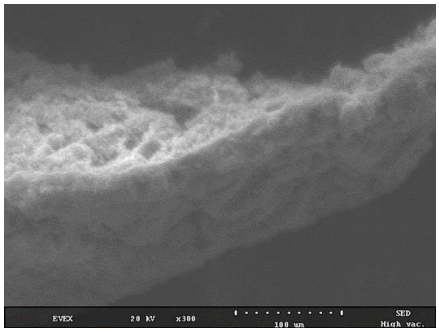

Magnification x200

Fig. 87—SEM Images for BG-6-7 Precipitates (Amorphous part).

Element	Atomic (%)
Fe	30.48
O	68.14
Cl	1.38

Table 15—EDS Results for Granular Part of BG-6-7 Precipitates.

Element	Atomic (%)
Fe	27.65
O	69.89
Al	1.67
Cl	0.78

Table 16—EDS Results for Amorphous Part of BG-6-7 Precipitates.

The initial pH of the effluent samples containing 5 wt% KCl brine was approximately 7. The pH decreased as the acid was injected to reach the lowest pH of 3.94 **(Fig. 88)**. However, the lowest pH was quite high compared to the previous experiments. This indicated that most of the acid were spent during the treatment with minimal or no live acid left in the effluent samples. The high pH value with very low iron dissolution from ICP result can cause formation damage due to iron precipitation at pH >2 (Taylor et al. 1999; Crowe 1986). Thereafter, the pH rose as the core was flushed with brine.

The density of injected brine was around 1.029 g/cc. When the 5 PV of treatment fluid was injected, the density started to increase (after 1.5 PV injection) as the acid dissolved more Ca, Mg, Al, and Fe, which was consistent with the ICP results. As the live

acid became spent acid, fewer H^+ ions reacted with the carbonates resulting in less cation dissolution. Consequently, a gradual decrease in density was observed. When the flow was switched back to brine, the density returned to its original value **(Fig. 88)**. The maximum density seen in this experiment was less than in BG-6-12 effluents due to less iron dissolution from ICP results.

The HCl concentration ranged from 0.01 - 0.15 % **(Fig. 89)**. This was consistent with the high pH value.

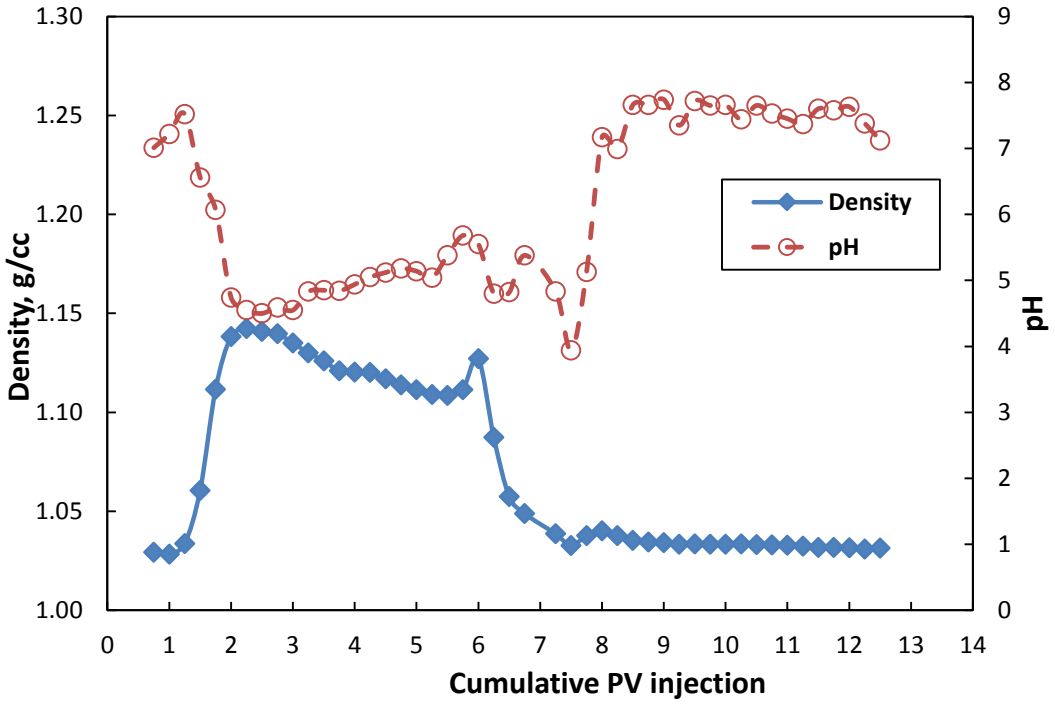

Fig. 88—Density and pH of Effluent Samples from Bandera-BG-6-7 at 300°F.

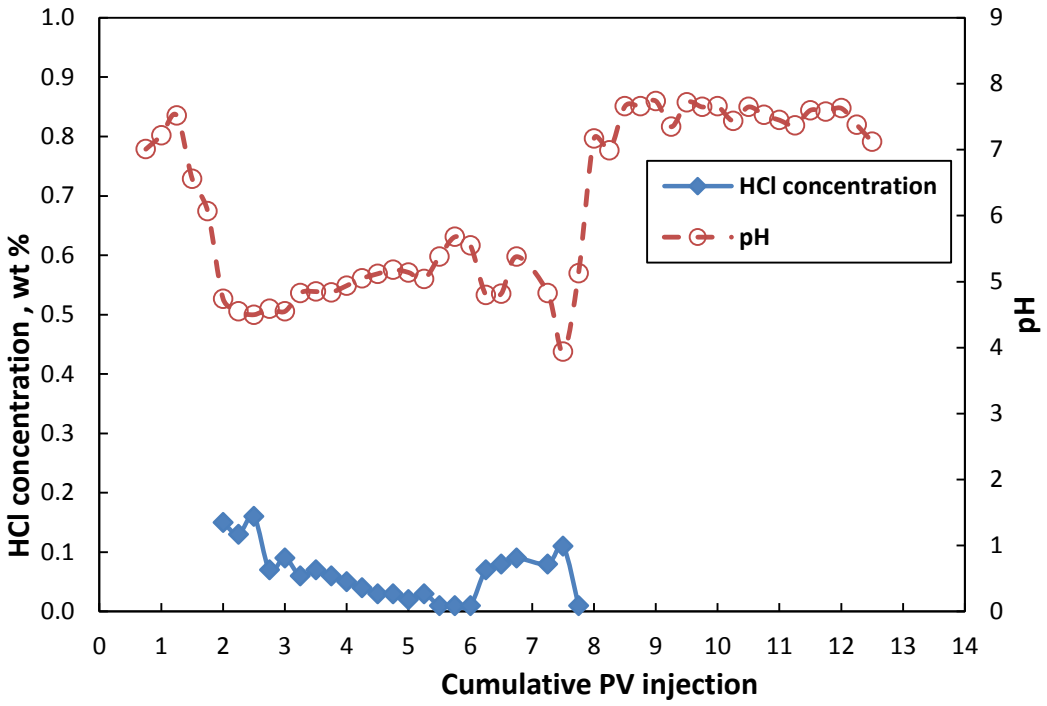

Fig. 89—HCl Concentration of Effluent Samples from Bandera-BG-6-7 at 300˚F.

The CT scan results indicated a decrease in the core porosity after the treatment, which means the cores were damaged. The porosity profile **(Fig. 90)** showed significant decline in porosity along the core after the treatment. The main reason behind this was formation damage due to iron precipitation in the core which was supported by ICP and pH result. **Table 17** shows the results comparison of urea-HCl at 250 and 300˚F.

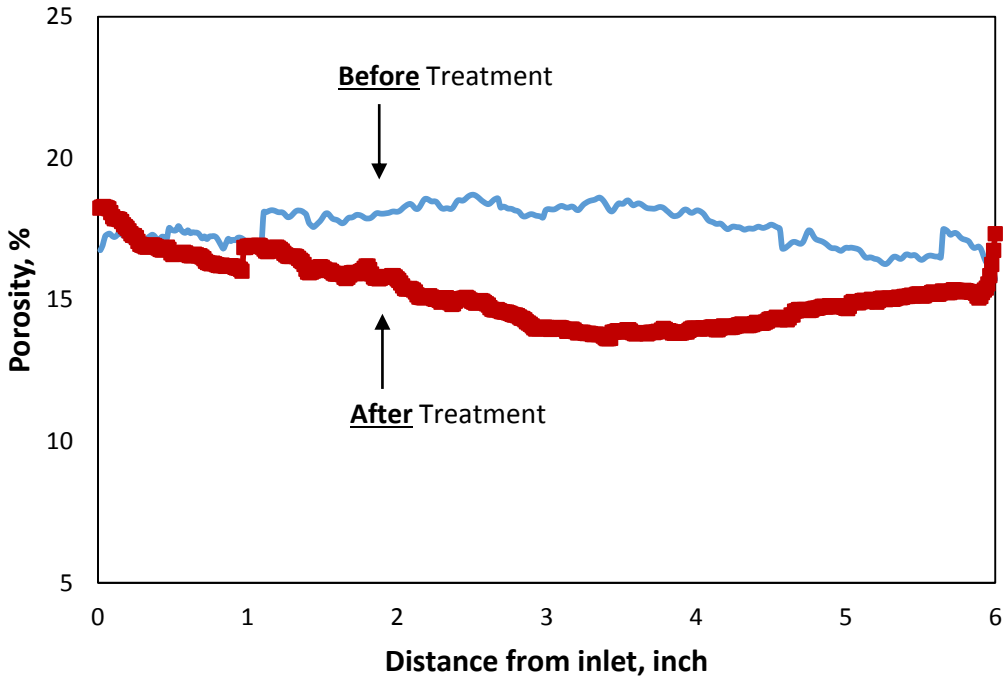

Fig. 90—Porosity Profile Before and After 30 wt% Urea-HCl Treatment for Bandera-BG-6-7.

Parameters		BG-6-12 (250°F)	BG-6-7 (300°F)
Permeability		+70 %	-2 %
ICP (mg/L)	Ca^{2+}	50,000	35,000
	Mg^{2+}	20,000	7,500
	Fe^{2+}	40,000	2,000-5,000
	Al^{3+}	5,000-10,000	1,000-3,000
	Si^{4+}	2,000-3,000	0
pH		0	4-5
HCl concentration (%)		9-10	0.1-0.18
Density (g/cm^3)		1.24	1.15

Table 17—Results Comparison between BG-6-12 and BG-6-7 (urea-HCl at 250 vs. 300°F)

Silurian Dolomite (SD-6-41) at 300˚F using Urea-HCl with Four Additives

At first, 5 wt% KCl brine was injected in the production direction, while heating up the system to 300°F until the pressure drop was stabilized. The pressure drop then increased as the flow was switched from brine to acid in an injection direction since the acid had a higher viscosity compared to 5 wt% KCl **(Fig. 91)**. After 5 PV of treatment, the stabilized pressure drop after the treatment was lower than that before the treatment. However, the acid breakthrough did not occur as in the case of urea-HCl at 250°F.

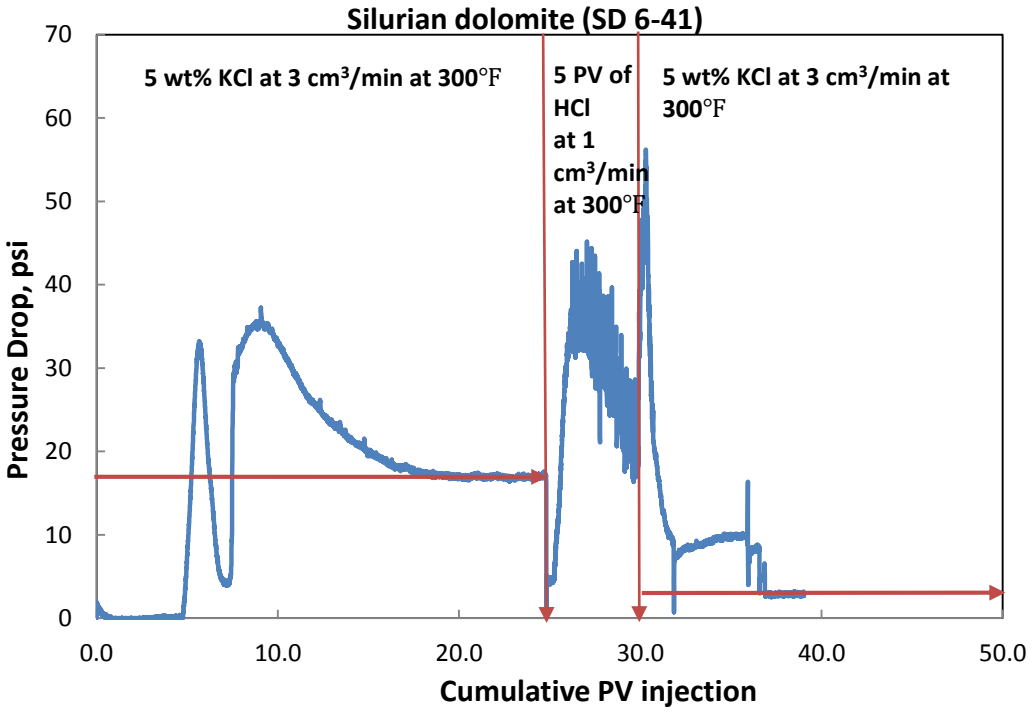

Fig. 91—Pressure Drop Profile Along the Silurian Dolomite SD-6-41 at 300˚F.

Some suspension and precipitates from the dolomite dissolution were observed in the effluent samples after 1.5 PV (pH = 6.14) acid injection **(Fig. 92)**. The calcium and

magnesium concentration from ICP **(Fig. 93)** also increased after 1.5 PV of treatment confirming the dissolution of dolomite by urea-HCl. However, the concentration of Ca^{2+} and Mg^{2+} were less than the previous treatment using urea-HCl at 250˚F. K^{+} concentration from 5 wt% KCl brine was also decreased during the reaction interval of acid with the core. **Fig. 94** shows the injection face, production face, and side view of SD-6-41 after acid treatment. Face dissolution was observed at the injection face of the core.

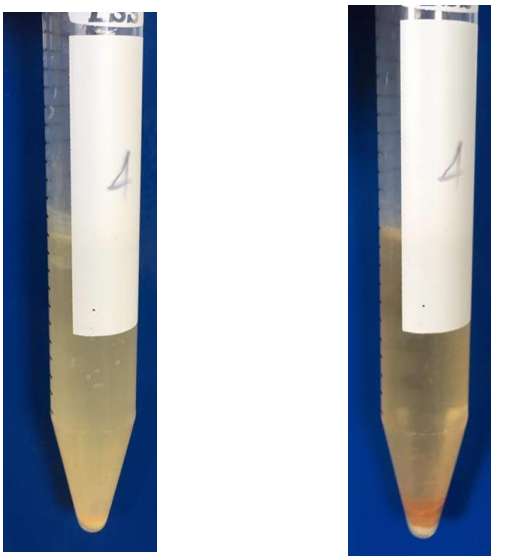

Fig. 92—Suspension and Precipitates of Silurian Dolomite SD-6-41.

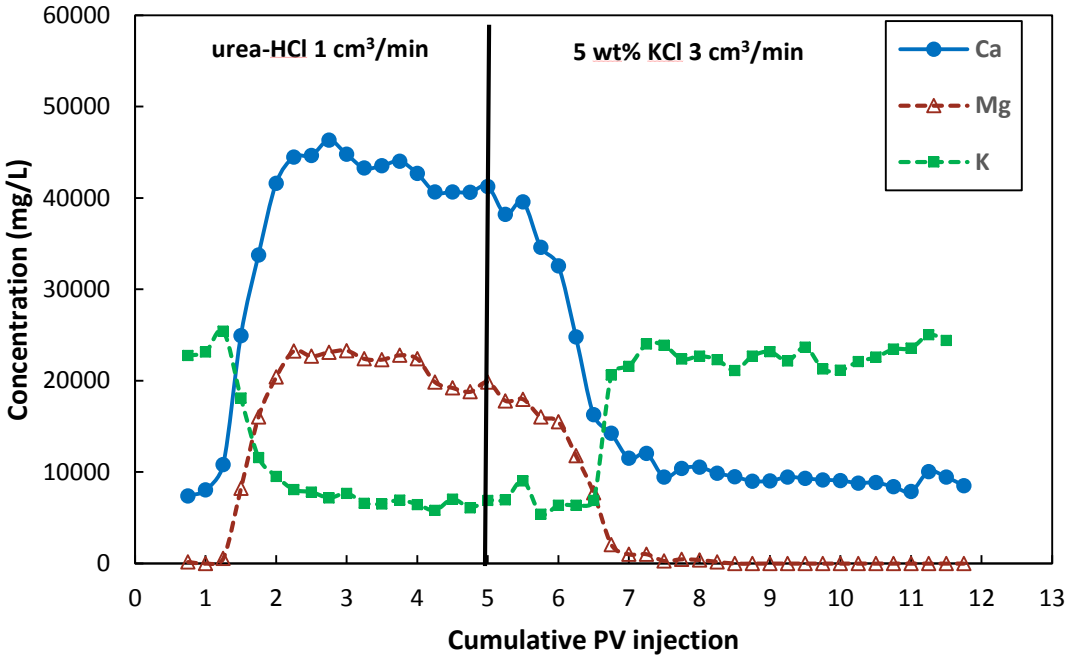

Fig. 93—ICP Analysis of the Effluent Samples- 30 wt% Urea-HCl with Silurian Dolomite SD-6-41 at 300˚F.

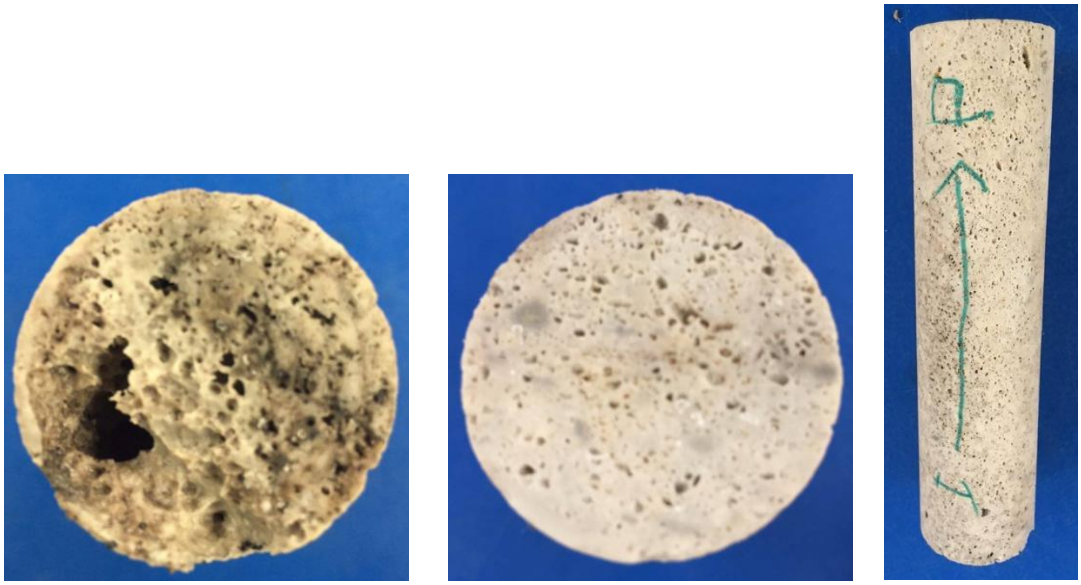

Fig. 94—Injection Face, Production Face, and Side View of Silurian Dolomite SD-6-41 After Acid Treatment.

The initial pH of the effluent samples containing 5 wt% KCl brine was approximately 7. The pH decreased as the acid was injected to reach the lowest pH of 4.61 **(Fig. 95)**. However, the lowest pH was quite high compared to the previous experiments. This indicated that most of the acid were spent during the treatment with minimal or no live acid left in the effluent samples. Thereafter, the pH rose as the core was flushed with brine.

The density of injected brine is around 1.029 g/cc. When the 5 PV of treatment fluid was injected, the density started to increase (after 1.5 PV injection) as the acid dissolved more Ca and Mg which was consistent with the ICP results. As the live acid became spent acid, fewer H^+ ions reacted with the carbonates resulting in less cation dissolution. Consequently, a gradual decrease in density was observed. When the flow was switched back to brine, the density returned to its original value **(Fig. 95)**.

The HCl concentration ranged from 0.01 - 0.17 % **(Fig. 96)** which was quite low compared to the experiment conducted at 250˚F.

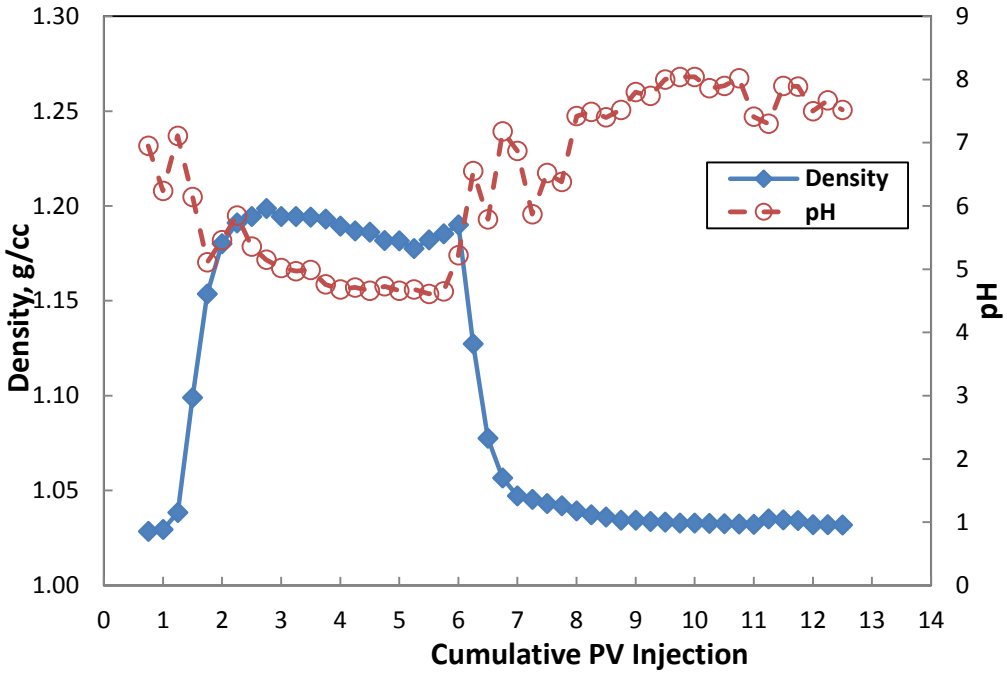

Fig. 95—Density and pH of Effluent Samples from Silurian Dolomite SD-6-41 at 300˚F.

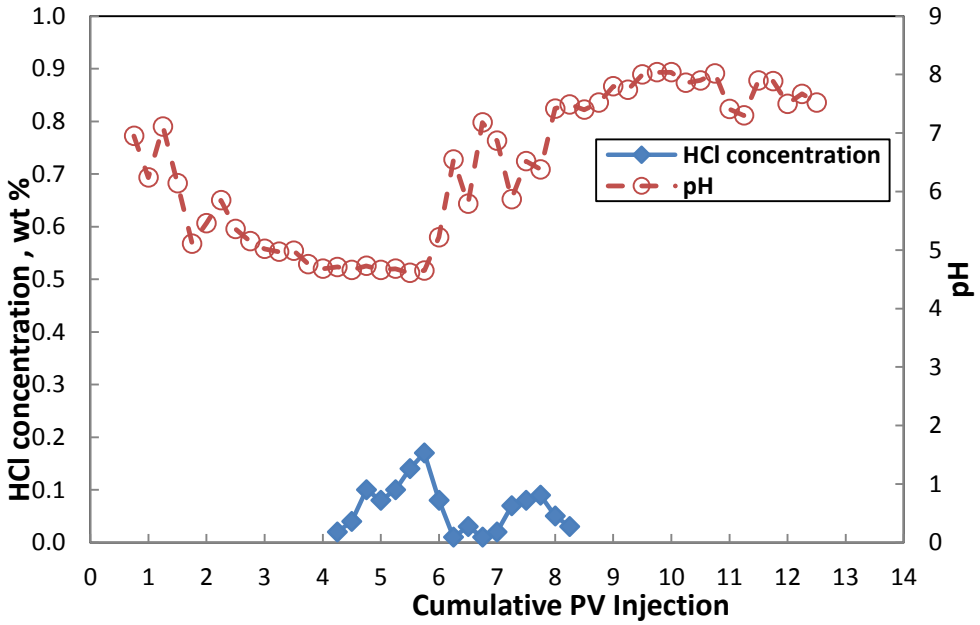

Fig. 96—HCl Concentration of Effluent Samples from Silurian Dolomite SD-6-41 at 250˚F.

The CT scan **(Fig. 97)** result showed the formation of 1 main wormhole along the core. However, the breakthrough did not occur after 5 PV of the acid injection. Some face dissolution was also observed from the CT scan at the injection face. **Table 18** gives the results comparison of urea-HCl at 250 and 300˚F on Silurian dolomite.

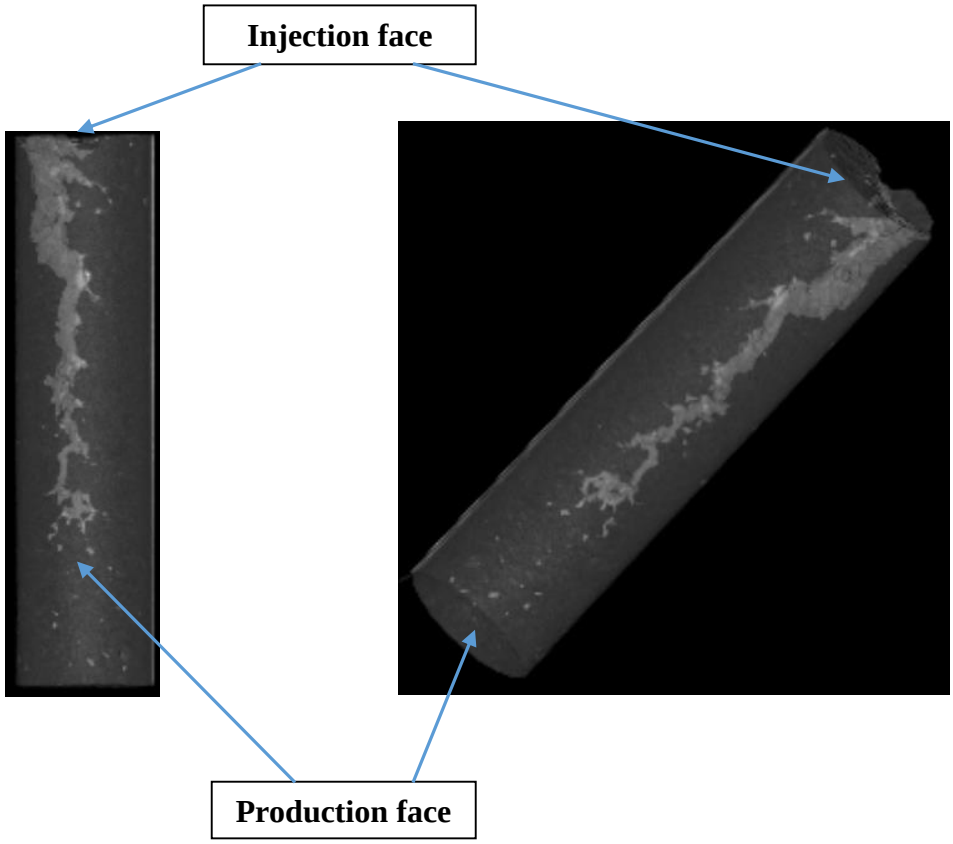

Fig. 97—Wormhole Propagation from CT Scan for Silurian Dolomite SD-6-41.

Parameters		SD-6-40 (250°F)	SD-6-41 (300°F)
Permeability		3	Not BT
ICP (mg/L)	Ca^{2+}	60,000-70,000	45,000
	Mg^{2+}	55,000-65,000	25,000
pH		0	4.5
HCl concentration (%)		9-11	0.2
Density (g/cm^3)		1.22	1.2

Table 18—Results Comparison between SD-6-40 and SD-6-41 (urea-HCl at 250 vs. 300˚F).

Fifth Set of Experiments: 15 wt% HCl including Four Additives -300˚F at 1 cm^3/min

The fifth set of experiments involved the injection of 15 wt% HCl with additives provided by a local service company into Grey Berea sandstone, Bandera sandstone, and Silurian dolomite cores to study the effect of acidizing on each lithology at 300°F. A flow rate of 1 cm^3/min was used throughout the experiments. 5 wt% KCl brine and 5 PV of treatment fluid were injected in the injection direction. The effluent samples from the coreflood experiments were collected after half PV of acid injection and every quarter PV until the end of each experiment. This set of results was used to compare with the stimulation by urea-HCl at 300°F.

Grey Berea Sandstone (G-6-17) at 300˚F using HCl with Four Additives

Regarding the pressure drop profile of Grey Berea sandstone (G-6-17) in **Fig. 98**, the stabilized pressure drop after the treatment was higher than that before the treatment. This can imply the damage in permeability from the treatment.

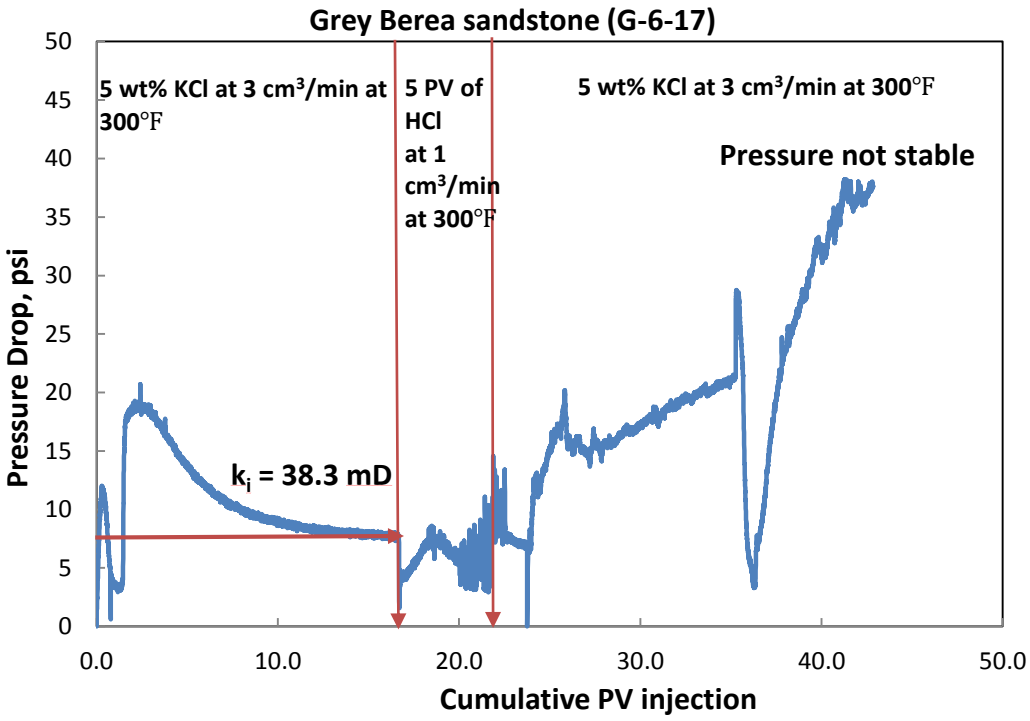

Fig. 98—Pressure Drop Profile Along the Berea-G-6-17 at 300˚F (HCl + 4 additives).

Some precipitates were observed in the effluent samples after 1.5 PV (pH = 5.9) acid injection **(Fig. 99)**. According to ICP results, a high iron concentration (50,000 ppm) was observed in the core effluent samples **(Fig. 100)**. This amount of dissolved iron was greater than the treatment by urea-HCl at 300˚F. The calcium and magnesium concentrations also increased after 1.75 PV of treatment confirming the dissolution by HCl. Al^{3+} was present due to the dissolution of kaolinite and feldspars. The peak concentration (30,000 ppm) of Al^{3+} was quite high compared to other experiments. This was the main reason for severe damage in the core due to clay instability (kaolinite) and fines migration at temperatures above 200°F in HCl (Coulter and Jennings 1999). The

injection, production face and side view of Berea-G-6-17 after acid treatment were shown in **Fig. 101**.

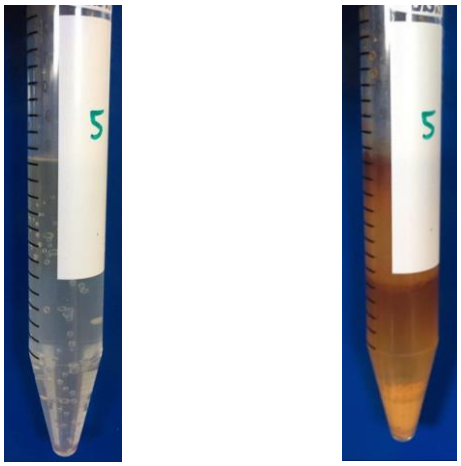

During coreflood **After 4 days**

Fig. 99—Precipitates from Effluent Samples of Berea-G-6-17.

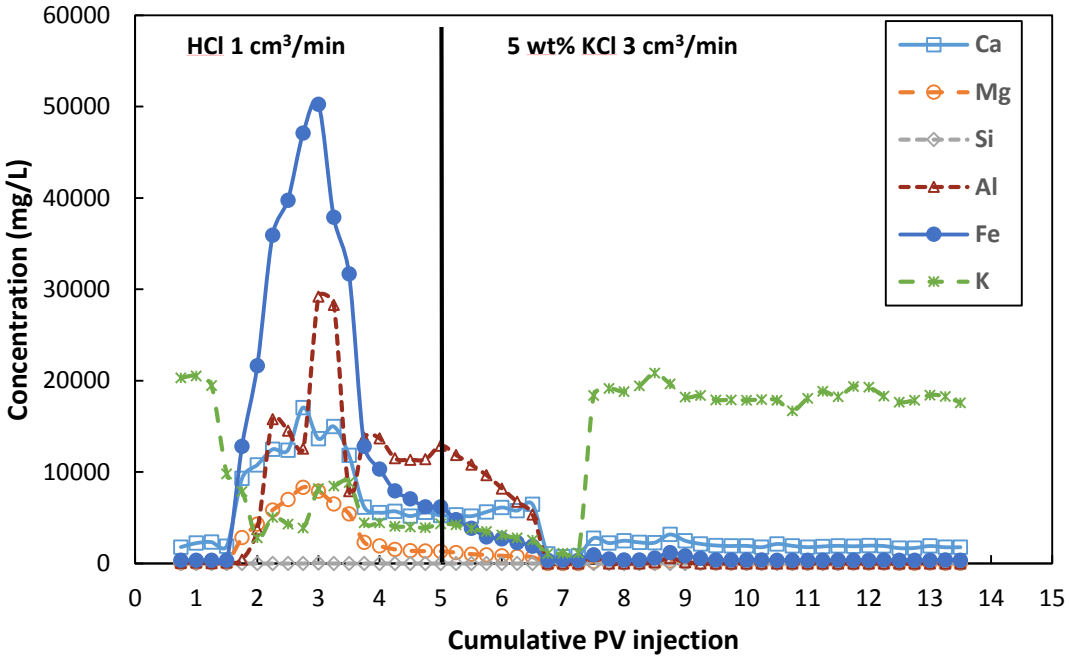

Fig. 100—ICP Analysis of 15 wt% HCl with Berea-G-6-17 at 300˚F.

Fig. 101—Injection Face, Production Face, and Side View of Berea-G-6-17 After Acid Treatment.

The initial pH of the effluent samples containing 5 wt% KCl brine was approximately 8. The pH sharply decreased as the acid was injected to reach a pH of 0 **(Fig. 102)**. This indicated that the effluent samples contained live acid and not all of the acid was spent to dissolve the carbonate minerals in the Grey Berea core. The pH of this experiment was lower compared to the treatment by urea-HCl at 300˚F but in the same range with the treatment by HCl at 250˚F. Subsequently, the pH rose as the core was flushed with brine.

The density of injected brine was around 1.029 g/cc. When the 5 PV of treatment fluid was injected, the density started to increase (after 1.75 PV injection) as the acid dissolved more Ca, Mg, Al, Si, and Fe. As the live acid became spent acid, less H^+ ions reacted with the carbonates resulting in fewer cations dissolution. Consequently, a gradual decrease in density was observed. When the flow was switched back to brine, the density returned to its original value **(Fig. 102)**. The peak of the density of this experiment was in the same range with the treatment by HCl at 250˚F but higher compared to the treatment by urea-HCl at 300˚F. This was due to higher iron dissolution in this experiment compared to the treatment by urea-HCl at 300˚F.

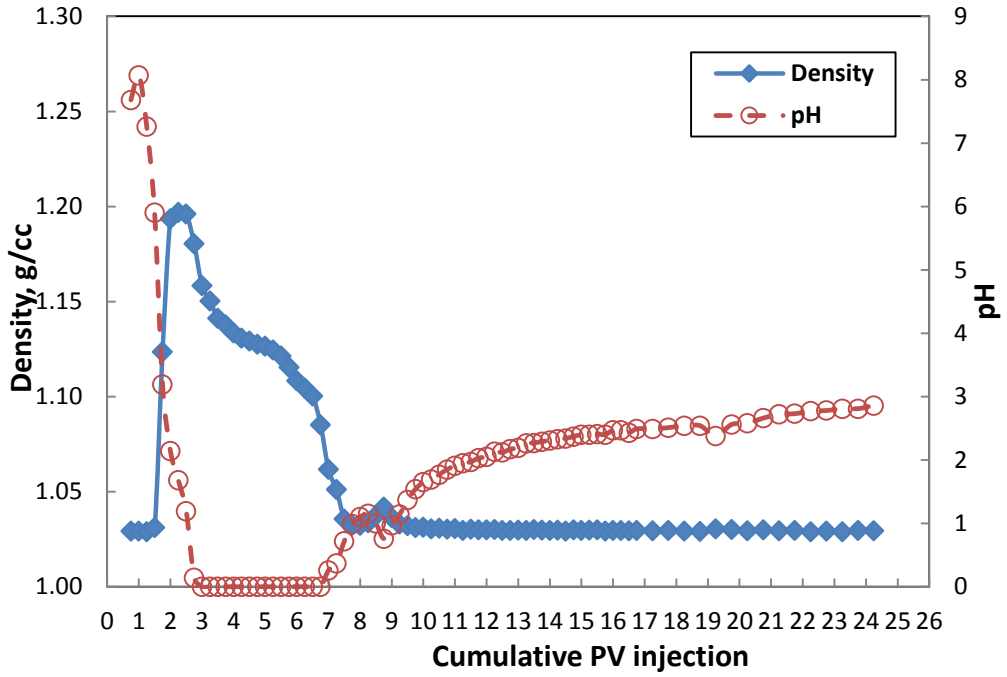

Fig. 102—Density and pH of Effluent Samples from Berea-G-6-17 at 300˚F.

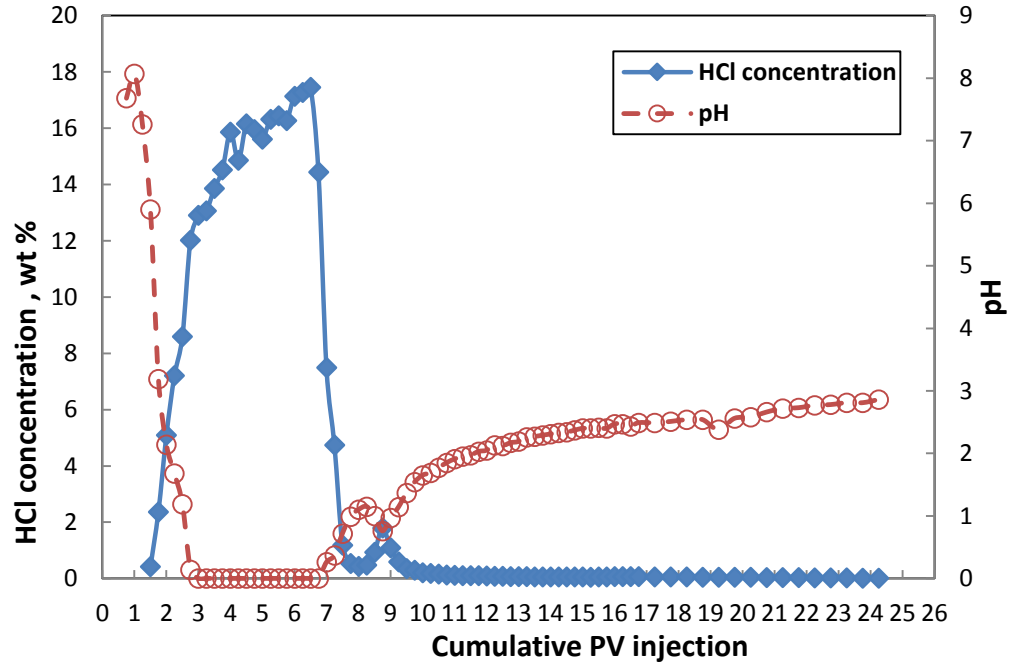

Fig. 103—HCl Concentration and pH of Effluent Samples from Berea-G-6-17 at 300˚F.

The HCl concentration of the effluent samples of Grey Berea (G-6-17) increased sharply after 1.75 PV of acid was injected to the maximum value around 17.46 wt% HCl **(Fig. 103),** which was close to the equivalent HCl concentration of 15 wt% HCl plus additives (18.76 %). After the flow had been switched back from acid to brine, HCl concentration decreased significantly after around 1.75 PV of brine injection to 0.02 wt% HCl. This confirmed that all the acid was pushed out by the brine. The maximum acid concentration in this experiment was significantly higher than the treatment by urea-HCl at 300˚F.

CT scan results showed almost the same porosity profile along the core (**Fig. 104). Table 19** shows the results comparison of urea-HCl and HCl at 300˚F, while **Table 20** gives the results comparison of HCl at 250 and 300˚F.

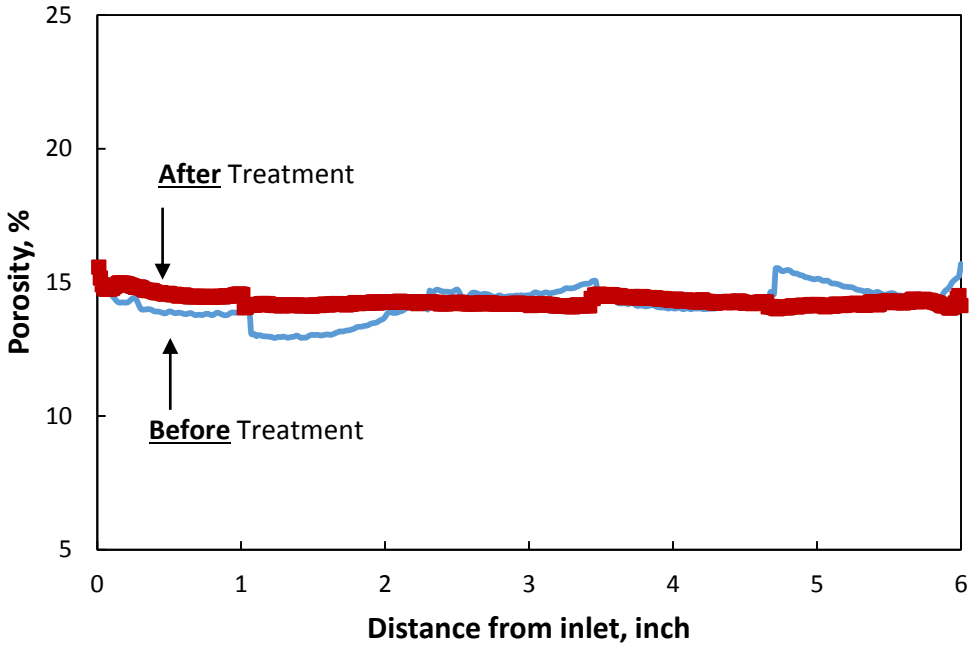

Fig. 104—Porosity Profile Before and After 15 wt% HCl Treatment for Berea-G-6-17.

Parameters		G-6-21 (UHC)	G-6-17 (HCl)
Permeability		-13 %	Not stabilized
ICP (mg/L)	Ca^{2+}	15,000	18,000
	Mg^{2+}	6,000	9,000
	Fe^{2+}	20,000	50,000
	Al^{3+}	2,000	30,000
	Si^{4+}	0	0
pH		2.5-3.5	0
HCl concentration (%)		1-2.5	16-18
Density (g/cm^3)		1.15	1.2

Table 19—Results Comparison between G-6-21 and G-6-17 (urea-HCl vs. HCl at 300˚F).

Parameters		G-6-27 (250°F)	G-6-17 (300°F)
Permeability		Not change	Not stabilized
ICP (mg/L)	Ca^{2+}	15,000	18,000
	Mg^{2+}	10,000	9,000
	Fe^{2+}	49,000	50,000
	Al^{3+}	15,000	30,000
	Si^{4+}	0	0
pH		0	0
HCl concentration (%)		18	16-18
Density (g/cm^3)		1.2	1.2

Table 20—Results Comparison between G-6-27 and G-6-17 (HCl at 250 vs. 300˚F).

Bandera Sandstone (BG-6-5) at 300˚F using 15 wt% HCl with Four Additives

Regarding the pressure drop profile of Bandera sandstone (BG-6-5) in **Fig. 105**, the stabilized pressure drop after the treatment was lower than that before the treatment. This can imply the enhancement in permeability resulted from the dissolution of the carbonate minerals in sandstone which will be confirmed from Ca^{2+} and Mg^{2+} dissolved as shown in the next section. The calculated final permeability increased **71%** from the initial permeability.

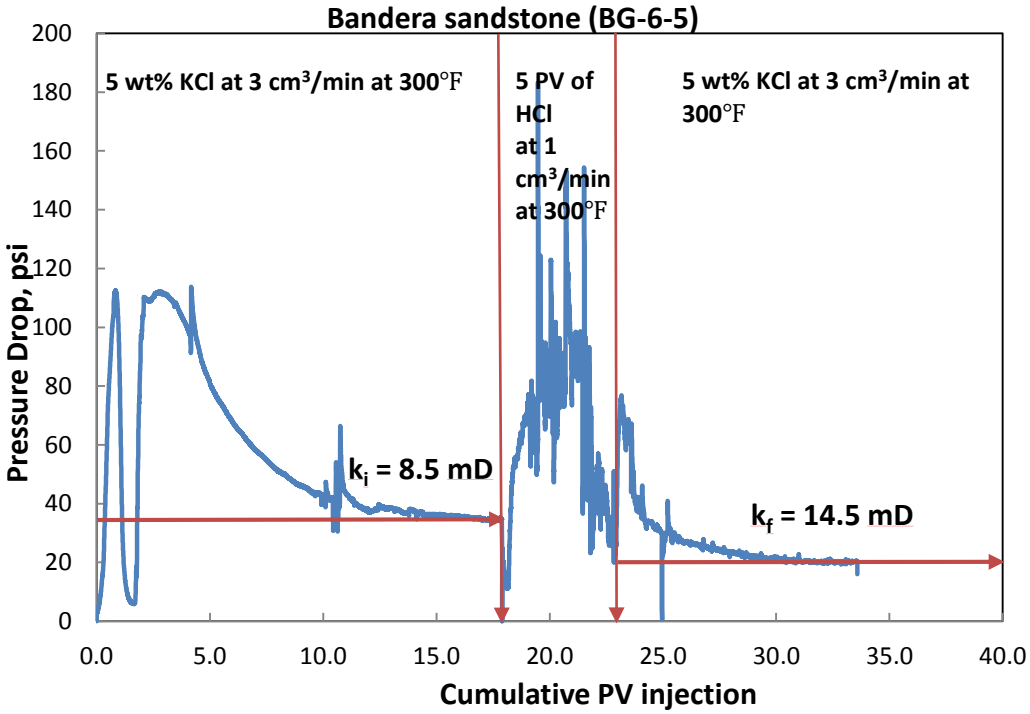

Fig. 105—Pressure Drop Profile Along the Bandera-BG-6-5 at 300˚F.

Some suspension and precipitates were also observed in the effluent samples after 1.75 PV (pH = 3.9) acid injection **(Fig. 106)**. According to ICP results **(Fig. 107)**, the iron

concentration was relatively low (10,000-17,500 ppm) compared to the previous experiments conducted by HCl at 250˚F, but still higher than the treatment by urea-HCl at 300˚F. The calcium and magnesium concentrations also increased after 1.5 PV of treatment confirming the dissolution by HCl. The maximum concentration of Ca and Mg in this experiment were almost two times of highest concentration in the experiment conducted by urea-HCl at 300˚F. This could be the main reason of stimulation in permeability of this experiment. Al^{3+} was present due to the dissolution of kaolinite and feldspars. K^{+} concentration from 5 wt% KCl brine was also decreased during the reaction interval of acid with the core. **Fig. 108** shows the injection face, production face, and side view of Bandera-BG-6-5 after acid treatment.

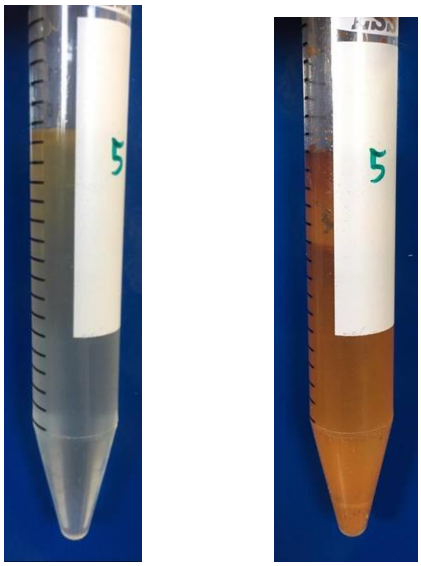

During coreflood **After 4 days**

Fig. 106—Suspension and Precipitates of Bandera-BG-6-5.

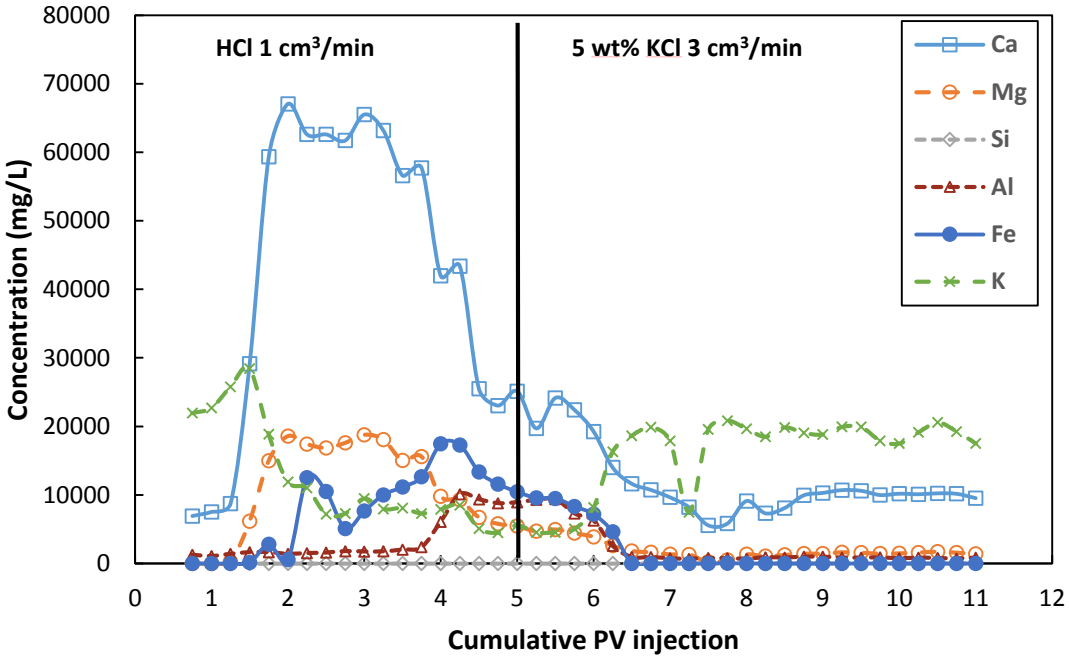

Fig. 107—ICP Analysis of the Effluent Samples-15 wt% HCl with Bandera-BG-6-5 at 300˚F.

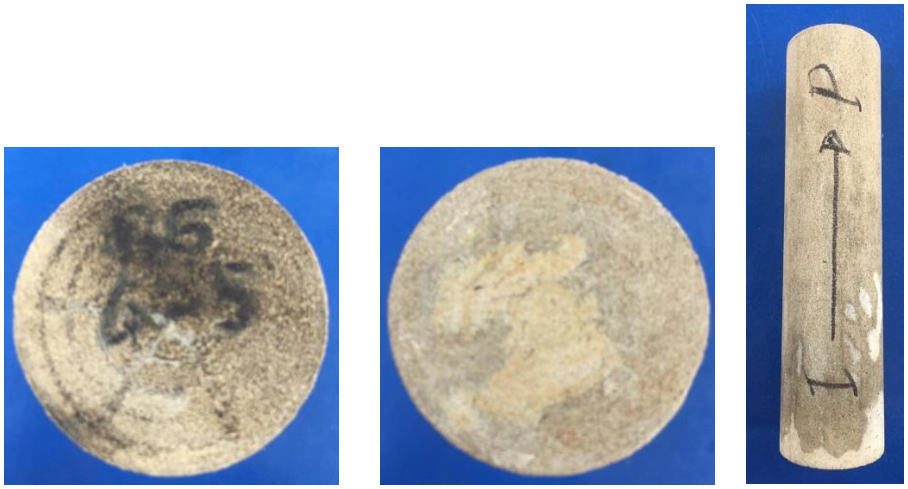

Fig. 108—Injection Face, Production Face, and Side View of Bandera-BG-6-5 After Acid Treatment.

The same procedure with BG-6-12 was applied for SEM-EDS analysis on BG-6-5 precipitates. The SEM images showed both beam burning and amorphous parts with no crystallization **(Fig. 109 and Fig. 110)**, which suggested severe fines migration resulted from the treatment. The EDS results of both granular and amorphous parts in atomic percentage indicated mainly Fe and O **(Table 21 and Table 22)**.

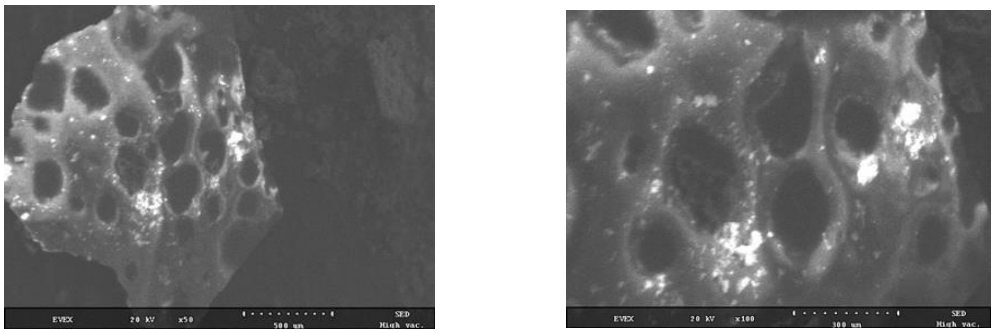

Magnification x50 **Magnification x100**

Fig. 109—SEM Images for BG-6-5 Precipitates (Beam burning part).

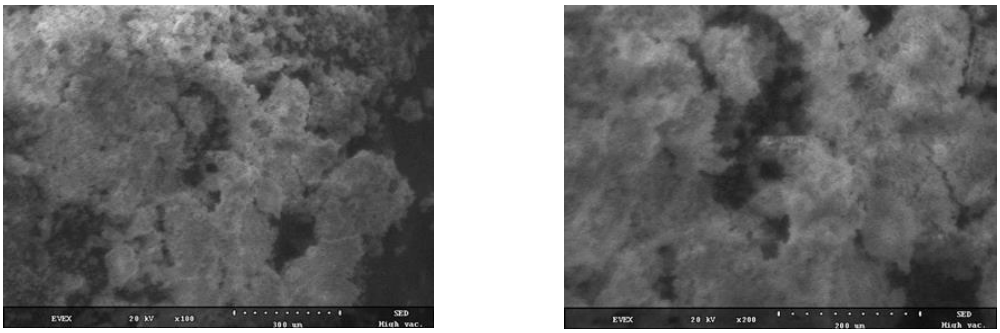

Magnification x100 **Magnification x200**

Fig. 110—SEM Images for BG-6-5 Precipitates (Amorphous part).

Element	Atomic (%)
Fe	20.21
O	77.26
Al	1.12
Cl	1.4

Table 21—EDS Results for Beam Burning Part of BG-6-7 Precipitates.

Element	Atomic (%)
Fe	27.75
O	67.12
Al	3.41
Cl	1.72

Table 22—EDS Results for Amorphous Part of BG-6-7 Precipitates.

The initial pH of the effluent samples containing 5 wt% KCl brine was approximately 8. The pH sharply decreased as the acid was injected to reach the lowest pH of 0 **(Fig. 111)**. This indicated that the effluent samples contained live acid and not all of the acid was spent to dissolve the carbonate minerals in the core. The pH of this experiment was lower compared to the treatment by urea-HCl at 300˚F but in the same range with the treatment by HCl at 250˚F. Subsequently, the pH rose as the core was flushed with brine.

The density of injected brine was around 1.029 g/cc. When the 5 PV of treatment fluid was injected, the density started to increase (after 1.75 PV injection) as the acid

dissolved more Ca, Mg, Al, Si and Fe, which was consistent with the ICP results. As the live acid became spent acid, fewer H^+ ions reacted with the carbonates resulting in less cation dissolution. Consequently, a gradual decrease in density was observed. When the flow was switched back to brine, the density returned to its original value **(Fig. 111)**. The peak of the density of this experiment was in the same range with the treatment by HCl at 250˚F but higher compared to the treatment by urea-HCl at 300˚F. This was due to higher iron and carbonate minerals dissolution in this experiment compared to the treatment by urea-HCl at 300˚F.

The HCl concentration increased sharply after 4 PV of treatment fluid injection to the maximum value around 14.49 wt% HCl **(Fig. 112)**. After the flow had been switched back from acid treatment to brine, HCl concentration decreased significantly after around 1.5 PV of brine injection to 0.12 wt% HCl. This confirmed that most of the acid were pushed out by the brine. The maximum acid concentration in this experiment was higher than the treatment by urea-HCl at 300˚F.

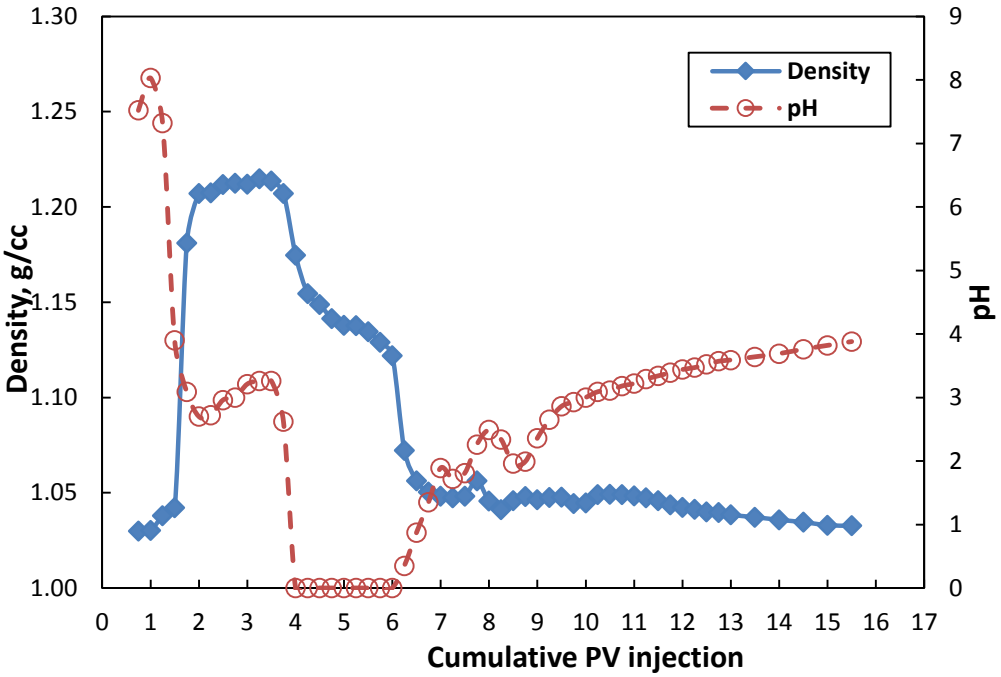

Fig. 111—Density and pH of Effluent Samples from Bandera-BG-6-5 at 300˚F.

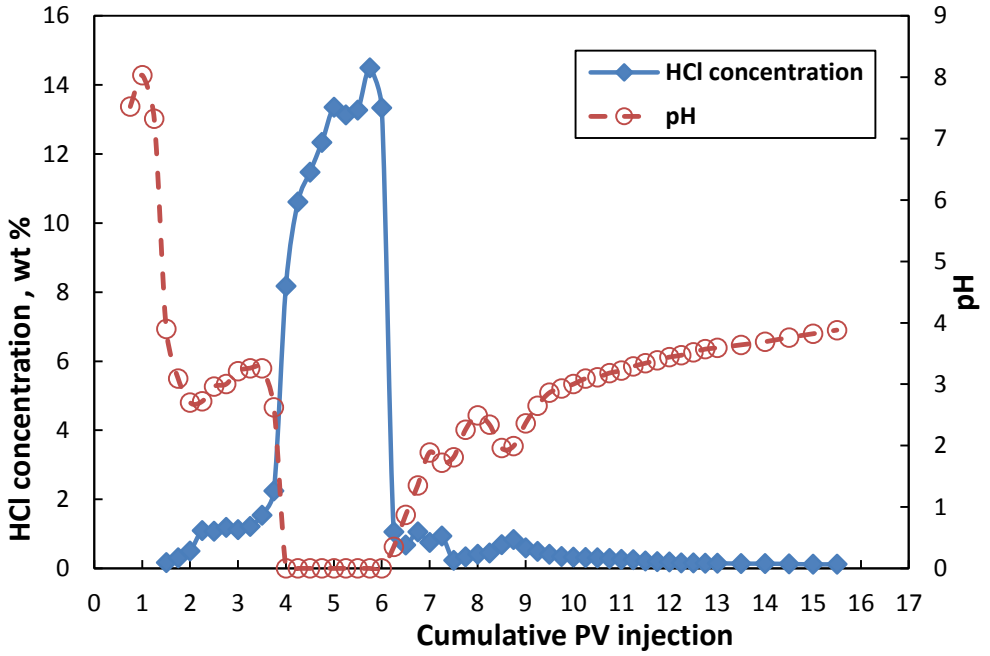

Fig. 112—HCl Concentration of Effluent Samples from Bandera-BG-6-5 at 300˚F.

CT scan results adversely showed the porosity reduction along the core may be due to iron precipitation in the core **(Fig. 113).** The possible explanations were the effect fines migration confirmed by SEM results and iron precipitation in the core. **Table 23** shows the results comparison of urea-HCl and HCl at 300˚F, while **Table 24** gives the results comparison of HCl at 250 and 300˚F.

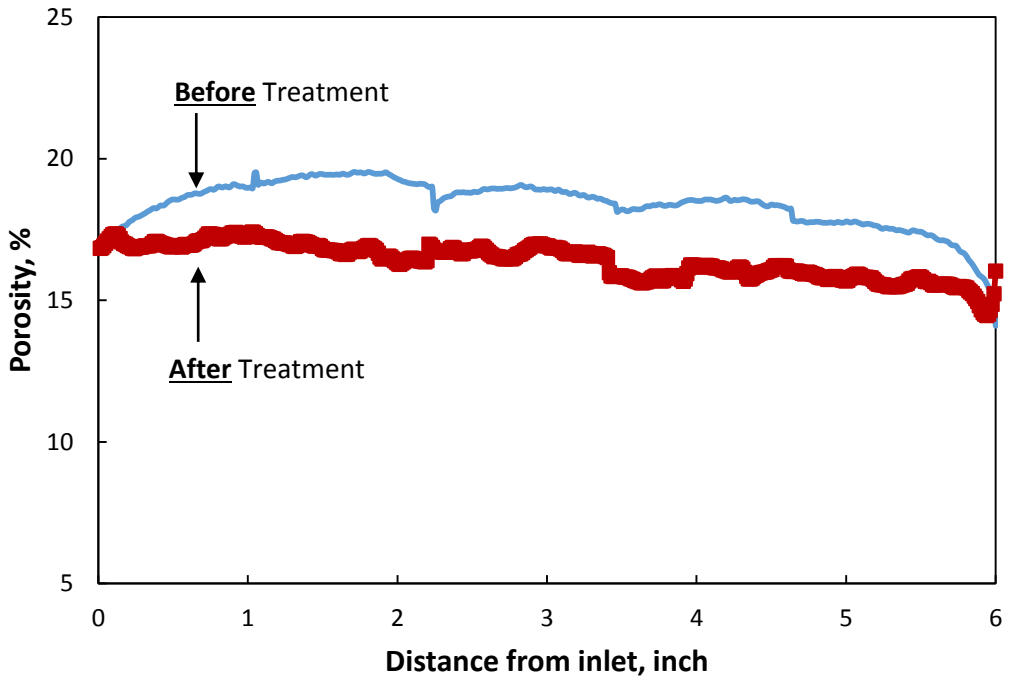

Fig. 113—Porosity Profile Before and After 15 wt% HCl Treatment for Bandera-BG-6-5.

Parameters		BG-6-7 (UHC)	BG-6-5 (HCl)
Permeability		-2 %	+71 %
ICP (mg/L)	Ca^{2+}	35,000	60,000-70,000
	Mg^{2+}	7,500	20,000
	Fe^{2+}	2,000-5,000	10,000-17,500
	Al^{3+}	1,000-3,000	10,000
	Si^{4+}	0	0
pH		4-5	0
HCl concentration (%)		0.1-0.18	14-15
Density (g/cm^3)		1.15	1.21-1.22

Table 23—Results Comparison between BG-6-7 and BG-6-5 (urea-HCl vs. HCl at 300°F).

Parameters		BG-6-6 (250°F)	BG-6-5 (300°F)
Permeability		+111 %	+71 %
ICP (mg/L)	Ca^{2+}	70,000-80,000	60,000-70,000
	Mg^{2+}	20,000	20,000
	Fe^{2+}	20,000-25,000	10,000-17,500
	Al^{3+}	5,000	10,000
	Si^{4+}	0	0
pH		0	0
HCl concentration (%)		12-14	14-15
Density (g/cm^3)		1.21	1.21-1.22

Table 24—Results Comparison between BG-6-6 and BG-6-5 (HCl at 250 vs. 300°F).

Silurian Dolomite (SD-6-33) at 300˚F using HCl with Four Additives

At first, 5 wt% KCl brine was injected in the production direction while heating up the system to 300°F until the pressure drop was stabilized. The pressure drop then increased as the flow was switched from brine to acid in an injection direction since the acid has a higher viscosity compared to 5 wt% KCl **(Fig. 114)**. After 5 PV of treatment, the stabilized pressure drop after the treatment was lower than that before the treatment. However, the acid breakthrough did not occur as in the case of urea-HCl at 250°F.

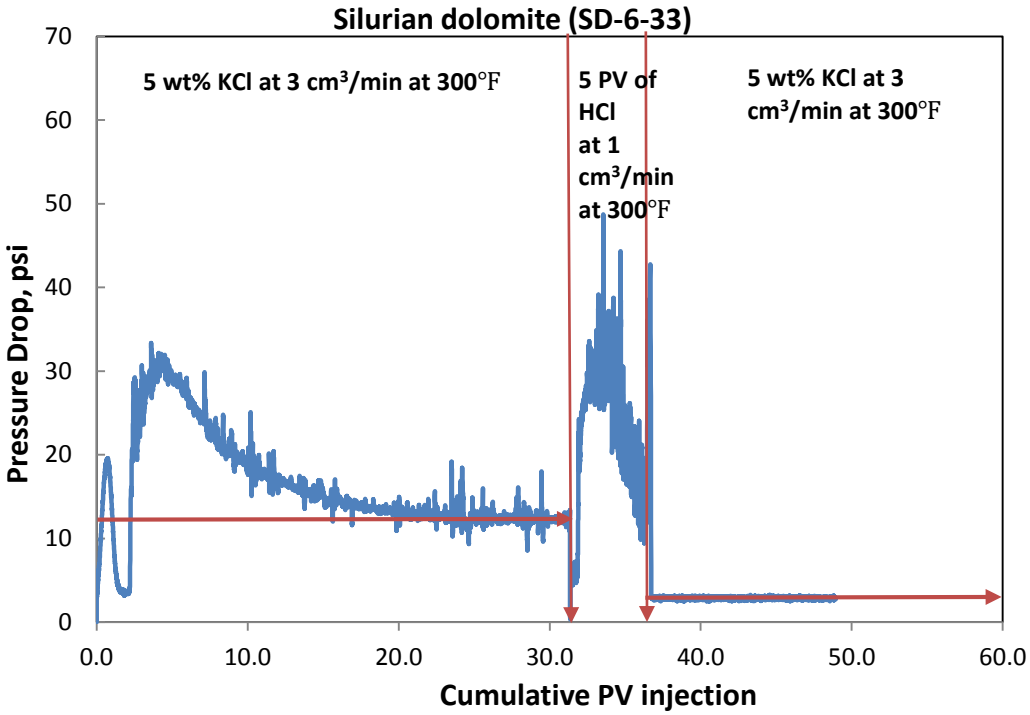

Fig. 114—Pressure Drop Profile Along the Silurian Dolomite SD-6-33 at 300˚F.

Some suspension and precipitates from the dolomite dissolution were observed in the effluent samples after 1.75 PV (pH = 3.47) acid injection **(Fig. 115)**. The calcium and

magnesium concentration from ICP **(Fig. 116)** increased after 1.5 PV of treatment confirming the dissolution of dolomite by HCl. The dissolved carbonate minerals in this experiment were slightly lower than the treatment by the treatment by HCl at 250˚F. However, the concentration of Ca^{2+} and Mg^{2+} were less than the treatment using urea-HCl at 300˚F. K^{+} concentration from 5 wt% KCl brine also decreased during the reaction interval of acid with the core. **Fig. 117** shows the injection face, production face, and side view of SD-6-41 after acid treatment. The most severe face dissolution was observed at the injection face of the core.

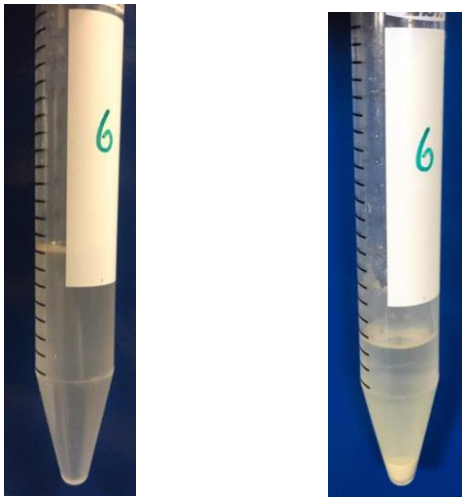

Fig. 115—Suspension and Precipitates of Silurian Dolomite SD-6-33.

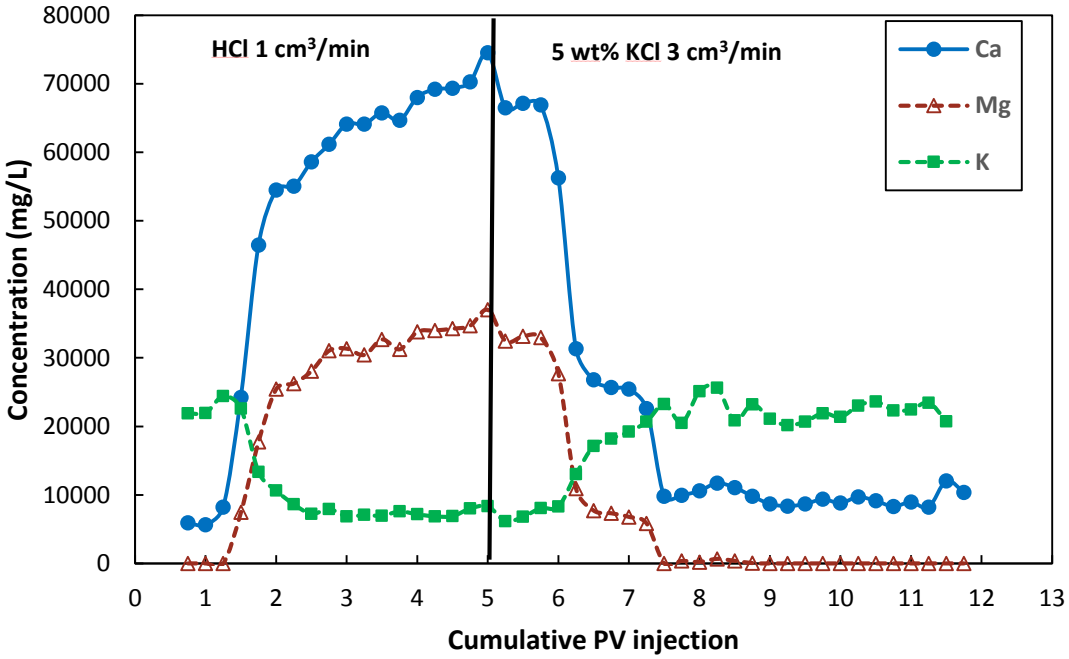

Fig. 116—ICP Analysis of the Effluent Samples- 15 wt% HCl with Silurian Dolomite SD-6-33 at 300˚F.

Fig. 117—Injection Face, Production Face, and Side View of Silurian Dolomite SD-6-33 After Acid Treatment.

The initial pH of the effluent samples containing 5 wt% KCl brine was approximately 8. The pH sharply decreased as the acid was injected to reach the lowest pH of 2.47 **(Fig. 118)**. The pH value was in the same range with the experiment conducted by HCl at 250°F but lower than the pH of the treatment by urea-HCl at 300°F. This indicated that most of the acid were spent during the treatment with minimal or no live acid left in the effluent samples. After that, the pH rose as the core was flushed with brine.

The density of injected brine was around 1.029 g/cc. When the 5 PV of treatment fluid was injected, the density started to increase (after 1.5 PV injection) as the acid dissolved more Ca and Mg, which was consistent with the ICP results. As the live acid became spent acid, fewer H^+ ions reacted with the carbonates resulting in less cation dissolution. Consequently, a gradual decrease in density was observed. When the flow was switched back to brine, the density returned to its original value **(Fig. 118)**. The peak density of this experiment was also in the same range with both the experiment conducted by urea-HCl at 300°F and HCl at 250°F.

The HCl concentration increased after 5 PV of acid was injected to the maximum value around 0.99 wt% HCl **(Fig. 119)**. After the flow had been switched back from acid treatment to brine, HCl concentration decreased significantly after around 1.25 PV of brine injection to 0.04 wt% HCl. This confirmed that most of the acid were pushed out by the brine. Moreover, almost the same carbonate minerals dissolution, pH, spent acid concentration, and density were observed comparing the treatment by HCl at 250 and 300°F.

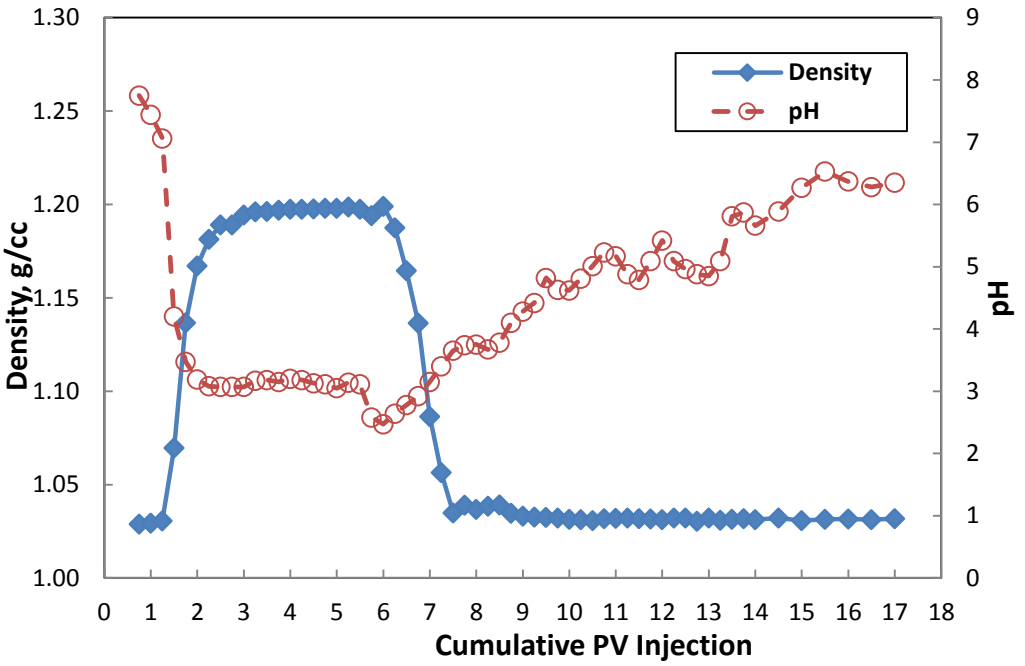

Fig. 118—Density and pH of Effluent Samples from Silurian Dolomite SD-6-33 at 300˚F.

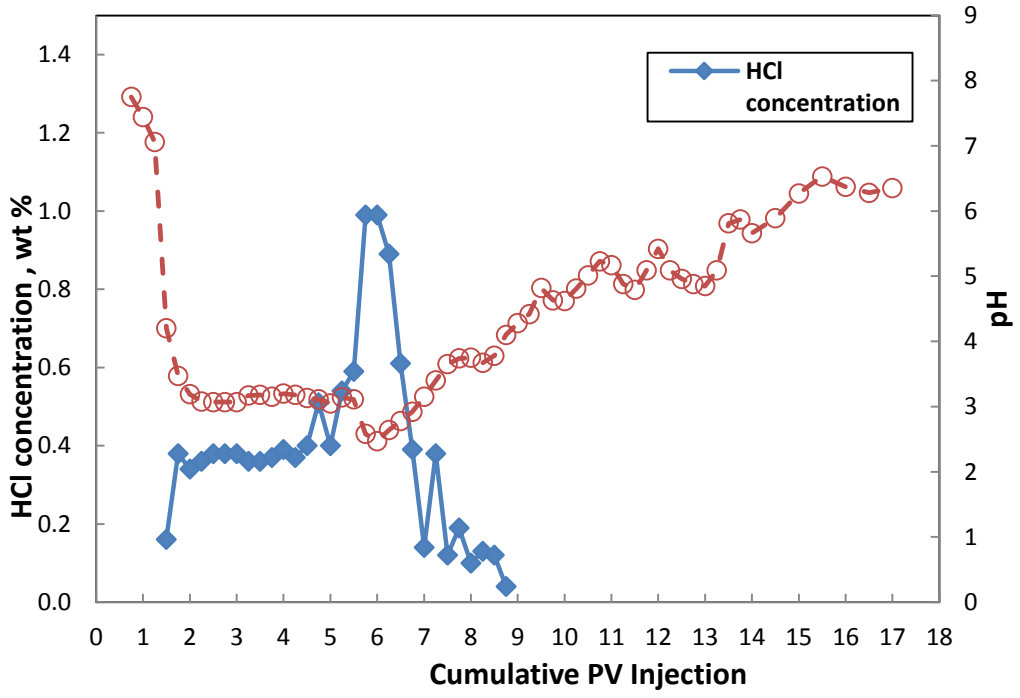

Fig. 119—HCl Concentration of Effluent Samples from Silurian Dolomite SD-6-33 at 300˚F.

The CT scan **(Fig. 120)** results showed the formation of two wormholes along the core. However, the breakthrough did not occur after 5 PV of the acid injection. The most severe face dissolution was also observed from the CT scan at the injection face. **Table 25** shows the results comparison of urea-HCl and HCl at 300˚F, while **Table 26** gives the results comparison of HCl at 250 and 300˚F.

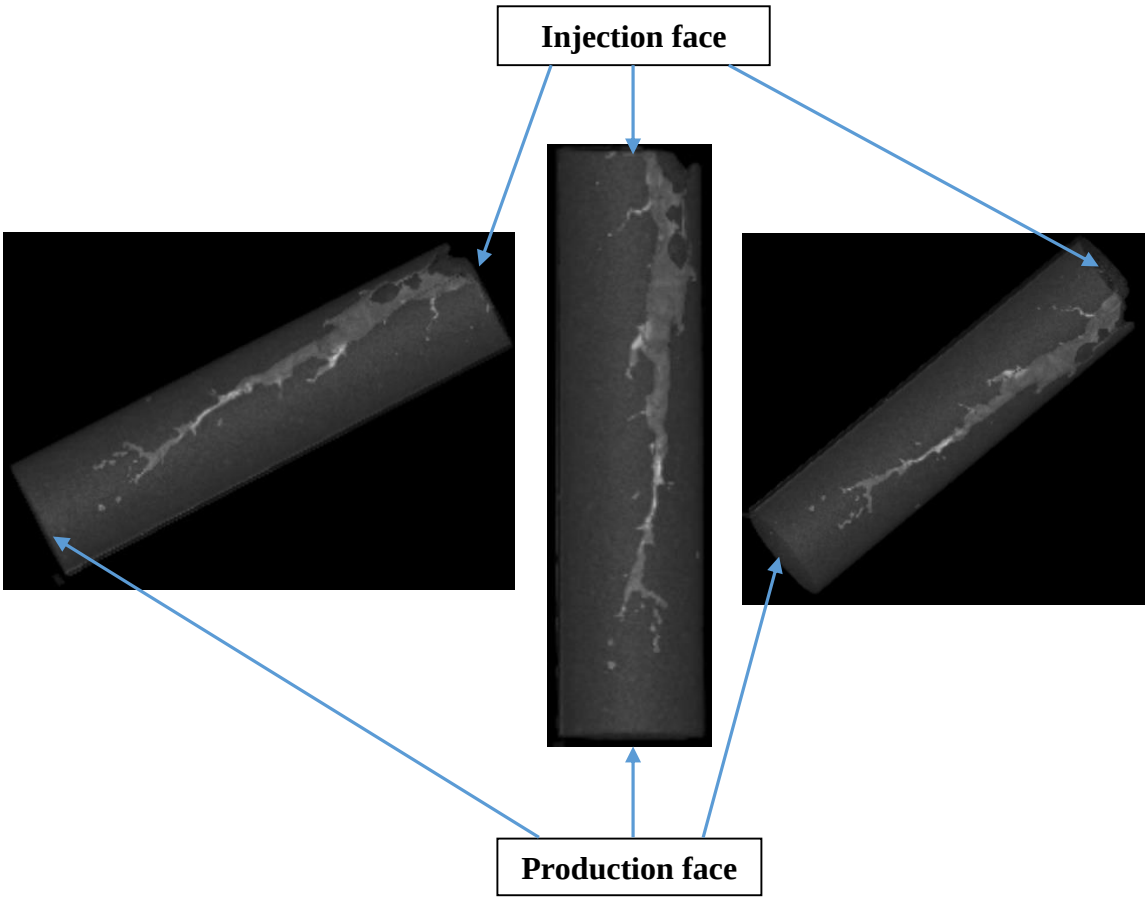

Fig. 120—Wormhole Propagation from CT Scan for Silurian Dolomite SD-6-42.

Parameters		SD-6-41 (UHC)	SD-6-33 (HCl)
Permeability		Not BT	Not BT
ICP (mg/L)	Ca^{2+}	45,000	70,000
	Mg^{2+}	25,000	30,000-35,000
pH		4.5	2.5-3
HCl concentration (%)		0.2	1
Density (g/cm^3)		1.2	1.2

Table 25—Results Comparison between SD-6-41 and SD-6-33 (urea-HCl vs. HCl at 300˚F).

Parameters		SD-6-42 (250°F)	SD-6-33 (300°F)
Permeability		Not BT	Not BT
ICP (mg/L)	Ca^{2+}	80,000-100,000	70,000
	Mg^{2+}	30,000-40,000	30,000-35,000
pH		2.2	2.5-3
HCl concentration (%)		1.6	1
Density (g/cm^3)		1.2	1.2

Table 26—Results Comparison between SD-6-42 and SD-6-33 (HCl at 250 vs. 300˚F).

CHAPTER IV

CONCLUSIONS AND RECOMMENDATIONS

Clay instability (fines migration), iron precipitation in the cores, and the possible decomposition of urea at high BHT are the main problems occurring during acid treatments. The carbonate minerals dissolution is the key mechanisms in stimulation results from the treatments. The advantages of using the new in-situ-generated acid in this research included the retardation effect from urea which was beneficial for less washout and deep penetration in dolomite cores. Moreover, there is no need for clay stabilizers due to the in-situ-generated NH_4Cl from hydrolysis process. In addition, the in-situ-generated acid system provided less corrosive to metal equipment. According to the results obtained, the following conclusions can be drawn:

1. Urea-HCl can efficiently worked as a standalone treatment fluid at 250°F for all lithology.

2. The generated NH_4Cl from urea-HCl hydrolysis can act as a clay stabilizer and lessen formation damage effect.

3. High spent acid concentration was observed in urea-HCl at 250°F suggesting that lower acid concentration in the future.

4. At 300°F, urea-HCl caused slightly damage for both sandstone (The possible hypothesis is the decomposition of urea-HCl).

5. Urea-HCl provided a better performance over HCl for Berea sandstone cores. The major cause is due to fines migration in HCl treatment at high temperature > 200°F.

6. HCl yielded a better results than Urea-HCl for Bandera sandstone cores due to more carbonate minerals dissolution in HCl and the iron precipitation in the cores at pH >2 in case of urea-HCl

7. Despite higher permeability enhancement, fines migration was still observed for Bandera sandstone cores in HCl cases according to SEM results.

8. Urea-HCl yielded better results at 250°F than 300°F in Berea and Bandera. The possible explanation could come from the decomposition at high temperature.

9. Increase corrosion inhibitor load caused slightly stimulation compared to original case since acid could dissolve more carbonate mineral.

10. Addition of silica inhibitor resulted in less stimulation compared to the normal case due to more iron precipitation in the core (less amount of iron dissolution from ICP results).

11. Urea-HCl are capable of creating one main wormhole, less washout, deeper penetration in Silurian dolomite cores compared to regular HCl cases due to retardation effect of urea.

12. Breakthrough can be achieved only in urea-HCl treatment at 250°F.

Regarding the results from this study, the recommendations for future work can be summarized as follows:

1. Study of the surface reaction rate by a rotating disk reactor.

2. Optimization of urea-HCl concentration for Berea and Bandera sandstone treatments at 250°F.

3. The fate of urea-HCl in sandstone cores at 300°F.

4. Investigation of higher acid injection rate for Silurian dolomite.

5. Run FTIR at 250 and 300°F for 0, 1, 2, 3, 4, and 5 hrs to see the decomposition products.

This study's outcome showed a promising results in developing a more cost-effective and efficient design of acid treatments as an alternative to a regular HCl in the dissolution of carbonates in dolomite cores and in the preflush stage for sandstone cores. However, the repetition of coreflooding experiments in various conditions are necessary and the cause and mitigation plan of the damage occurred should be thoroughly understood to ensure the efficient implementation in the field.

REFERENCES

Averill, B.A. and Eldredge, P. 2012. *General Chemistry: Principles, Patterns, and Applications*. New York: Prentice Hall.

Bartko, K. M., Newhouse, D. P., Andersen, C. A. et al. 1995. The Use of CT Scanning in the Investigation of Acid Damage to Sandstone Core. Presented at the SPE Annual Technical Conference and Exhibition, Dallas, Texas, 22-25 October. SPE-30457-MS. http://dx.doi.org/10.2118/ 30457-MS.

Chang, F. F., Nasr-El-Din, H. A., Lindvig, T. et al. 2008. Matrix Acidizing of Carbonate Reservoirs Using Organic Acids and Mixture of HCl and Organic Acids. Presented at the SPE Annual Technical Conference and Exhibition, Denver, Colorado, 21-24 September. SPE-116601-MS. http://dx.doi.org/10.2118/116601-MS

Chapman, M. E. 1933. Some of the Theoretical and Practical Aspects of the Acid Treatment of Limestone Wells. *Oil and Gas Journal*. October 12: 10.

Chatelain, J. C., Silberberg, I. H., and Schechter, R. S. 1976. Thermodynamic Limitations in Organic-Acid/Carbonate Systems. *SPE J.* **16** (4): 189-195. SPE-5647-PA. http://dx.doi.org/10.2118/5647-PA.

Chiu, T. -J., Caudell, E. A., and Wu, F. L. 1993. Development of an Expert System to Assist with Complex Fluid Design. *SPE Computer Applications* **5** (1): 18-20. SPE-24416-PA. http://dx.doi.org/10.2118/24416-PA.

Coulter, G. R. and Jennings, A. R., Jr. 1999. A Contemporary Approach to Matrix Acidizing. *SPE Prod & Oper* **14** (2): 144-149. SPE-56279-PA. http://dx.doi.org/10.2118/56279-PA.

Crowe, C. W. 1986. Prevention of Undesirable Precipitates from Acid Treating Fluids. Presented at the SPE International Meeting on Petroleum Engineering, Beijing, China, 17-20 March. SPE- 14090-MS. http://doi:10.2118/14090-MS.

Estiu, G. and Merz, K. M. 2004. The Hydrolysis of Urea and The Proficiency of Urease. *Journal of the American Chemical Society* **126** (22): 6932–6944. http://dx.doi:10.1021/ja049327g.

Frasch, H. 1896. Increasing the flow of oil wells. U.S. Patent No. 556,669.

Frenier, W. W., Wilson, D., Crump, D. et al. 2000. Use of Highly Acid-Soluble Chelating Agents in Well Stimulation Services. Presented at the SPE Annual Technical Conference and Exhibition, Dallas, Texas, 1-4 October. SPE-63242-MS. http://dx.doi.org/10.2118/63242-MS.

Frenier, W. W., Fredd, C. N., and Chang, F. 2001. Hydroxyaminocarboxylic Acids Produce Superior Formulations for Matrix Stimulation of Carbonates. Presented at the SPE European Formation Damage Conference, The Hague, The Netherlands, 21-22 May. SPE-68924-MS. http://dx.doi:10.2118/68924-MS.

Frenier, W. W., Rainey, M., Wilson, D. et al. 2003. A Biodegradable Chelating Agent is Developed for Stimulation of Oil and Gas Formations. Presented at the SPE/EPA/DOE Exploration and Production Environmental Conference, San Antonio, Texas, 10-12 March. SPE-80597-MS. http://dx.doi.org/10.2118/80597-MS.

Garzon, F. O., Nasr-El-Din, H. A., Al-Mutairi, S. H., et al. 2007. Lessons Learned from Re-pickling Old/Sour Gas Wells. Presented at the SPE Middle East Oil and Gas Show and Conference, Manama, Bahrain, 11-14 March. SPE 105633-MS. http://doi:10.2118/105633-MS.

Geology.uprm.edu. Terrigenous Sediments and Rocks. http://geology.uprm.edu/Morelock/terrigenous.htm (accessed 3 February 2016).

Gidley, J., Brezovec, E., and King, G. 1996. An Improved Method for Acidizing Oil Wells in Sandstone Formations. *SPE Prod & Fac* **11** (01): 4-10. SPE-26580-PA. http://dx.doi:10.2118/26580-PA.

Godfrey, P., Brown, R., Hunter, A. 1997. The Shape of Urea. *Journal of Molecular Structure*. **413–414**: 405–414. http://dx.doi:10.1016/S0022-2860(97)00176-2.

Harris, F. 1961. Applications of Acetic Acid to Well Completion, Stimulation and Reconditioning. *J Pet Technol* **13** (07): 637-639. SPE-63-PA. http://dx.doi:10.2118/63-PA.

Hill, A. D. and Rossen, W. 1994. Fluid Placement and Diversion in Matrix Acidizing. Presented at the University of Tulsa Centennial Petroleum Engineering Symposium, Tulsa, Oklahoma, 29–31 August. SPE-27982-MS. http://dx.doi:10.2118/27982-MS.

Izgec, O., Demiral, B., Bertin, H. et al. 2005. CO_2 Injection in Carbonates. Presented at the SPE Western Regional Meeting, Irvine, California, 30 March-1 April. SPE-93773-PA. http://dx.doi.org/10.2118/93773-MS.

Jiang, L., Lecerf, B., Jones, T. G. et al. 2013. Aqueous Solution and Method for Use Thereof. U.S. Patent No.20,150,037,234.

Kalfayan, L. and Metcalf, A. 2000. Successful Sandstone Acid Design Case Histories: Exceptions to Conventional Wisdom. Presented at the SPE Annual Technical Conference and Exhibition, Dallas, Texas, 1-4 October. SPE-63178-MS. http://dx.doi.org/10.2118/63178-MS.

Kalfayan, L. 2008. *Production Enhancement with Acid Stimulation*, second edition. Tulsa, Oklahoma: PennWell.

King, G. E. 1986. Acidizing concepts-Matrix vs. Fracture acidizing. *J Pet Technol* **38** (05): 507–508. SPE-15279-PA. http://dx.doi:10.2118/15279-PA.

Li Y. -H., Fambrough, J. D., and Montgomery, C. T. 1998. Mathematical Modeling of Secondary Precipitation from Sandstone Acidizing. *SPE J.* **3** (04): 393-401. SPE-53001-PA. http://dx.doi.org/10.2118/53001-PA.

Mahmoud, M., Nasr-El-Din, H. A., and DeWolf, C. 2011. Removing Formation Damage and Stimulation of Deep Illitic-Sandstone Reservoirs Using Green Fluids. Presented at the SPE Annual Technical Conference and Exhibition, Denver, Colorado, 30 October-2 November. SPE-147395-MS. http://dx.doi:10.2118/147395-MS.

McLeod, H. O., Ledlow, L. B., and Till, M. V. 1983. The Planning, Execution, and Evaluation of Acid Treatments in Sandstone Formations. Presented at the SPE Annual Technical Conference and Exhibition, San Francisco, California, 5-8 October. SPE-11931-MS. http://dx.doi.org/10.2118/11931-MS.

McLeod, H. O. 1984. Matrix Acidizing. *J Pet Technol* **36** (12): 2055-2069. SPE-13752-PA. http://dx.doi.org/10.2118/SPE-13752-PA.

McLeod, H. O. 1989. Significant Factors for Successful Matrix Acidizing. Presented at the SPE Centennial Symposium at New Mexico Tech, Socorro, New Mexico, 16-19 October. SPE-20155-MS. http://dx.doi:10.2118/20155-MS.

Nitters, G., Roodhart, L., Jongma, H. et al. 2000. Structured Approach to Advanced Candidate Selection and Treatment Design of Stimulation Treatments. Presented at the SPE Annual Technical Conference and Exhibition, Dallas, Texas, 1-4 October. SPE-63179-MS. http://dx.doi:10.2118/63179-MS.

Putnam, S. W. 1933. Development of Acid Treatment of Oil Wells Involves Careful Study Of Problems of Each. *Oil and Gas Journal*. February 23: 8.

Robert, J. A. and Crowe, C. W. 2000. Carbonate Acidizing Design. In *Reservoir Stimulation*, third edition, Michael J. Economides and Kenneth G. Nolte, Chap. 17, 1-15. Chishester, England: John Wiley & Sons Ltd.

Sargent, R., Alender, J., and Moss, T. 1997. Method for Using Urea Hydrochloride. U.S. Patent No. 5,672,279.

Schaber, P. M., Colson, J., Higgins, S. et al. 2004. Thermal Decomposition (pyrolysis) of Urea in an Open Reaction Vessel. *Thermochimica acta* **424** (1): 131-142. http://dx.doi:10.1016/j.tca.2004.05.018

Shaughnessy, C. M. and Kunze, K. R. 1981. Understanding Sandstone Acidizing Leads to Improved Field Practices. *J Pet Technol* **33** (7): 1196-1202. SPE-9388-PA. http://dx.doi.org/10.2118/9388-PA.

Schauhoff, S. and Kissel, C. 2000. New Corrosion Inhibitors for High Temperature Applications. *Materials and Corrosion* **51** (3): 141-6.

Schechter, R. S. 1992. *Oil Well Stimulation*. New York: Prentice Hall.

Simon, D. and Anderson, M. 1990. Stability of Clay Minerals in Acid. Presented at the SPE Formation Damage Control Symposium, Lafayette, Louisiana, 22-23 February. SPE-19422-MS. http://dx.doi.org/10.2118/19422-MS.

Smith, C. F., Crowe, C. W., and Nolan, T. J. 1969. Secondary Deposition of Iron Compounds Following Acidizing Treatments. *J Pet Technol* **21** (9): 1121-1129. SPE 2358-PA. http://doi:10.2118/2358-PA.

Smith, C. and Hendrickson, A. 1965. Hydrofluoric Acid Stimulation of Sandstone Reservoirs. *J Pet Technol* **17** (02): 215-222. SPE-980-PA. http://dx.doi.org/10.2118/980-PA.

Taylor, K. C. and Nasr-El-Din, H. A. 1999. A Systematic Study of Iron Control Chemicals - Part 2. Presented at the SPE International Symposium on Oilfield Chemistry, Houston, Texas, 16-19 February. SPE 50772-MS. http://doi:10.2118/50772-MS.

Taylor, K. C., Nasr-El-Din, H. A., and Saleem, J. A. 2001. Laboratory Evaluation of Iron-Control Chemicals for High-Temperature Sour-Gas Wells. Presented at the SPE International Symposium on Oilfield Chemistry, Houston, Texas 13-16 February. SPE-65010-MS. http://doi:10.2118/65010-MS.

Thomas, R. L., Nasr-El-Din, H. A., Lynn, J. et al. 2001. Precipitation During the Acidizing of a HT/HP Illitic Sandstone Reservoir in Eastern Saudi Arabia: A Laboratory Study. Presented at the SPE Annual Technical Conference and Exhibition, New Orleans, Louisiana, 30 September-3 October. SPE-71690-MS. http://dx.doi.org/10.2118/71690-MS.

Tuttle, R. 1987. Corrosion in Oil and Gas Production. *J Pet Technol* **39** (07): 756-62. SPE-17004-PA. http://dx.doi.org/SPE-17004-PA.

Walker, J. and Wood, J. K. 1903. LIV.—Hydrolysis of Urea Hydrochloride. *Journal of the Chemical Society, Transactions* **83**: 484-491. http://dx.doi.org/10.1039/CT9038300484

Walker, J., and Hambly, F. J. 1895. Transformation of Ammonium Cyanate into Urea. *J. Chem. Soc.* **67**: 746–767.

Walker, M. L., Dill, W. R., Besler, M. R. et al. 1991. Iron Control in West Texas Sour-Gas Wells Provides Sustained Production Increases. *J Pet Technol* **43** (05): 603-607. SPE-20122-PA. http://dx.doi:10.2118/20122-PA.

Walsh, M. P., Lake, L. W., and Schechter, R. S. 1982. A Description of Chemical Precipitation Mechanisms and Their Role in Formation Damage during Stimulation by Hydrofluoric Acid. *J Pet Technol* **34** (09): 2,097–2,112. SPE-10625-PA. http://dx.doi.org/10.2118/10625-PA.

Warner, R. C. 1942. The Kinetics of the Hydrolysis of Urea and of Arginine. *Journal of Biological Chemistry* **142** (2): 705-723.

Werner, E. A. 1918. XIII.—The Constitution of Carbamides. Part V. The Mechanism of the Decomposition of Urea when Heated in Solution with Alkalis and with Acids, Respectively. The Hydrolysis of Metallic Cyanates. *Journal of the Chemical Society, Transactions* **113**: 84-99.

Werner, E. A. 1920. CXVII.—The Constitution of Carbamides. Part XI. The Mechanism of the Synthesis of Urea from Ammonium Carbamate. The Preparation of Certain Mixed Tri-Substituted Carbamates and Dithiocarbamates. *Journal of the Chemical Society, Transactions* **117**: 1046-53.

Williams, B. B., Gidley, J. L., and Schechter, R. S. 1979. *Acidizing Fundamentals,* Monograph Series. Richardson, Texas: SPE.

Wilson, J. R. 1935. Well Treatment. U.S. Patent No. 1,990,969.

Wöhler, F. 1829. On the Decomposition of Urea and Uric Acid at High Temperature. *Ann.Phys.Chem* **15**: 619-30.